Technical Appendix D: Climate Model Data and Assumptions

Contents

Integrating Climate Policies and Data

The Council first started using climate model data to inform its power planning in the Seventh Power Plan. There are a few substantive ways in which climate data affects the power plan. First, long-term trends in temperature will alter the magnitude and seasonal pattern of electricity demand. Next, since temperature determines whether precipitation falls as rain or snow at a location, then trends in temperature will also alter (magnitude and seasonal pattern of) snowpack on mountains and streamflow in rivers, and thus potential electricity generation from hydro-projects along the river. Furthermore, since temperatures at the extremes (i.e., very high and very low) are correlated with very low wind speeds, then trends in temperature could alter the potential electricity generation from wind farms. Additionally, state policies and laws enacted to reduce greenhouse gas emissions will affect existing resource operations and limit future resource choices. The combined effects of those policies, temperature and other factors will impact the availability of new resources, including energy efficiency and demand response. All these effects must be taken into account to ensure that the Council's resource strategy will result in an adequate, efficient, economical and reliable future power supply. This section focuses on how climate model data are incorporated into the Council's analytical tools, including updates to the approach for the Ninth Power Plan.

Climate Model Data

In 1988, the United Nations Environment Programme (UNEP) and the World Meteorological Organization (WMO) established the Intergovernmental Panel on Climate Change (IPCC), which was subsequently endorsed by the United Nations General Assembly.[1] The IPCC was established to assess available scientific, technical, and socio-economic information concerning climate change, its potential effects, and options for adaptation and mitigation. The IPCC's purpose is to collect and review the most recent scientific information produced worldwide relevant to the understanding of climate change. It does not conduct any research on its own nor does it monitor climate-related data. It is open to all member countries of the United Nations and currently has 195 participating countries that review all scientific material to ensure an objective and complete assessment of current information.[2]

In November of 2014, the IPCC completed its Fifth Assessment Report (AR5)[3] which, among other topical sections, includes a comprehensive assessment of the physical science basis of climate change. In particular, a working group of the IPCC analyzed global climate models (also abbreviated as GCMs) developed by various international participating organizations.[4] The various GCMs forecast long-term changes in the Earth's climate including the effects of greenhouse gases on temperature

[1] See "*IPCC Factsheet: Timeline – highlights of IPCC history*" at https://www.ipcc.ch/site/assets/uploads/2024/04/IPCCFactSheet_Timeline.pdf.
[2] See https://archive.ipcc.ch/organization/organization.shtml.
[3] See "*AR5 Climate Change 2014: Mitigation of Climate Change*" at https://www.ipcc.ch/report/ar5/wg3.
[4] See "*CMIP5 - Coupled Model Intercomparison Project Phase 5*" at https://pcmdi.llnl.gov/mips/cmip5.

and precipitation. The models also take into consideration the interaction of the atmosphere, oceans, and land surfaces. Each of these models has been calibrated to some degree and crosschecked against other such models to provide greater confidence in their forecasting ability.

There were at least 31 different GCMs that were used to project future changes in temperature and precipitation. Every one of these models, to varying degrees, forecasted a warming trend for the Earth. Each used sophisticated mathematical techniques to simulate changes in temperature as a function of atmospheric and other conditions. Like all fields of scientific study, however, there are uncertainties associated with GCM analyses, such as the effects of weather and ocean conditions, that are not as well-understood as scientists would like. Nonetheless, scientists are generally confident about GCM projections for large-scale global areas.

Unfortunately, forecasts on a large spatial scale are of little use to power planners in smaller sub-regions, such as the Pacific Northwest. Therefore, methods to downscale output from the GCMs to a more granular scale were developed by the River Management Joint Operating Committee (RMJOC) which consists of staff from three federal agencies, Bonneville Power Administration (BPA), the Army Corps of Engineers, and the Bureau of Reclamation, as well as climate scientists from the University of Washington and Oregon State University. The downscaling methodology and resulting finer spatial scaled GCM data are described in detail in a RMJOC report.[5]

The RMJOC climate model data were developed for the Pacific Northwest region and are considered as "in-region." The Council's analytical tools use the RMJOC and other related climate model data to simulate operations of power systems in the Northwest. The "in-region" climate model data are discussed in detail from the section "*Incorporating Climate Model Data into Analytical Tools*" to those sections under "*Climate Scenario Solar Generation Profiles*" in this Appendix.

In developing this Power Plan, the Council's analytical tools also simulate power systems in the Western Electricity Coordinating Council[6] (WECC) that are outside of the Pacific Northwest. However, since the RMJOC climate model data are not available for these WECC "out-of-region" power systems, other sources of climate model data are used, and they are discussed in the last section "*Out-of-Region Climate Data*".

Incorporating Climate Model Data into Analytical Tools

The Council uses climate model data to inform hydro conditions, loads, and renewable profiles. The downscaled climate model data include projected future daily maximum and minimum temperatures and daily averaged precipitation for roughly every four-by-four square mile area within the Pacific Northwest region. The forecasted temperature and precipitation data are inputs into various

[5] See "*Climate and Hydrology Datasets for RMJOC Long-Term Planning Studies: Second Edition (RMJOC-II) Part I: Hydroclimate Projections and Analyses*" at https://www.bpa.gov/-/media/Aep/power/hydropower-data-studies/rmjoc-ll-report-part-l.pdf.

[6] See https://www.wecc.org/.

hydrological models to develop a reasonable range of natural (unregulated) river flows.[5] When irrigation withdrawals and returns and evaporation are taken into account, the natural flows then become the modified flows. More specifically, the RMJOC climate model modified flows were calculated with the effects of historical irrigation depletions of year 2008, which were also used in developing the 2010 Level Modified Streamflows.[7] The modified flows at various locations along rivers in the region are among the many inputs into the Council's adequacy model and capital expansion model, GENESYS and OptGen, respectively, to simulate operations of various hydro-projects for power generation and other non-power functions (for example, flood risk management).

Furthermore, the climate model temperatures are also used, among other inputs, in the Council's load-forecast models to estimate future electricity demand.[8] The forecasted demand is then used to provide a starting point for not only the broader regional power system analysis, but also potentially available energy efficiency and demand response.[9]

Unlike the streamflow and temperature data, climate model forecasted wind speed data are not included in the RMJOC data sets. Fortunately, they are available at the Climatology Lab at the University of California, Merced.[10] The downloaded daily averaged wind speed are then used to estimate a set of future hourly wind generations which become inputs in the GENESYS and OptGen models.

Lastly, even though climate model forecasted solar radiation data (also not included in the RMJOC data sets) are available for download from the Climatology Lab, they are not directly used to model future solar generation since there are concerns about the GCMs' ability to accurately simulate cloud cover over the downscaled spatial grids.[11] Instead, climate model diurnal temperature ranges are used as a proxy for the projected solar radiation. These climate model diurnal temperature ranges along with historical diurnal temperature ranges and historical solar radiation data are combined to estimate a set of future hourly utility-scale and behind-the-meter solar generations. The utility scale solar generation becomes an input into the GENESYS and OptGen models, while the behind-the-meter solar shape is used to calculate levelized costs.[12] Both types of solar generation include effects of smoke modeled from historical wildfire patterns.[13]

For simplicity, the climate scenario modified streamflows, forecasted climate wind and solar generation, and electric demand forecasted using climate scenario temperature data are referred to

[7] See https://www.oregon.gov/owrd/WRDReports/appendix_d_flow-data-set-res-sim-analysis.pdf for more details.
[8] See Technical Appendix F - Electricity Demand Forecast in the Ninth Power Plan for more details.
[9] The Council also used these projected temperatures to estimate the savings potential for specific weather sensitive efficiency measures, such as heating measures, to reflect how those opportunities will save under future temperatures. Also reference the section how climate model data are incorporated in Energy Efficiency (EE) and Demand Response (DR) models.
[10] Climatology Lab: https://www.climatologylab.org/maca.html.
[11] Discussions during the Climate and Weather Advisory Committee Meeting on 12/04/2024.
[12] See Technical Appendix J - Rooftop Solar Methodology and Potential in the Ninth Power Plan for more details.
[13] See wildfire methodology section in Technical Appendix G - New Generating Resources for more details.

as climate-informed data. Along with other types of data, they are used in the Council's adequacy model, GENESYS, to assess adequacy reserve margins (ARM). Then the ARM, the climate-informed data, and other relevant resource data, are used as inputs into the Council's regional capital expansion model, OptGen, to develop 20-year resource strategies for the Ninth Plan.

Summary of the RMJOC Climate Model Data and Scenarios

For the Ninth Plan, the Council decided to continue to use climate data developed by the RMJOC, as was done in the previous 2021 Power Plan. A comprehensive analysis of the RMJOC climate data is available in a report (RMJOC I).[14] In the report, RMJOC staff selected 19 climate scenarios for reservoir regulation studies to model and analyze climate impacts on hydro power, flood risk management, water supply, ecosystem, and biological operations, among other topics of interest. Results of the hydro-regulation studies are published in another RMJOC Report (RMJOC II).[15] Methods for selecting the previous subset are described in detail in the "*Climate Change Scenario Selection Process"* supporting material of the 2021 Power Plan.[16] Since data from any selected RMJOC climate scenarios are inputs into many of the Council's models used for the Ninth Power Plan, this section is a summary of the climate scenarios from the RMJOC I report.

The RMJOC climate data were developed from a subset of GCMs from the Coupled Model Intercomparison Project Phase 5 (CMIP5) which were completed in 2014.[17] Subsequently, from 2019 to 2022, a newer set of GCMs became available from CMIP6.[18] Some members of the Council's Climate and Weather Advisory Committee (CWAC) have suggested using climate data from the newer set of CMIP6 GCMs. However, the streamflow data, which is used as an input in the Council's adequacy and capital expansion models, is not an output of GCMs. Rather, it was the RMJOC staff, many of whom have background in regional hydrology, that calculated streamflow data from temperature and precipitation data, which are outputs of CMIP5 GCMs. The RMJOC streamflow data were calculated using various hydrological models tuned for the Pacific Northwest region. There is yet no regional streamflow data calculated from outputs of CMIP6 GCMs, and therefore, the Council continues to use climate data from the CMIP5 GCMs.

---

[14] "*Climate and Hydrology Datasets for RMJOC Long-Term Planning Studies: Second Edition (RMJOC-II) Part I: Hydroclimate Projections and Analyses*" at https://www.bpa.gov/-/media/Aep/power/hydropower-data-studies/rmjoc-ll-report-part-l.pdf.

[15] https://www.bpa.gov/-/media/Aep/power/hydropower-data-studies/rmjoc-ll-report-part-ll.PDF.

[16] https://www.nwcouncil.org/2021powerplan_climate-change-scenario-selection-process.

[17] See "*CMIP5 - Coupled Model Intercomparison Project Phase 5*" at https://pcmdi.llnl.gov/mips/cmip5.

[18] See "*CMIP6 - Coupled Model Intercomparison Project Phase 6*" at https://pcmdi.llnl.gov/CMIP6.

Global Climate Models Selected by the RMJOC

Climate scientists at Oregon State University and the University of Washington, in collaboration with RMJOC staff, selected 10 GCMs from CMIP5 that better replicate historical climate data for the Pacific Northwest region and the larger western North America and northeast Pacific. The 10 selected GCMs are listed in Table D - 1.

Table D - 1: The 10 Global Climate Models selected by the RMJOC

1. CanESM2	6. HadGEM2-CC
2. CCSM4	7. HadGEM2-ES
3. CNRM-CM5	8. inmcm4
4. CSIRO-Mk3-6-0	9. IPSL-CM5-MR
5. GFDL-ESM2M	10. MIROC5

For each of the 10 GCMs, output data were calculated for several representative concentration pathways (RCPs). The RCP is in units of watts per square meter and represents the difference of energy flux radiated by the atmosphere back to the surface between the chosen pre-industrial year of 1765 and the year 2100. For example, for GCMs with RCP8.5, the atmosphere for the year 2100 will radiate to the surface with an *additional* 8.5 W/m^2 energy flux than it did for the year 1765. This increase in energy radiated on the surface of the Earth, or positive radiative forcing, will lead to higher warming for 2100 relative to 1765. Furthermore, it has been estimated that relative to 1765, radiative forcings for 1950, 1980 and 2011 were about 0.57 W/m^2, 1.25 W/m^2 and 2.29 W/m^2 respectively (see IPCC AR5 WG1 Figure SPM.5[19]). Thus, positive radiative forcing has been increasing over the recent decades and so has warming. The RMJOC selected GCMs with RCP4.5 and RCP8.5.

Up to the time of the RMJOC Report,[20] greenhouse gas emissions most closely followed those consistent with RCP8.5 radiative forcing. Since then, there has been debate about the plausibility of RCP8.5 over the long term.[21] However, RCP8.5 is still considered a likely scenario and appropriate for planning purposes out to at least 2050,[22] which is about the time horizon of this study. Moreover, for the Columbia River Basin there is a large overlap in regional GCM projections of temperature and

[19] Intergovernmental Panel on Climate Change, Assessment Report 5, WG1 Figure SPM.5: https://www.ipcc.ch/report/ar5/wg1/summary-for-policymakers/figspm-05.
[20] See "*Climate and Hydrology Datasets for RMJOC Long-Term Planning Studies: Second Edition (RMJOC-II) Part I: Hydroclimate Projections and Analyses*" at https://www.bpa.gov/-/media/Aep/power/hydropower-data-studies/rmjoc-ll-report-part-l.pdf.
[21] Hausfather, Z., & Peters, G. P. (2020). Emissions - the "business as usual" story is misleading. Nature, 577(7792), 618-620. https://doi.org/10.1038/d41586-020-00177-3.
[22] Schwalm, C. R., Glendon, S., & Duffy, P. B. (2020). RCP8.5 tracks cumulative CO2 emissions. Proceedings of the National Academy of Sciences, 117(33), 19656-19657. https://doi.org/10.1073/pnas.2007117117.

precipitation from RCP4.5 and RCP8.5 to 2050.[23] Therefore, the Council decided to use only GCMs with RCP8.5 for the Ninth Plan, matching the RMJOC decision to also choose the RCP8.5 GCMs for its hydro-regulation studies.

The 10 selected CMIP5 GCMs have spatial grids with resolutions between 47 miles to 186 miles. However, grids with these distances are too coarse to adequately capture the complex terrain and highly varied climate across the Columbia River Basin. Also, the coarse spatial grids might not be close to locations of interest for representative cities of the 13 Northwest balancing authorities (such as airports), whose climate scenario temperature data are used in the Council's load forecast models. Therefore, to make the climate data more useful, the RMJOC transformed the original coarse grid into a more granular grid of about 4 miles by 4 miles using two statistical methods: the Bias-Corrected Spatial Disaggregation (BCSD) downscaling and Multivariate Adaptive Constructed Analog (MACA) downscaling.

With the two downscaling methods, RMJOC staff were able to calculate for the 10 GCMs downscaled temperature and precipitation data on many grid points over the Northwest. Because of using two downscaling methods, the original 10 CMIP5 GCMs in Table D - 1 expanded to 20 downscaled GCMs and are listed in Table D - 2. The downscaling method is expressed in bold texts.

Table D - 2: The 20 RMJOC downscaled Global Climate Models

CanESM2_**BCSD**	CanESM2_**MACA**	HadGEM2-CC_**BCSD**	HadGEM2-CC_**MACA**
CCSM4_**BCSD**	CCSM4_**MACA**	HadGEM2-ES_**BCSD**	HadGEM2-ES_**MACA**
CNRM-CM5_**BCSD**	CNRM-CM5_**MACA**	inmcm4_**BCSD**	inmcm4_**MACA**
CSIRO-Mk3-6-0_**BCSD**	CSIRO-Mk3-6-0_**MACA**	IPSL-CM5-MR_**BCSD**	IPSL-CM5-MR_**MACA**
GFDL-ESM2M_**BCSD**	GFDL-ESM2M_**MACA**	MIROC5_**BCSD**	MIROC5_**MACA**

The climate data (precipitation and temperature) from the 20 downscaled GCMs in Table D - 2 were used as inputs into hydrological models to generate natural streamflow data. It should be noted that these natural streamflows do not take into consideration any irrigation, evaporation, or regulation from hydro-projects. RMJOC staff used four hydrological models: the Variable Infiltration Capacity (VIC) Model developed at the University of Washington (VIC-P1), at the Oak Ridge National Laboratory (VIC-P2), and at the National Center for Atmospheric Research (VIC-P3), and the Precipitation Runoff Modeling System (PRMS-P1) Model.

Thus, the four hydrological models produced 80 climate scenarios of natural streamflows from the 20 downscaled GCMs in Table D - 2. Since it is not practical to list all 80 scenarios in a table, an example is presented for one downscaled GCM to show the transformation of its climate data into climate scenario streamflows. The downscaled CanESM2_**BCSD** model listed in Table D - 2 will produce four scenarios: CanESM2_**BCSD**_***VIC_P1***, CanESM2_ **BCSD**_***VIC_P2***, CanESM2_**BCSD**_***VIC_P3***, and

[23] Rupp, D. E., Abatzoglou, J. T., & Mote, P. W. (2017). Projections of 21st century climate of the Columbia River Basin. Climate Dynamics, 49(5), 1783-1799. https://doi.org/10.1007/s00382-016-3418-7.

CanESM2_**BCSD**_ ***PRMS_P1***, where the hydrological models are expressed in italic bold texts. These four scenarios have different streamflows but the same temperature since hydrological modeling does not affect temperature. Therefore, even though there are 80 scenarios with climate model natural streamflows, there are only 20 unique scenarios for climate model temperatures as listed in Table D - 2.

RMJOC staff performed extensive analyses of the 80 climate scenarios, and the following are excerpts from the executive summary in the RMJOC Report[24]:

- Temperatures have already warmed about 1.5°F in the region since the 1970s (which refers the 30 years from 1970 to 1999). They are expected to warm another 1 to 4°F by the 2030s (which refers to the middle decade of the near-future 30 years, from 2020 to 2049).
- Temperatures are likely to warm 3 to 6°F over what is currently observed in the basin by the 2070s if RCP4.5 emissions pathways are attained. If current trajectory RCP8.5 emissions pathways are realized, though, 4 to 10°F of warming above what is currently observed will be likely by the 2070s (which refers to the middle decade of the far-future 30 years, from 2060 to 2089).
- Warming is likely to be greatest in the interior, with a greater range of possible outcomes, with less pronounced warming near the coast.
- Future precipitation trends are more uncertain, but a general upward trend is likely for the rest of the 21st century, particularly in the winter months. Already dry summer months could become drier.
- Average winter snowpacks are very likely to decline over time as more winter precipitation falls as rain instead of snow, especially in the US side of the Columbia Basin.
- By the 2030s, higher average fall and winter flows, earlier peak spring runoff, and longer periods of low summer flows are very likely. The earliest and greatest streamflow changes are likely to occur in the Snake River Basin, although that is also the basin with the greatest modeling and forecast uncertainty.
- In the Willamette Basin, fall and winter flows are likely to increase. A slight decrease in spring flows is possible, with a longer period of low summer flows more likely than not.

The 19 RMJOC Climate Scenarios

Because a hydro-regulation study for just one scenario requires considerable time and resources to complete, the RMJOC staff decided to study hydro-regulation for only a representative subset of the 80 scenarios. The representative subset of 19 climate scenarios is listed in Table D - 3 below.

[24] See "*Climate and Hydrology Datasets for RMJOC Long-Term Planning Studies: Second Edition (RMJOC-II) Part I: Hydroclimate Projections and Analyses*" at https://www.bpa.gov/-/media/Aep/power/hydropower-data-studies/rmjoc-ll-report-part-l.pdf.

Table D - 3: The 19 Climate Scenarios Selected by the RMJOC for Hydro-Regulation Studies

A: CanESM2_RCP85_**BCSD**_***VIC_P1***	**K:** GFDL_ESM2M_RCP85_**MACA**_***VIC_P2***
B: CanESM2_RCP85_**MACA**_***PRMS_P1***	**L:** HadGEM2-CC_RCP85_**BCSD**_***VIC_P1***
C: CCSM4_RCP85_**BCSD**_***VIC_P1***	**M:** HadGEM2-CC_RCP85_**MACA**_***VIC_P1***
D: CCSM4_RCP85_**MACA**_***VIC_P3***	**N:** inmcm4_RCP85_**BCSD**_***PRMS_P1***
E: CNRM-CM5_RCP85_**BCSD**_***VIC_P2***	**O:** inmcm4_RCP85_**BCSD**_***VIC_P2***
F: CNRM-CM5_RCP85_**MACA**_***VIC_P1***	**P:** inmcm4_RCP85_**MACA**_***VIC_P3***
G: CNRM-CM5_RCP85_**MACA**_***VIC_P3***	**Q:** IPSL-CM5A-MR_RCP85_**MACA**_***VIC_P2***
H: CSIRO-Mk3-6-0_RCP85_**BCSD**_***PRMS_P1***	**R:** MIROC5_RCP85_**BCSD**_***PRMS_P1***
I: GFDL_ESM2M_RCP85_**BCSD**_***VIC_P2***	**S:** MIROC5_RCP85_**BCSD**_***VIC_P3***
J: GFDL_ESM2M_RCP85_**MACA**_***VIC_P1***	

These 19 scenarios were selected by the RMJOC to cover a wide range of differences in hydrological conditions between the 2030's time period (the 30 years from 2020 to 2049) and a historical period (the 30 years from 1976 to 2005) for 14 hydro-projects throughout the Columbia River Basin. A map of the 14 hydro-projects in the red circles is plotted Figure D - 1.

Figure D - 1: The 14 Hydro-Projects in the Red Circles[25]

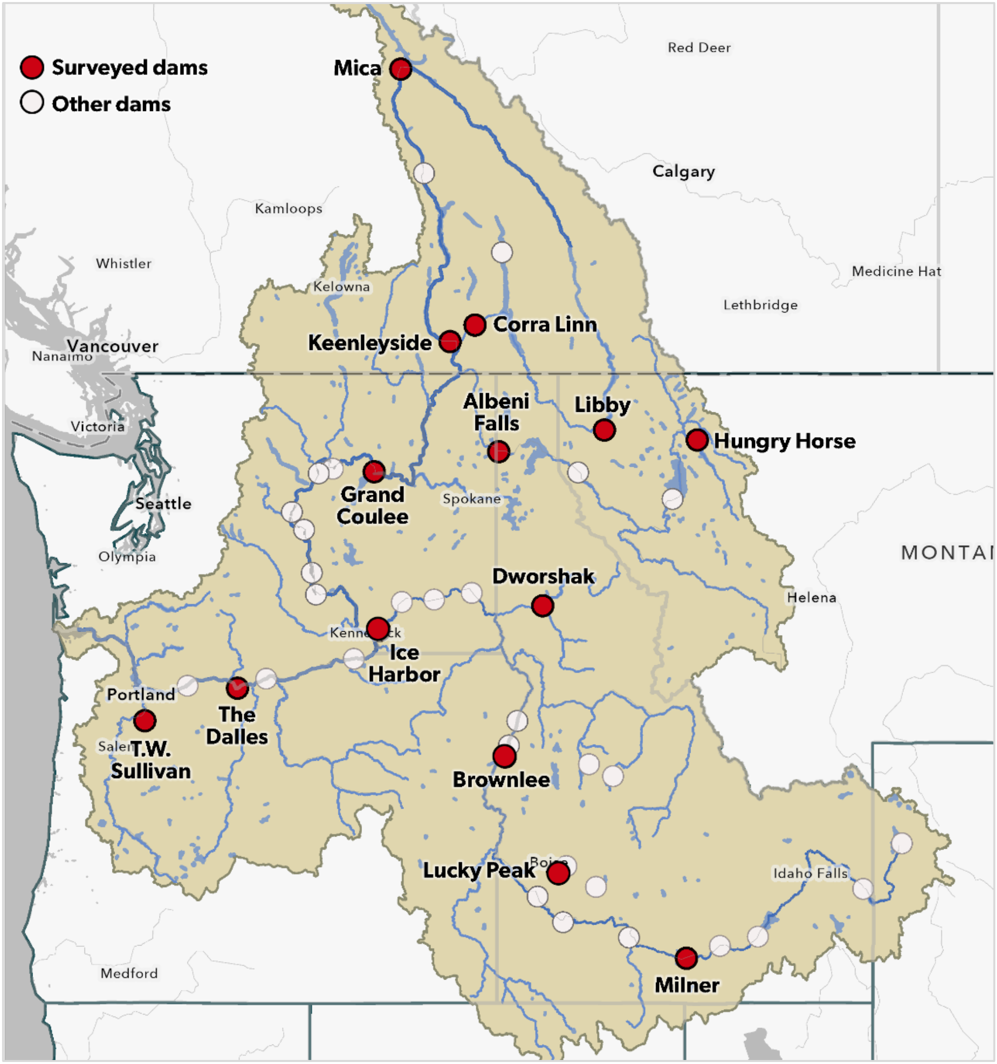

Figure D - 1 shows a map of the 14 hydro-projects, plotted in the red circles, whose streamflow metrics were used to select the 19 RMJOC climate scenarios. The 14 hydro-projects are Mica, Keenleyside (or Arrow), and Cora Linn in Canada, and Hungry Horse, Libby, Albeni Falls, Grand Coulee, Dworshak, Ice Harbor, The Dalles, T. W. Sullivan, Brownlee, Lucky Peak, and Milner in the United States. The hydrological conditions are characterized by six streamflow metrics: river-flow volume for the entire year and for the winter, spring, and summer periods, winter-to-spring volume ratio, and annual half-volume timing (which is the date on which half the annual volume at The Dalles has passed). RMJOC staff then developed an algorithm based on these six streamflow metrics for the

[25] Figure D-1 reproduces the same information on the 14 hydro-projects as Figure 76 in "*Climate and Hydrology Datasets for RMJOC Long-Term Planning Studies: Second Edition (RMJOC-II) Part I: Hydroclimate Projections and Analyses*" at https://www.bpa.gov/-/media/Aep/power/hydropower-data-studies/rmjoc-ll-report-part-l.pdf.

14 hydro-projects to select the subset of 19 out of 80 climate scenarios.[26] For these 19 climate scenarios, RMJOC staff also performed hydro-regulation studies and published the results and analyses in another RMJOC report.[27]

The RMJOC shared its climate model and related data with the Council, which include modified streamflows (which do contain effects of irrigation and evaporation, but not regulation from hydro projects), flood-control and refill rule-curves, and operating constraints for various hydro-projects. These hydro data are needed for the Council's resource adequacy and capital expansion models, GENESYS and OptGen, respectively. Analyses of the climate model streamflow data are presented in a subsequent section.

In addition to the hydro related data, the RMJOC also shared climate model temperature data at 26 locations in the Northwest that could represent the 13 Northwest balancing authorities. The temperature data are inputs into Council's load forecast model.[28] Some representative regional temperatures are analyzed in detail in a later section.

As discussed previously, climate model wind and solar data are not available from the RMJOC data set but are available at the Climatology Lab at the University of California, Merced.[29] The calculations of climate scenario wind and solar generations, which are inputs into the Council's simulation models, are described in detail in subsequent sections.

Finally, since the full designation for each of the 19 climate scenarios in Table D - 3 is quite long, for convenience, in subsequent sections the scenarios are referenced by the assigned alphabetical indices, from A to S, which are printed in bold texts. It should also be noted that the pair of scenarios in each of the four sets, (F, G), (J, K), (N, O) and (R, S), have the same climate temperature since they come from the same GCM and are calculated with the same downscaling method but differ only in the hydrological models used (which does not affect temperature). Because of duplications in temperatures in these four pairs of scenarios, there are only 15 unique scenarios for climate temperatures in contrast to the 19 unique scenarios for climate streamflows.

The Subset of RMJOC Climate Scenarios for the Power Plan

As discussed in a previous section, for the Ninth Plan, the Council proposed to use the same representative subset of three climate scenarios out of the 19 RMJOC climate scenarios as was done in the previous 2021 Power Plan. The selected RMJOC climate scenarios and their relevant properties

[26] See "*Climate and Hydrology Datasets for RMJOC Long-Term Planning Studies: Second Edition (RMJOC-II) Part I: Hydroclimate Projections and Analyses*" at https://www.bpa.gov/-/media/Aep/power/hydropower-data-studies/rmjoc-ll-report-part-l.pdf.
[27] https://www.bpa.gov/-/media/Aep/power/hydropower-data-studies/rmjoc-ll-report-part-ll.PDF.
[28] See Technical Appendix F - Electricity Demand Forecast in the Ninth Power Plan for more details.
[29] Climatology Lab: *https://www.climatologylab.org/maca.html*.

are presented in this section. Furthermore, there is also a discussion on adding another climate scenario to the existing three scenarios in the subset so that together they are more representative of the entire ensemble of 19 RMJOC climate scenarios. Council staff presented the two proposed subsets and their analyses to the Climate and Weather Advisory Committee (CWAC). After some discussions, the CWAC in general agreed with using the same three climate scenarios for the Ninth Plan.

The Three Selected Climate Scenarios

The three selected RMJOC climate scenarios are: CanESM2_RCP85_**BCSD**_***VIC_P1***, designated as **A**; CCSM4_RCP85_**BCSD**_***VIC_P1***, designated as **C**; and CNRM-CM5_RCP85_**MACA**_***VIC_P3***, designated as **G**. All 19 RMJOC climate scenarios are listed in Table D - 3 in the previous section.

Methods for selecting scenarios A, C and G are described in detail in the "*Climate Change Scenario Selection Process"* supporting material of the previous 2021 Power Plan.[30] However, it should be noted that the selection methods utilized variables and simulation tool that have been replaced with different variables and a new simulation model in the current Ninth Plan. Therefore, to avoid any confusion, the "*Climate Change Scenario Selection Process"* supporting material of the previous 2021 Power Plan is referenced in a footnote but not presented here. Nevertheless, the methods developed previously for selecting A, C and G are still valid and are discussed briefly in this section.

In summary, the methods used were based on selecting a subset (of climate scenarios) whose four distributions of winter and summer hydro-generation, regional winter heating-degree-days (HDDs), and regional summer cooling-degree-days (CDDs), could be considered representative of the corresponding four distributions from the ensemble of all 19 scenarios. Specifically, winter is represented by the months December, January, and February, while summer is represented by months June, July, and August.

Comparisons of the four distributions are presented in box-and-whiskers plots (or boxplots for short). An illustration of a boxplot is presented in Figure D - 2 below. The boxplot allows for quantitative comparisons of distributional statistics such as the 25th, 50th (the median), and 75th percentiles. The grey box in Figure D - 2, which starts from the 25th percentile (at the bottom of the box) and ends at the 75th percentile (the top of the box), contains the central 50% of the population of the distribution. The length of the box is defined as the inter-quartile-range (IQR) and is used to delineate outliers (if any): those data that lie beyond one-and-a-half times the IQR from the box.

[30] https://www.nwcouncil.org/2021powerplan_climate-change-scenario-selection-process.

Figure D - 2: An Illustrative Example of Box and Whiskers Plot

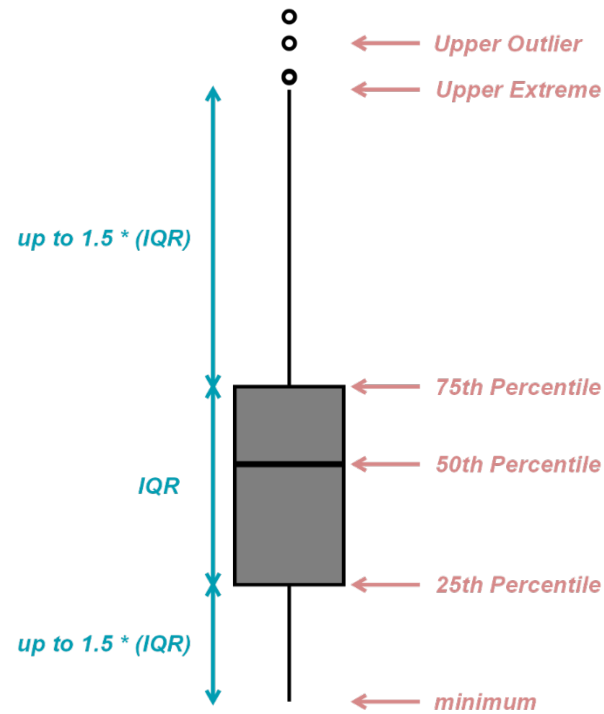

First, comparisons of the winter and summer monthly average hydro-generation are presented as Figure D - 3 below.

Figure D - 3: Comparison of Winter (left) and Summer (right) Hydro Generation Between Selected Scenarios and Ensemble

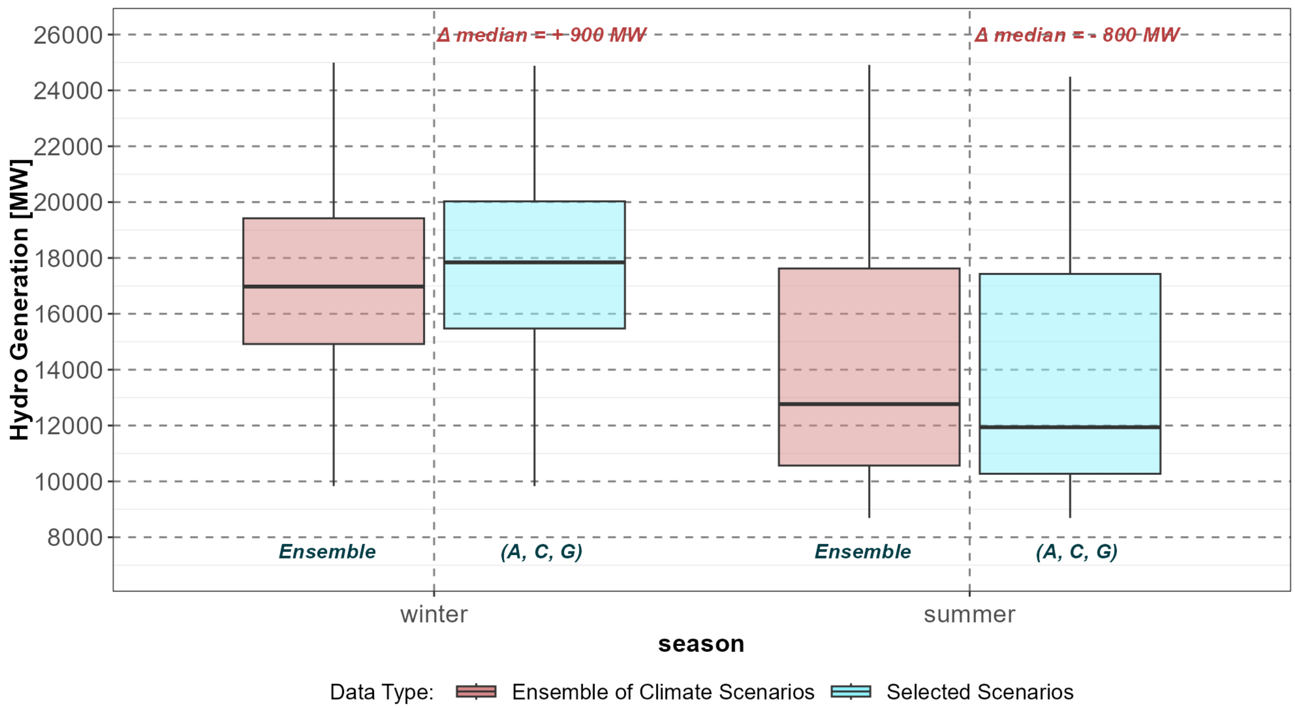

In Figure D - 3, average monthly hydro-generations of the ensemble distribution of all 19 climate scenarios are plotted in the light red boxplots while that of the distributions of the selected (A, C, G) scenarios are plotted in the light blue boxplots. Generations for the winter and summer seasons are plotted on the left side and right side, respectively. Furthermore, the difference between the median generations of the (A, C, G) distribution and the ensemble distribution is listed above the light blue boxplots. For winter hydro-generation, the light blue (A, C, G) distribution is *slightly higher* than the light red ensemble distribution, with the blue median being about 900 MW higher than the red median. In contrast, for summer hydro-generation, the blue (A, C, G) distribution is *slightly lower* than the red ensemble distribution, with the blue median being about 800 MW lower than the red median.

Next, comparisons of the winter Heating Degree-Days (HDDs) and summer Cooling Degree-Days (CDDs) are presented as Figure D - 4 below.

Figure D - 4: Comparison of Winter (left) and Summer (right) Degree-Days Between Selected Scenarios and Ensemble

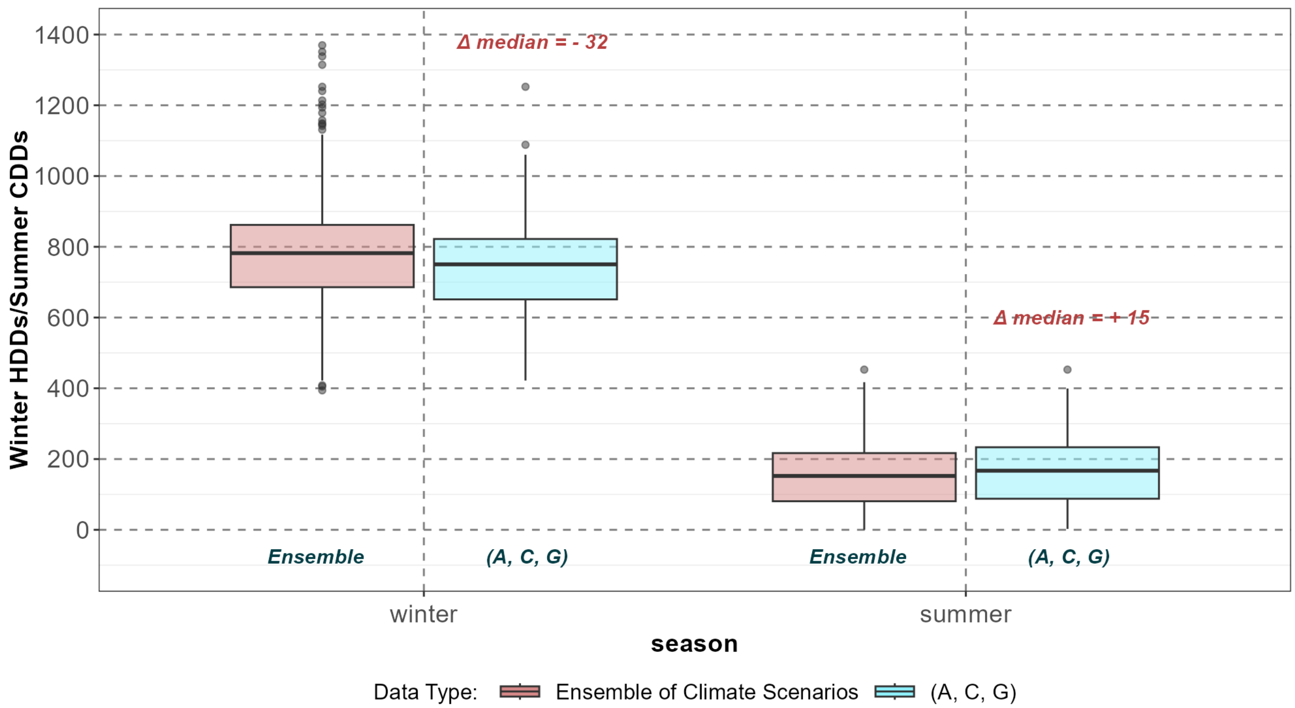

In Figure D - 4, monthly degree-days (HDDs or CDDs) of the ensemble distribution of all 19 climate scenarios are plotted in the light red boxplots while those of the distribution of the selected (A, C, G) scenarios are plotted in the light blue boxplots. HDDs for winter and CDDs for summer are plotted on the left side and right side, respectively. Furthermore, the difference between the median degree-days of the (A, C, G) distribution and the ensemble distribution is listed above the blue boxplots. For winter HDDs, the blue (A, C, G) distribution is *slightly lower* than the red ensemble distribution, with the blue median being 32 degree-days lower than the orange median. In contrast, for summer CDDs, the blue (A, C, G) distribution is slightly higher than the red ensemble distribution, with the blue median being 15 degree-days higher than the orange median.

Therefore, the four distributions of the selected (A, C, G) scenarios are slightly different from the corresponding distributions of the ensemble, with opposite trends between winter and summer.

Selecting an Additional RMJOC Climate Scenario

Subsequent to the completion of the 2021 Power Plan, further analysis showed that by adding one more RMJOC climate scenario, namely **J**: GFDL_ESM2M_RCP85_**MACA**_***VIC_P1***, to the already selected A, C and G, the four distributions of the expanded subset (A, C, G, J) are much closer to the corresponding four distributions of the ensemble.

Specifically, in Figure D - 5, average monthly hydro-generations of the ensemble distribution of all 19 climate scenarios are plotted in the red boxplots while those of the distribution of the selected scenarios (A, C, G) plus scenario J are plotted in the blue boxplots. Generations for the winter and summer seasons are plotted on the left side and right side, respectively. Furthermore, the difference between the median generations of the (A, C, G, J) distribution and the ensemble distribution is listed above the blue boxplots. For winter hydro-generation, the blue (A, C, G, J) distribution is a very close match to the red ensemble distribution, with the blue median being only about 28 MW higher than the red median. Furthermore, for summer hydro-generation, the blue (A, C, G, J) distribution could also be considered a very close match to the red ensemble distribution, despite the blue median being about 464 MW lower than the orange median.

Figure D - 5: Comparison of Winter (left) and Summer (right) Hydro-Generation Between Selected Scenarios Plus Scenario J vs Ensemble

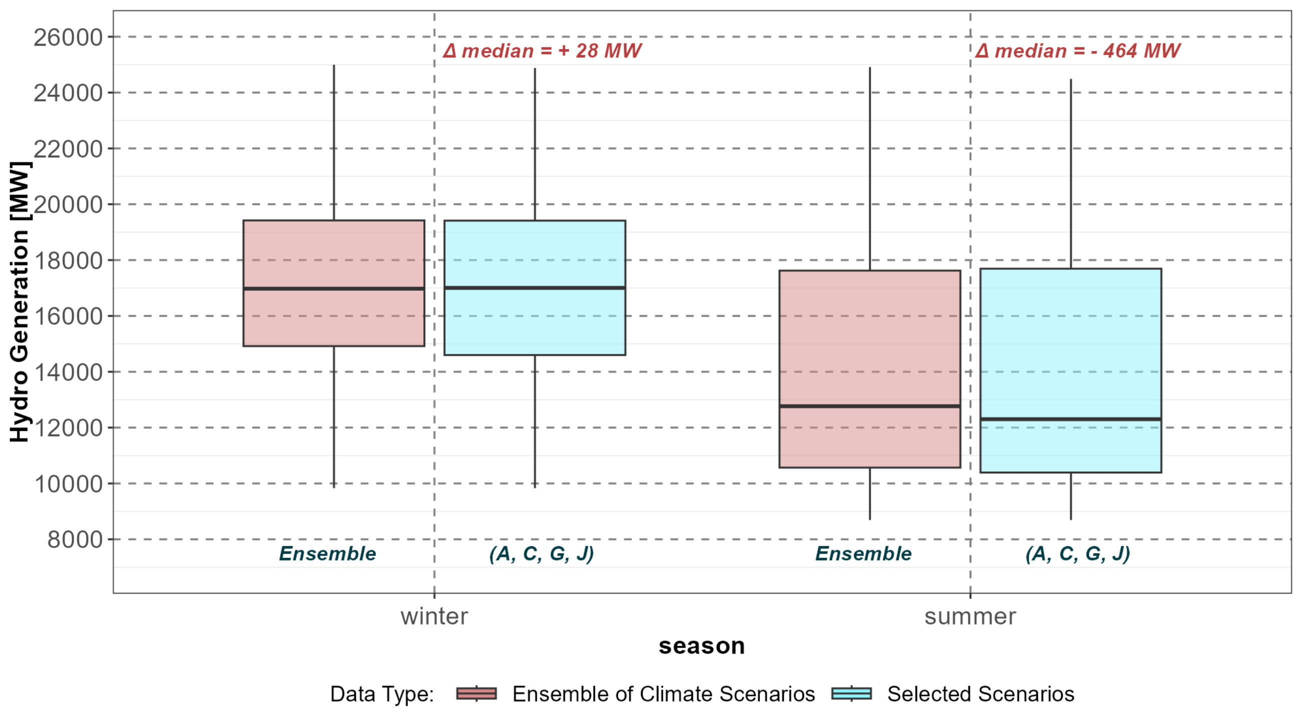

Finally, comparisons of the winter HDDs and summer CDDs are presented in Figure D - 6 below.

Figure D - 6: Comparison of Winter (left) and Summer (right) Degree-Days Between the Selected Scenarios Plus J vs the Ensemble

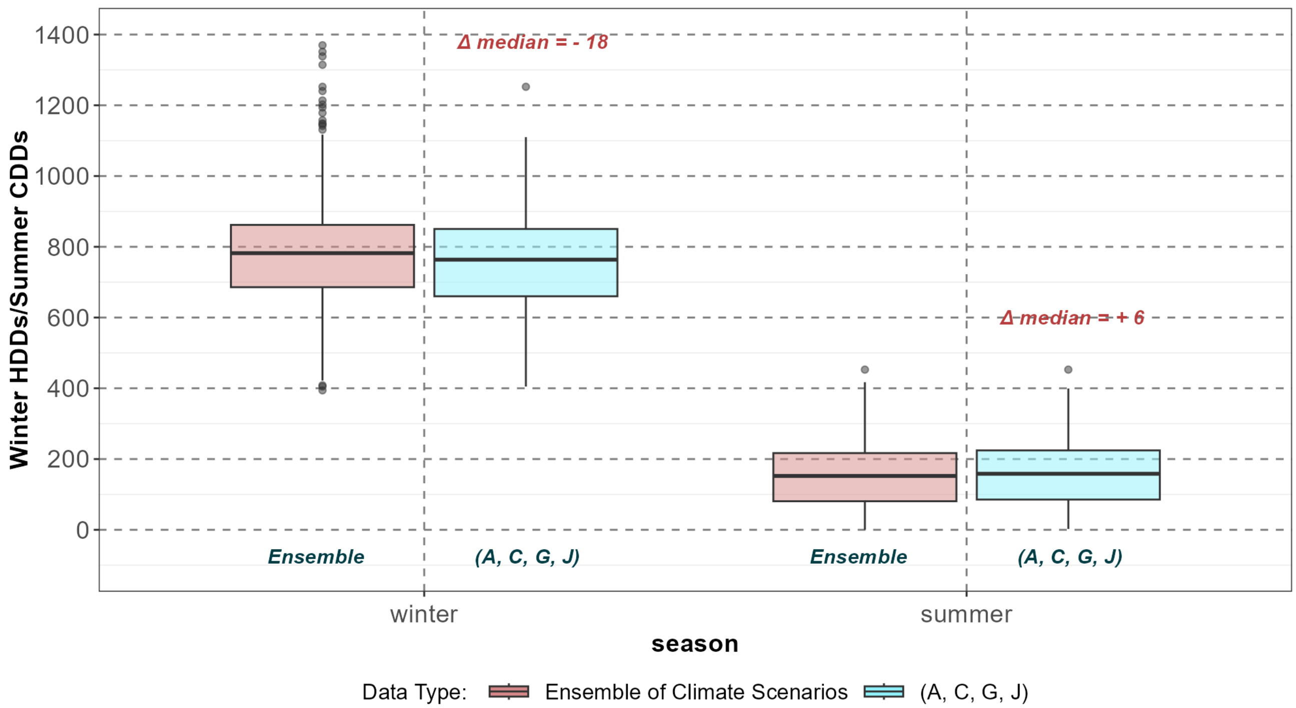

In Figure D - 6, the monthly degree-days (HDDs or CDDs) of the ensemble distribution of all 19 climate scenarios are plotted in the red boxplots while those of the distribution of the selected scenarios (A, C, G) plus scenario J are plotted in the blue boxplots. HDDs for winter and CDDs for summer are plotted on the left side and right side, respectively. Furthermore, the difference between the median degree-days of the (A, C, G, J) distribution and the ensemble distribution is listed above the blue boxplots. For winter HDDs, the blue (A, C, G, J) distribution is very close to the red ensemble distribution, with the blue median being only 18 degree-days lower than the red median. Moreover, for summer CDDs, the blue (A, C, G, J) distribution is also very close to the red ensemble distribution, where the blue median is only 6 degree-days higher than the red median.

Therefore, compared to the original selected (A, C, G) subset, the four distributions of the adding J are much closer to the corresponding distributions of the ensemble. Thus, adding J would result in a more representative of the ensemble.

Staying With the Original Three Selected Climate Scenarios

The Council considered using climate data by adding in scenario J for the Ninth Plan due to the final suite being more representative of the entire ensemble of 19 RMJOC climate scenarios. However, scenario J seems to have opposite climate trends in winter.

First, according to the RMJOC report,[31] the GFDL-ESM2M GCM, from which climate scenario J is derived, is forecasted to have higher winter temperature (throughout the region) and higher precipitation (over most of the region) in the future time period from 2020 to 2049 than in the historical time period, from 1970 to 1999. Since having higher winter temperature and precipitation over most of the region would in general lead to higher winter streamflows, then for scenario J, the future time period should have higher winter hydro-generation than the historical time period.

But as show in Figure D - 7, it is the opposite trend. The boxplots in Figure D - 7 are the winter hydro-generation of the ensemble distribution of all 19 climate scenarios (the orange boxplot) in Figure D - 5 disaggregated into its 19 component scenarios separately. The 19 scenarios are represented by the letters A to S along the x-axis. Since the hydro-generations were calculated using climate model streamflows that were adjusted using the historical irrigation depletions of 2008, then for a fair comparison, historical winter hydro-generation is also calculated using the 2010 Level historical modified flows (80 water-years from 1929 to 2008) which were adjusted with the same irrigation depletions of 2008. The historical winter hydro-generation is plotted in the gray boxplot on the right side, represented as scenario "T."

Therefore, Figure D - 7 shows that winter hydro-generation of climate scenario J, plotted in one of the three light blue boxplots inside the dashed green oval, is lower than the historical winter hydro-generation plotted in the gray boxplot for scenario "T." This is opposite to the expected higher winter generation discussed previously.

[31] See Figures 28, 29 and 35 in "*Climate and Hydrology Datasets for RMJOC Long-Term Planning Studies: Second Edition (RMJOC-II) Part I: Hydroclimate Projections and Analyses*" at https://www.bpa.gov/-/media/Aep/power/hydropower-data-studies/rmjoc-ll-report-part-l.pdf.

Figure D - 7: Winter Hydro-Generations for the 19 Climate Scenarios and Historical

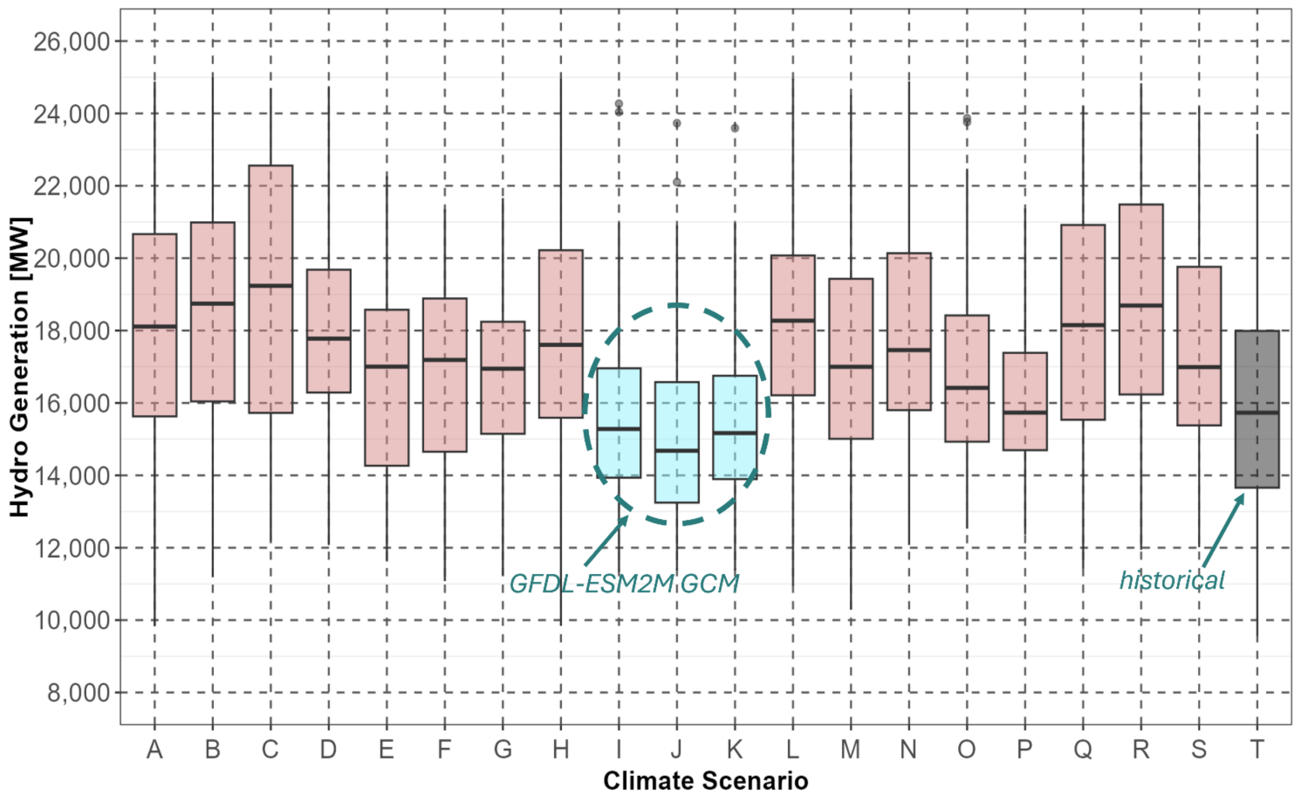

Furthermore, climate scenarios I, J and K, represented by the three light blue boxplots, are all derived from the GFDL-ESM2M GCM (see Table D - 3), and their winter hydro-generations are all below the historical winter hydro-generation in the gray boxplot.

In addition, the remaining 16 climate scenarios, A to H, and L to S (seeTable D - 3), represented by the 16 light red boxplots in Figure D - 7, are derived from eight of the remaining nine GCMs (where the HadGEM2-ES GCM in Table D - 1 has been excluded). It could be seen that winter hydro-generations of (the 16 climate scenarios derived from) these eight GCMs are higher than the historical winter hydro-generation (in the gray boxplot). This trend is consistent with their warmer winter temperature and higher winter precipitation as presented in the RMJOC report.[32]

The opposite trends of future winter hydro-generation (which was presented to the CWAC[33]) suggest that scenario J, or more generally, climate scenarios derived from the GFDL-ESM2M GCM, could be significantly underestimating historical streamflows. However, a better understanding would require

[32] See Figures 28, 29 and 35 in "*Climate and Hydrology Datasets for RMJOC Long-Term Planning Studies: Second Edition (RMJOC-II) Part I: Hydroclimate Projections and Analyses*" at https://www.bpa.gov/-/media/Aep/power/hydropower-data-studies/rmjoc-ll-report-part-l.pdf.

[33] Climate and Weather Advisory Committee meeting on 7/15/2024: https://www.nwcouncil.org/meeting/climate-and-weather-advisory-comm-kick-off-2024-07-15.

further systematic analysis by climate scientists. Therefore, even though including scenario J would make the suite more representative of the ensemble of 19 RMJOC scenarios, the Council decided it was prudent to exclude this scenario for the Ninth Plan due to its anomalous lower winter hydro-generation. Council staff proposed to stay with the original three-scenario subset (A, C, G) during meetings of the CWAC.[34] While some members of the CWAC supported including the additional scenario J to increase diversity of the climate data, ultimately there was no objection to the Council using climate data from the three-scenario subset (A, C, G).

The Climate Scenario Years Used in the Ninth Power Plan

Data in the RMJOC climate scenarios are of daily time-step and start on 1/1/1950 and end on 12/31/2099, totaling 150 years of data. For analysis, RMJOC staff chose time periods spanning 30 years. For example, the historical period is the 30-year span from 1970 to 1999, and is referred to as the 1980s for simplicity; a near-future period is the 30-year span from 2020 to 2049, and is called the 2030s; and finally, a distant future period spans the 30-years period from 2060 to 2089, called the 2070s.[35]

For modeling hydro-operations under the influence of climate scenario data, the RMJOC also used the same three sets of 30-year time-periods, the 1980s, the 2030s, and the 2070s. For those three sets of time-periods, they also developed hydro-regulation rule-curves, such a flood control, and operation constraints for the various hydro-projects in their hydro-regulation models.[36] The RMJOC shared with the Council the climate scenario data (from 1950 to 2099) and the associated hydro-regulation rule curves and constraints for the 2030s and the 2070s.

As decided by the Council, the Ninth Plan is developed for the 20-years from 2027 to 2046, which conveniently can draw upon as inputs the 150 years of climate scenario data, and the RMJOC hydro-regulation rule curves and constraints for the 2030s (from 2020 to 2049). Thus, during meetings of the CWAC, the staff proposed using climate scenario data for the 2030s set of climate scenario years and the RMJOC 2030s set of rule-curves and constraints, since they have been incorporated into various Council simulation models.[37] A few committee members expressed their preference of using a few more climate scenario years beyond 2049 to capture stronger climate trends, which the Council staff

---

[34] Climate and Weather Advisory Committee meeting on 8/1/2024: https://www.nwcouncil.org/meeting/climate-and-weather-and-conservation-resources-adv-comm-combined-meeting-2024-08-21, and on 12/4/2024: https://www.nwcouncil.org/meeting/climate-and-weather-advisory-committee-2024-12-04.

[35] *Climate and Hydrology Datasets for RMJOC Long-Term Planning Studies: Second Edition (RMJOC-II) Part I: Hydroclimate Projections and Analyses*" at https://www.bpa.gov/-/media/Aep/power/hydropower-data-studies/rmjoc-ll-report-part-l.pdf.

[36] "Climate and Hydrology Datasets for RMJOC Long-Term Planning Studies: Second Edition (RMJOC-II) Part II: Columbia River Reservoir Regulation and Operations—Modeling and Analyses" at https://www.bpa.gov/-/media/Aep/power/hydropower-data-studies/rmjoc-ll-report-part-ll.PDF.

[37] Climate and Weather Advisory Committee meetings on 7/15/2024: https://www.nwcouncil.org/meeting/climate-and-weather-advisory-comm-kick-off-2024-07-15, and on 8/1/2024: https://www.nwcouncil.org/calendar/climate-and-weather-advisory-committee-2024-08-01.

also shares. However, the hydro-regulation rule curves and operation constraints for a few years beyond 2049 are not readily available. Therefore, the Council decided to use the available data from the 2030s climate scenario years (from 2020 to 2049) only.

Another consideration for incorporating climate data into the Council's models is the sampling method for the climate scenario years for temperature, water, wind, and solar data. More specifically, because temperature and precipitation output (both sets of data are used to calculate streamflow) from the GCMs are not independent, the temperature year and water year selected for each simulation run must be the same climate year. Mixing climate scenario years for temperature and precipitation could lead to unlikely occurrences.

For a rather simplified example, at a specific location in the region, if temperatures were mostly above freezing during fall and winter for a particular climate year, then most of the precipitation during that period would fall as rain, resulting in higher streamflow but depositing a smaller snowpack in the mountains. Then during spring and early summer, streamflow would be lower due to contribution from a smaller snowpack.

Alternatively, if fall and winter temperatures were mostly below freezing, then precipitation would mostly fall as snow, resulting in lower streamflow but creating a larger snowpack. Then spring and early summer of that climate year should see higher streamflow due to contribution from the larger snowpack.

These two simple examples illustrate that even with the same amount of seasonal precipitation, temperature can have a significant influence on the timing and magnitude of streamflow. Thus, pairing temperature and streamflow patterns from two different climate scenario years could lead to unlikely situations such as having freezing temperatures during winter (from one climate year) but with winter precipitation falling as rain (from another climate year) that leads to higher streamflow and smaller snowpack.

In addition to using the same climate year for temperature and water in a simulation run, it is important to also use the same climate year for wind and solar data. The reason for doing so is that all the climate data should represent the same weather systems simulated in a GCM. In other words, the weather systems that bring temperatures and precipitations into a region also carry along the wind and cloud cover (which influences solar radiation). Using the same climate scenario years for the four types of data enables them to be considered temporally coincident, and the impact of weather on operations of the power system can be modeled consistently.

The following sections provide a more comprehensive description of the climate model data and methods to adapt them for the Ninth Power Plan.

In-Region Climate Scenario Data

There are four types of climate scenario data used in the Power Plan: streamflow, temperature, wind generation, and solar generation. They are analyzed and presented in the following sections.

As discussed previously, the climate scenario streamflow data were produced by the RMJOC, and they are used directly (among other data) in the Council's resource adequacy model and capital expansion model, GENESYS and OptGen, respectively, to simulate operations and generations of the hydro system. The streamflow data are daily averages and located at 74 hydro-projects and gauging stations simulated in both models.[38] Since there are many years of corresponding historical streamflow data available, comparisons of historical data to climate model data will enable discovery of climate trends, if any. In addition, since hydro-generation is a major component of the regional power system, it is also of interest to analyze for very high and very low streamflows.

Similar to the climate scenario streamflow data, the climate temperature data were also produced by the RMJOC, and they are used, among other data, in the Council's load forecasting model, developed by Itron,[39] to produce loads at the 13 balancing authorities (BAs) in the region. The temperature data are daily minima and maxima and located at 26 locations throughout the region. Analogous to the historical streamflow data, there are many years of corresponding historical temperature data available and comparing them with climate temperature data will allow discovery of climate trends, if any. Moreover, since very high or very low temperatures lead to very high loads, and thus it is important to analyze frequencies and magnitudes of the extreme temperatures.

The remaining two climate scenario data, wind speed and solar radiation, are not included in the RMJOC data set. Fortunately, identical or very similar climate scenario wind and solar data are available at the Climatology Lab.[40]

Five representative locations were selected to model wind fleet generation for the region, and their corresponding climate wind speed data were downloaded from the Climatology Lab. The data are daily averages which undergo further calculations to become hourly wind generations and thus inputs in the Council's models. Some calculations include bias-corrections of the data in historical years to replicate statistical properties such as, the correlations between historical wind and historical temperature data, and the monthly distributions of historical wind data. The methodologies are discussed in detail in a following section.

Finally, three representative locations were selected to model solar generation for the region, and their corresponding climate solar radiation data are also available from the Climatology Lab. However, during a meeting of the CWAC, some climate scientists expressed concern that the original GCMs might not be able to model cloud cover (and therefore solar radiation) accurately over small geographical areas due to the coarse spatial grids used in the GCMs. Thus, alternative methods were developed to model solar generation, and details of which are presented in a subsequent section.

[38] In the Council's models, there are a few hydro-projects classified as "small or independent hydro" that do not use climate scenario streamflows. They are modeled as renewable resources with historical monthly generation shapes. On average, their aggregate generation is about 1,100 aMW.
[39] See Appendix F – Electricity Demand Forecast in the Ninth Power Plan for more details.
[40] Climatology Lab: https://www.climatologylab.org/maca.html.

Many GCMs have systematic errors or biases in their output which are differences between the output and some baseline values, for example, a set of historical observations or widely accepted output of climate and weather models. The biases are often due to coarse resolution used and simplified physical processes assumed in the GCMs. Therefore, to enable more realistic and thus more believable GCM output, they undergo bias-corrections[41,42] to align themselves more closely with historical observations or widely accepted data. For streamflow and temperature data from the RMJOC climate scenarios, climate scientists and RMJOC staff have already performed appropriate bias-corrections.[43] For climate scenario wind and solar data downloaded from other sources, they also undergo bias-corrections which are discussed in more detail in subsequent sections.

Trends in Historical and Climate Scenario Streamflows

As discussed above, the Council has decided to use data from three of the 19 climate scenarios developed by the RMJOC for the Ninth Plan analysis. In this section, analyses of both historical and climate model streamflows are presented which show the climate trends that will influence the generation portfolios developed for the Power Plan.

Trends in Historical Streamflows

The RMJOC in 2013 began the development of climate scenario data, including modified streamflows. In that process, the RMJOC used the 2010 Level Modified Streamflow data set, which are historical streamflows that would have been observed if irrigation depletions (as of year 2008) existed in the past and if the effects of river regulation were removed (except at the upper Snake, Deschutes, and Yakima basins, where current upstream reservoir regulation practices are included).[44] In this section, the historical 2010 Level Modified Streamflows (referred henceforth as “historical streamflows” for simplicity) are analyzed for possible climate trends.

The historical streamflow set consists of 80 water-years of daily streamflows from 1929 to 2008 at many sites of interest throughout the Columbia River Basin, including at all hydro projects modeled in GENESYS. By definition, a water-year begins in October and ends in September of the following year. For example, the 1987 water-year begins on October 1, 1986, and ends on September 30, 1987. For the same water-year, the annual volume and monthly pattern of streamflow measured at stream gauging stations in different sub-basins, for example, Mica and The Dalles (TDA), can be vastly different. Nevertheless, streamflow at TDA, which is located near the mouth of the Columbia River, is

---

[41] https://glisa.umich.edu/wp-content/uploads/2021/03/Global-Climate-Model-Bias-and-Bias-Correction.pdf .
[42] https://climate.copernicus.eu/sites/default/files/2021-01/infosheet7.pdf.
[43] *Climate and Hydrology Datasets for RMJOC Long-Term Planning Studies: Second Edition (RMJOC-II) Part I: Hydroclimate Projections and Analyses*” at https://www.bpa.gov/-/media/Aep/power/hydropower-data-studies/rmjoc-ll-report-part-l.pdf.
[44]See https://www.oregon.gov/owrd/WRDReports/appendix_d_flow-data-set-res-sim-analysis.pdf for more details of 2010 Level Modified Streamflows. However, in 2020, the Bonneville Power Administration published a new modified streamflow data: the *2020 Level Modified Streamflows*. See https://www.bpa.gov/-/media/Aep/power/historical-streamflow-reports/2020-level-modified-streamflow-seasonal-volumes-and-statistics.pdf.

commonly used to classify a water-year (i.e., a critical or dry year, an average year, or a wet year) for the entire Columbia River Basin.

Because the historical streamflow record spans 80 years, it is worthwhile to investigate whether they have fundamentally changed over time, that is, if trends in the volume and pattern of streamflow are observable. Thus, in Figure D - 8, TDA streamflows for the first 30 water-years, from 1929 to 1958 (plotted in gray), are compared with those for the last 30 water-years (plotted in light blue), from 1979 to 2008. With respect to 2010 Level Modified Streamflows, the 30 years from 1929 to 1958 are the first 30 years, while the 30 years from 1979 to 2008 are the last 30 years. For simplicity, in subsequent sections, streamflows for the two sets of 30 years will be referred to as “first 30 years” and “last 30 years,” respectively.

Figure D - 8: Comparison of The Dalles Daily Streamflows for Two Historical Time Periods

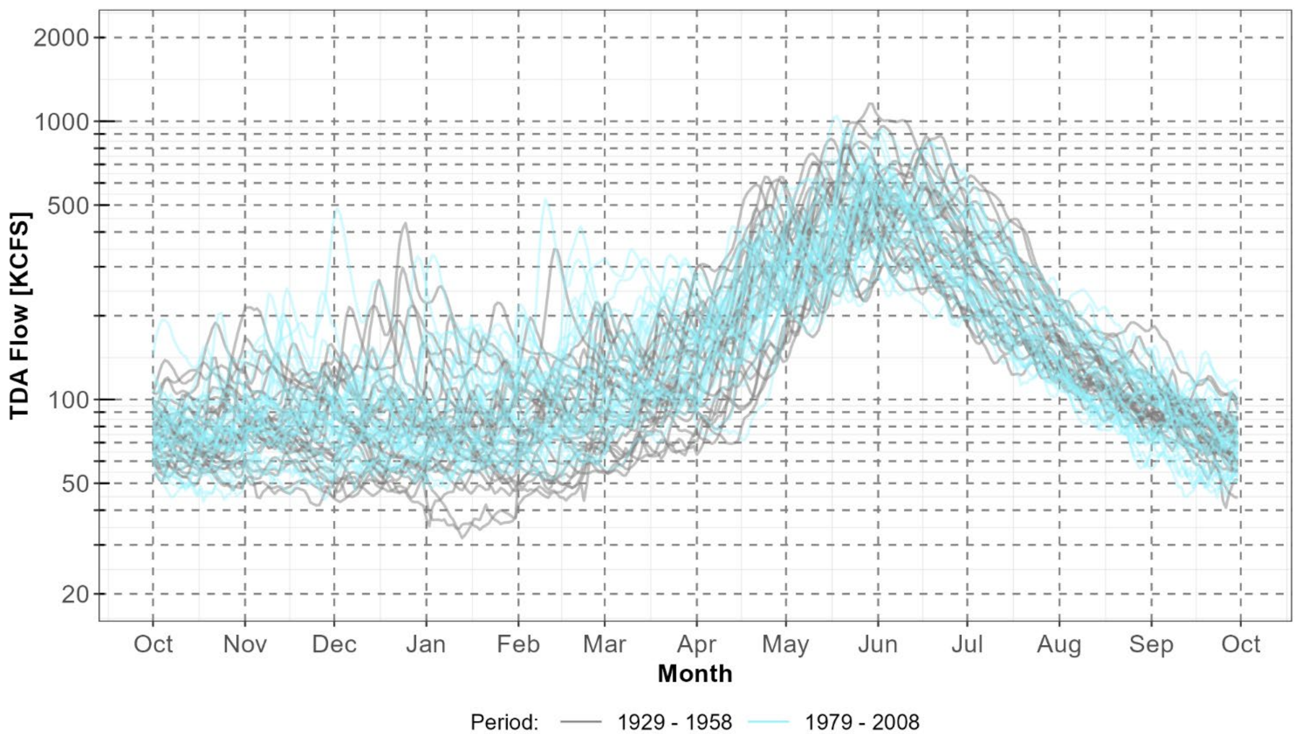

On the x-axis are the months from October to the next September for a water year. On the y-axis are the TDA flows in thousand cubic feet per second (or KCFS).[45] The plots in Figure D - 8 are called trace plots because streamflows for the 60 water-years are plotted separately in 60 traces. Furthermore, the traces are plotted in log scale so that visual comparisons are easier for streamflows with both large and small magnitudes. However, visual comparison of the 60 traces remains difficult because of the high amount of overlap. Nevertheless, the trace plots are still useful since they do allow for an

[45] The same axes are used in the following series of figures comparing different streamflows at TDA.

easy visual scan for outliers, that is, streamflows with significantly different monthly magnitudes and shapes.

The streamflow traces for the first 30 years (in gray curves) and the last 30 years (in light blue curves) look similar at a glance, except for two gray traces, representing water-years 1930 and 1937, which have very low streamflows in January. These are the lowest historical streamflows. Furthermore, there is a hint that flows for the last 30 years (in light blue curves) might be slightly higher from January to April.

In contrast, there is one gray trace representing 1948 that have very high flows, at or greater than 1,000 KCFS, from late May to early June. After 1948, there were three other years, 1972, 1974 (both not plotted due to being outside the two selected historical time periods) and 1997 where the flows were similarly very high for a few days in mid-May (plotted in a blue trace). These are the highest historical streamflows.

Beside the trace plots in Figure D - 8, two other types of plots are presented to compare TDA streamflows between the historical first 30 years and last 30 years.

First, Figure D - 9 shows the envelope plots, in which streamflows for the first 30 years are represented in the gray area while those for the last 30 years are represented in the light blue area. For each set of streamflows, the envelope data are obtained by extracting the maximum and minimum streamflow for each day over all 30 years. In addition to the envelope plots, the average daily streamflows are also plotted in Figure D - 9, the white dashed curve for the first 30 years and the dark blue dashed curve for the last 30 years.

Figure D - 9: Comparison of Maximum, Minimum, and Average TDA Daily Streamflows for Two Historical Time Periods

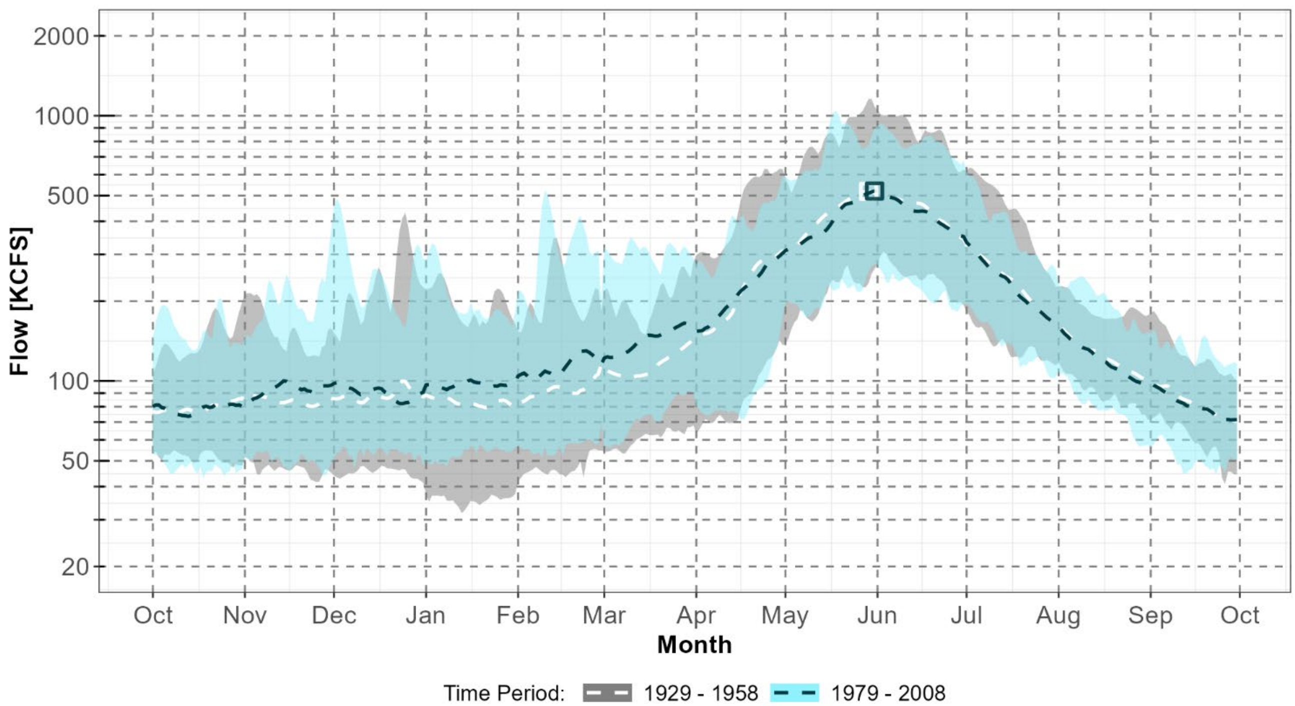

The envelope plots in Figure D - 9 show less data than the trace plots in Figure D - 8, but they allow for easier comparisons of the monthly shapes of the maxima and minima. For example, for most days from November to mid-April, streamflows for the last 30 years (in the light blue area) have higher maxima and minima than those for the first 30 years (in the gray area). Moreover, comparing the two dashed curves shows that, for most days from November to mid-April, the average streamflow is also higher for the last 30 years (in blue) than for the first 30 years (in white). For example, for January 15, the difference is 18.7 KCFS higher or +23% (relative to the average streamflow for the first 30 years).

Another interesting observation is the spring maximum of the TDA average streamflow. In Figure D - 9, the spring maxima for the averages are plotted as squares, in white for the first 30 years and in dark blue for the last 30 years. The spring maximum for the historical last 30 years occurs one day later than the maximum for the first 30 years. The difference is however too small from which to draw any conclusion about temporal shifts between the two historical periods.

In summary, between historical water-years 1929 to 1958 and 1979 to 2008, there appears to be a trend for higher flows at TDA from November to April. This trend is consistent with a portion of the climate change signal analyzed in RMJOC report I.[46] (However, the RMJOC climate trend of lower flows at TDA for the summer months is not present for the two sets of historical data. In addition, the

[46] See Figure 49 in "*Climate and Hydrology Datasets for RMJOC Long-Term Planning Studies: Second Edition (RMJOC-II) Part I: Hydroclimate Projections and Analyses*" at https://www.bpa.gov/-/media/Aep/power/hydropower-data-studies/rmjoc-ll-report-part-l.pdf.

trend of an earlier temporal shift in the spring maximum streamflow is also not evident. Therefore, analysis of Figure D - 9suggests that a portion of climate change impacts, namely the higher November through April streamflows, is already present in the historical streamflow data

Next, monthly boxplots of the same data are presented in Figure D - 10, which compares the monthly distributions of TDA daily streamflows between the historical first 30 years, from 1929 to 1958 (in gray), and the last 30 years, from 1979 to 2008 (in light blue).

Figure D - 10: Comparison of Monthly Distributions of TDA Daily Streamflows

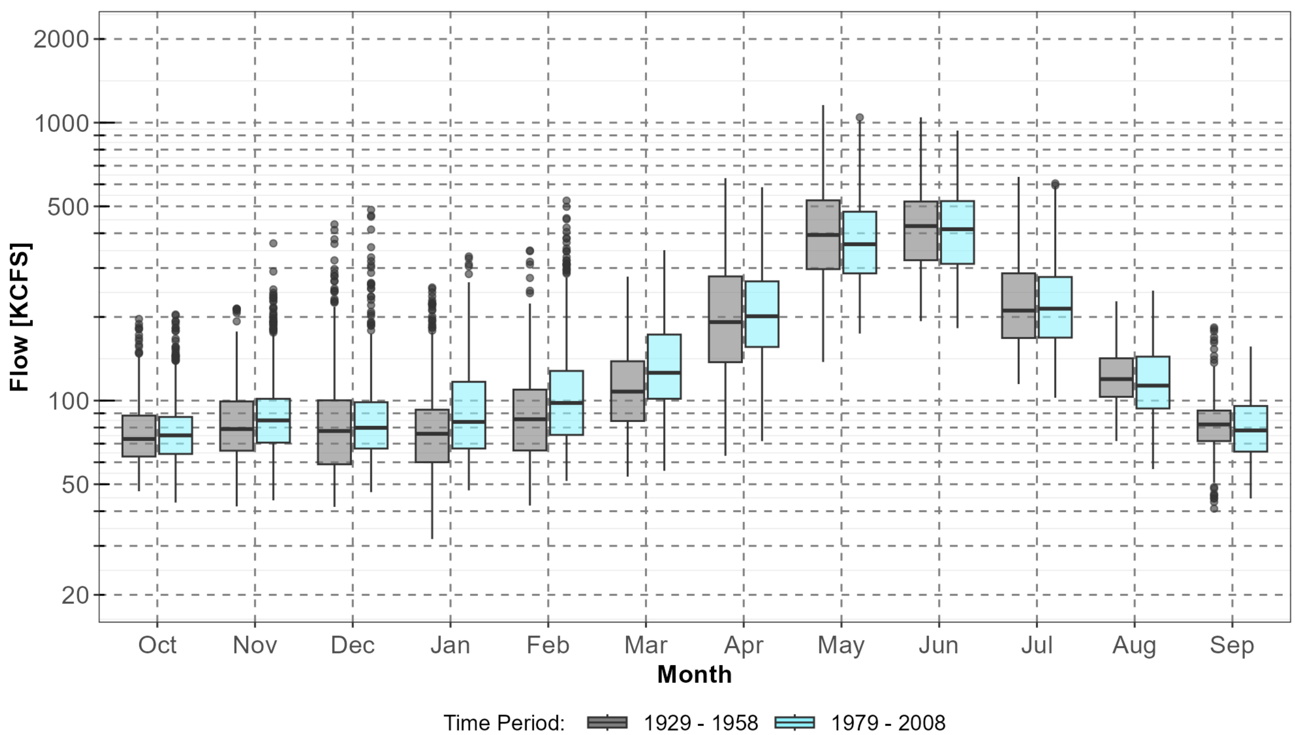

The side-by-side boxplot statistics allow for easy quantitative comparisons of the monthly distributions for the two sets of historical streamflows. However, comparisons of monthly shapes in terms of boxplots are more difficult than those comparisons in terms of envelope plots as presented in Figure D - 9.

In Figure D - 10, for November to March, most of the boxplot statistics (outliers, whiskers, median, 25th and 75th percentiles) show that streamflow is generally higher for the last 30 years. Furthermore, by comparing just the median, the higher streamflow for the last 30 years takes place over a longer period, from October to April. As for the summer months from June to August, the monthly distributions for both historical streamflow sets are similar.

Thus, the plots in Figure D - 10 support the observation in Figure D - 9 that the RMJOC projected climate-driven trend of increasing flows for October to March (or April) is present in the historical data. On the other hand, the trend of decreasing flows for summer months is not evident in the historical data.

Since the climate scenario modified flows were calculated using irrigation depletions of year 2008, then for consistency, in subsequent sections, they will be compared to the historical 2010 Level modified flows which were calculated using the same irrigation depletions of 2008.

Subsequent to the completion of the RMJOC climate scenario data in 2018, a newer historical streamflow data set became available in 2020, the 2020 Level Modified Streamflows which incorporated the effects of irrigation depletions of year 2018. For comparisons to climate scenario streamflows, using the 2010 Level Modified Streamflows is appropriate since both climate scenario and the 2010 modified streamflows have the effects of the same 2008 irrigation depletions. Nevertheless, it is still of interest to analyze for climate trends in the 2020 modified flows to compare and check for consistency with climate trends in the 2010 modified flows just analyzed in this section.

The resulting analysis of the more recent 2020 Level modified TDA flows (not shown here) also supports a similar trend of higher flows for the last 30 years (now from 1989 to 2018) for November to April. However, the 2020 Level modified flows also suggest the climate-driven trend of decreasing flows for the summer months, from June to September, which was not evident in the 2010 Level flows. Furthermore, for the 2020 Level flows, the average TDA flow for the last 30 years has a spring maximum occurring 8 days later than that for the first 30 years, in contrast to occurring just 1 day later for the 2010 Level flows as previously presented.

Trends in Climate Scenario Streamflows

For climate scenarios A, C and G, their TDA modified streamflows are also analyzed using the three types of plot: the trace, the envelope and the boxplot presented previously in Figure D - 8 to Figure D - 10, respectively. The analyses involve comparing historical streamflow for the last 30 years, from 1979 to 2008, with the three sets of climate scenario streamflows for the 30 years from 2020 to 2049. For simplicity, those 30 years from 2020 to 2049 will be referred to as the "next 30 years."[47] Similar analyses have already been done in an RMJOC report[48] for the No Regulation – No Irrigation (NRNI) streamflows, for a slightly different set of historical water-years and presented in different types of plots. Nevertheless, it is expected that climate trends for the TDA streamflow analyzed in the following sections are consistent with those presented in the RMJOC report.[48]

Climate Scenario A

In Figure D - 11, the 30 light blue traces are the historical daily TDA flows from 1979 to 2008 and the 30 light red traces are climate scenario A (CanESM2 GCM) daily TDA flows from 2020 to 2049.

[47] Referring 2020 to 2049 as the "next 30 years" was more accurate when this section was written during development of the previous 2021 Power Plan that started in 2019.

[48] *Climate and Hydrology Datasets for RMJOC Long-Term Planning Studies: Second Edition (RMJOC-II) Part I: Hydroclimate Projections and Analyses*" at https://www.bpa.gov/-/media/Aep/power/hydropower-data-studies/rmjoc-ll-report-part-l.pdf.

Figure D - 11: Comparison of Historical vs Climate Scenario A Daily Streamflows at TDA

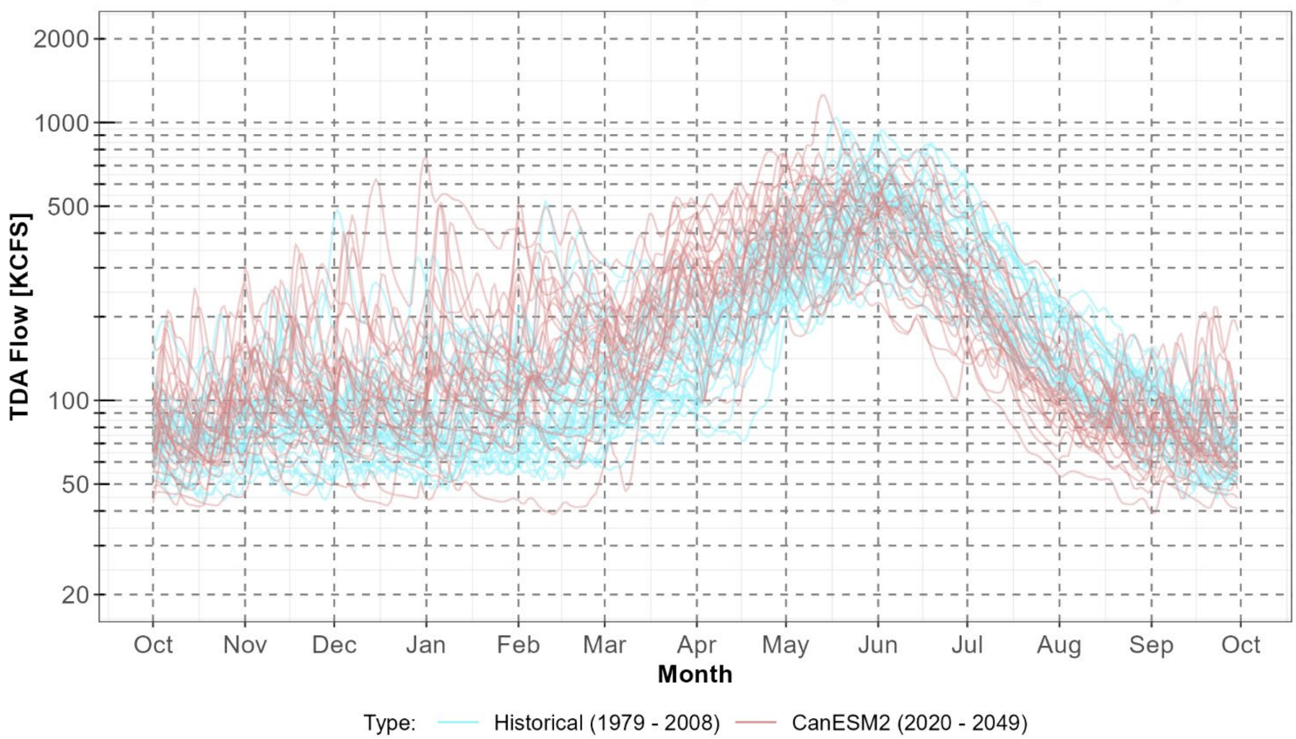

It is easy to see that as a distribution, from October to April, the 30 Scenario A climate traces are generally higher than the 30 historical traces. However, there are still one or two climate traces below the minimum historical traces for December to March. On the other hand, for the three summer months from June to August, the distribution of Scenario A traces is lower than the distribution of the historical traces. It should be noted that there are seven days in mid-May that the Scenario A climate trace representing water-year 2047 has flows at or higher than 1,000 KCFS.

Next, the envelope plots and the averages for the climate and historical traces in Figure D - 11 are presented in Figure D - 12, along with the squares indicating the spring maxima of the 30-year averages.

Figure D - 12: Comparison of Historical and Climate Scenario A Streamflows

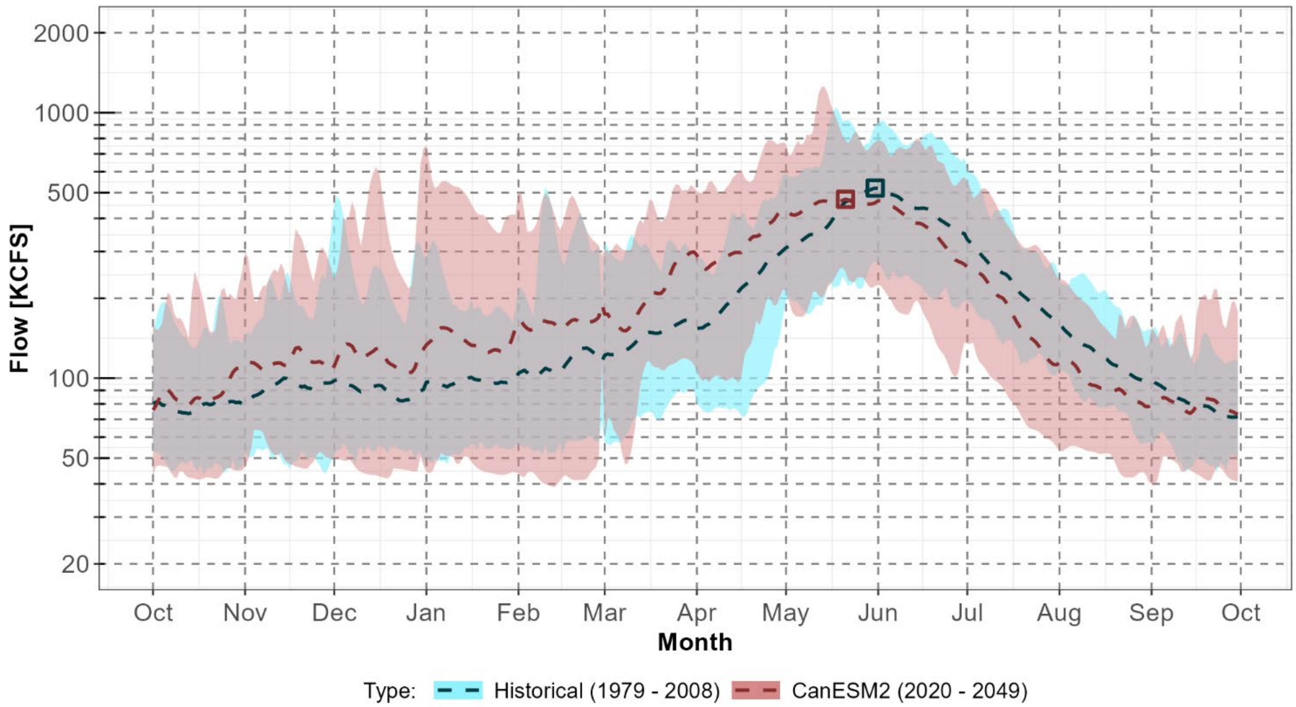

The envelope plots and averages in Figure D - 12 show that for most days from October to mid-May, the climate scenario streamflows, represented by the light red area and dark red dashed curve, are generally higher than the historical (last 30 years) flows, represented by the light-blue area and dark blue dashed curve. In contrast, for the summer months June to August, the climate scenario streamflows are generally lower than the historical flows.

Furthermore, the spring maxima of the average streamflows in Figure D - 12, plotted in the dark blue square for the historical data and dark red square for Scenario A data, show the climate Scenario A maximum occurring 10 days earlier, on May 21. It is worthwhile to analyze this shift in more details as follows. The average streamflow for scenario A in the red dashed curve has contributions from all 30 climate (light red) traces in Figure D - 11. There are 16 (among 30) climate traces where the dates of their spring maximum flows are earlier than May 21, with an average about 17 days earlier. On the other hand, there are 11 historical traces where the dates of their spring maximum flows are earlier than May 21, with an average about 7 days earlier. The earlier shift of the climate spring maximum flow is consistent with the findings in the RMJOC report.[49]

Lastly, the monthly distributions of the daily TDA streamflows for the historical last 30 years, in the light blue boxplots, and the climate scenario A next 30 years, in the light red boxplots, are presented in

[49] *Climate and Hydrology Datasets for RMJOC Long-Term Planning Studies: Second Edition (RMJOC-II) Part I: Hydroclimate Projections and Analyses*" at https://www.bpa.gov/-/media/Aep/power/hydropower-data-studies/rmjoc-ll-report-part-l.pdf.

Figure D - 13. Since the boxplots are rather compact, the monthly distributions for the historical first 30 years are also included and plotted in the gray boxplots.

Figure D - 13: Comparison of Monthly Distributions of Historical and Climate Scenario A Daily Streamflows at TDA

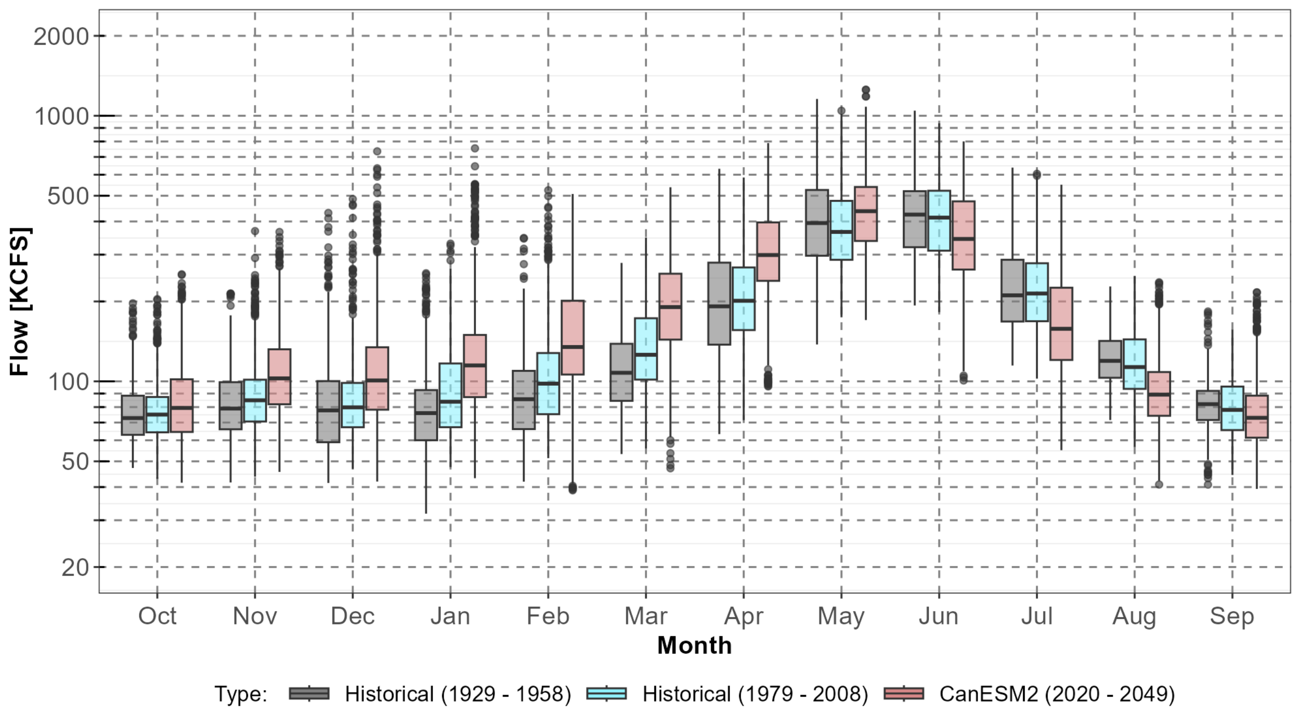

In Figure D - 13 shows a consistent climate trend of increasing flows from October to April and decreasing flows from June to September (except for July between the two historical periods) among the three distriubtions. Also, it could be seen that the differences between the red boxplots and the blue boxplots are larger than the differences between the blue boxplots and the gray boxplots. Therefore, the climate trends, from the historical first 30 years to the historical last 30 years, and from the historical last 30 years to the next 30 years, became stronger over time.

Furthermore, the time-gap between the historical first 30 years (1929 to 1958) and last 30 years (1979 to 2008) is 51 years, and the time-gap beween the historical last 30 years to the next 30 years (2020 to 2049) is 42 years. Therefore, between the the historical last 30 years to the next 30 years, the climate trends not only became stronger, but they became stronger over a shorter amount of time (42 years). This suggests that the climate trends are accelerating (i.e., the rate of change of the climate trends are increasing).

It should be noted that there are a few days in May where all three distributions of streamflows have very high flows, at or greater than 1,000 KCFS. Before and during days with these very high flows, the hydro-system would require careful regulations to avoid flooding. This topic will be discussed in more details in a subsequent section.

For numerical comparisons, Table D - 4 below lists differences between the medians of the three distributions of streamflows. This table helps to illustrate the accelerated climate trends of streamflows from October to April, and from June to September (except for July between the two historical periods).

Table D - 4: Boxplot Statistics for Figure D - 13

Month	$Median_{(last\ 30)} - Median_{(first\ 30)}$	$Median_{(Scen\ A)} - Median_{(last\ 30)}$
Oct	2.2	4.4
Nov	5.9	17.7
Dec	2.1	20.9
Jan	7.9	31.0
Feb	12.4	36.7
Mar	18.2	64.5
Apr	9.5	97.8
Jun	-10.9	-69.9
Jul	3.4	-56.4
Aug	-6.2	-24.0
Sep	-4.0	-5.2

Climate Scenario C

Next, Figure D - 14 to Figure D - 16 present the trace plots, envelope plots and boxplots, respectively, comparing TDA streamflows between the last 30 historical years and the scenario C (CCSM4 GCM) years from 2020 to 2049. Although the streamflow magnitudes, monthly shapes and monthly distributions are different between scenarios C and A, they both generally show the same climate trends relative to streamflows from the last 30 historical years, as discussed below.

In Figure D - 14, it is evident that, for the 30 climate scenario C light red traces, its distribution from November to April is higher than that of the 30 light-blue historical traces. However, there are still one or two climate traces below the minimum historical traces for March and April. In contrast, for the three summer months from June to August, the distribution of climate traces is lower than that of the historical traces.

Figure D - 14: Comparison of Historical vs Climate Scenario C Daily Streamflows at TDA

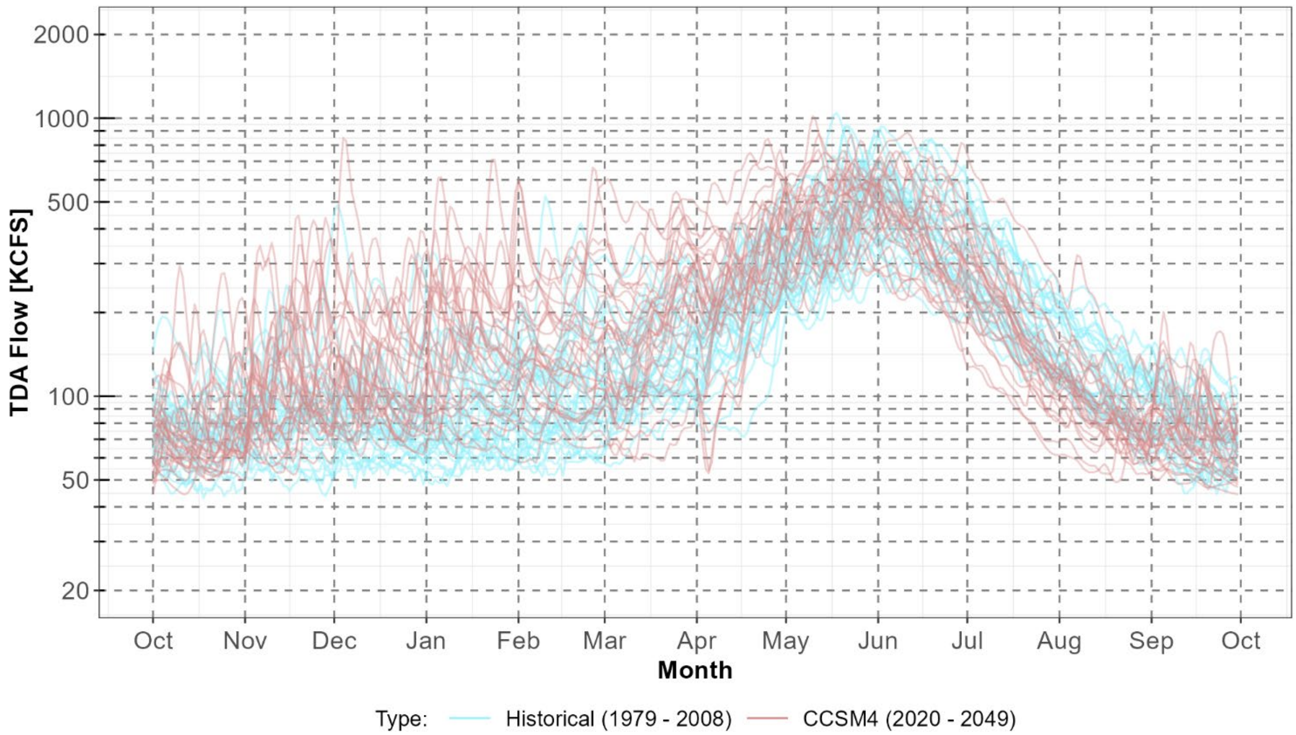

Next, Figure D - 15 presents the envelope and average (in the dashed curves) plots. They show that, from November to May, the climate scenario C streamflows, represented by the light red area and dark red dashed curve, are generally higher than the historical flows represented by the light-blue area and dark blue dashed curve. The opposite is observed for June to August, where the envelope and dashed curves show that the climate scenario C streamflow is lower than the historical streamflow. In addition, the spring maximum of the climate average, in the red square, occurs 9 days earlier than the spring maximum of the historical average, in the blue square. These observations are nearly identical to those from Figure D - 12 which compares scenario A streamflows with historical streamflows.

Figure D - 15: Comparison of Historical and Climate Scenario C Streamflows

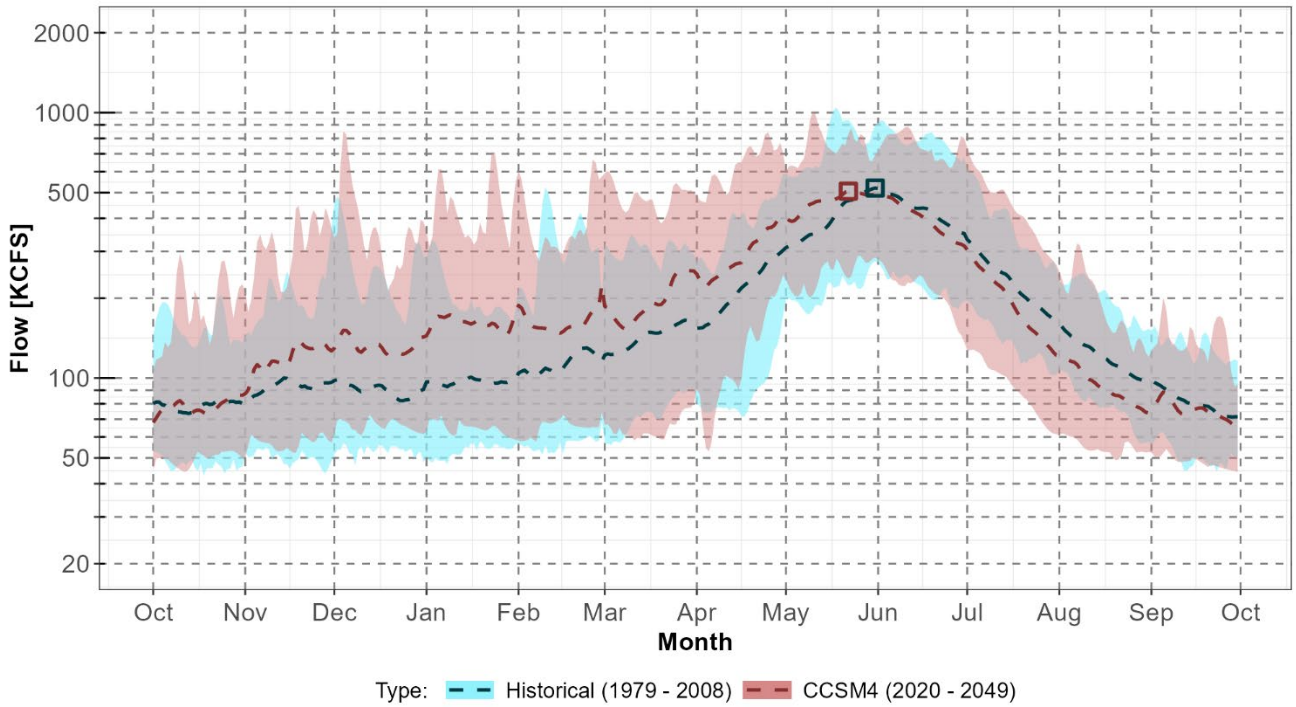

Finally, Figure D - 16 shows the monthly boxplot distributions of the daily TDA streamflows for the first 30 historical years, the last 30 historical years, and the climate scenario C years from 2020 to 2049, plotted in the gray, light blue, and light red boxplots, respectively.

Figure D - 16: Comparison of Monthly Distributions of Historical and Climate Scenario C Daily Streamflows at TDA

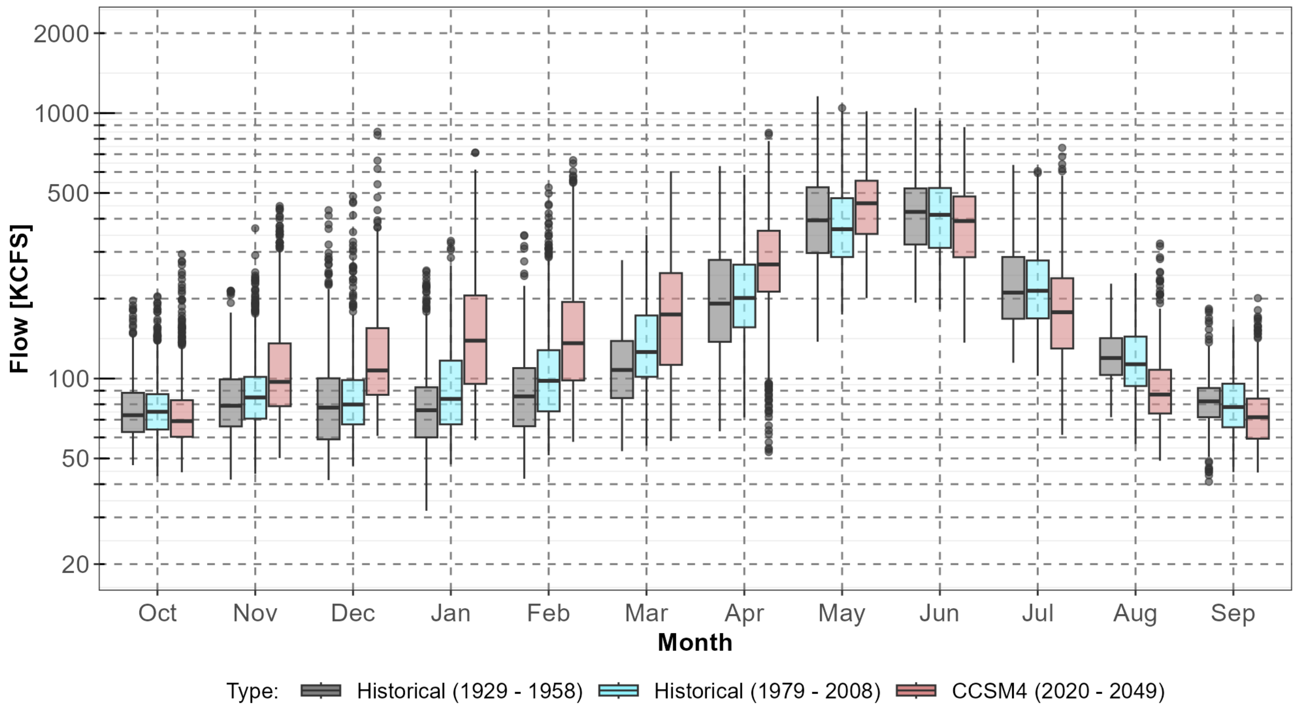

Figure D - 16 also shows the climate trends of increasing flows from November to April and decreasing flows from June to September (except for July) have accelerated between between the two historical periods and the scenario C period.

Differences of the medians among the three distributions of streamflows in Figure D - 16 are listed In Table D - 5, which support the climate trends are accelerating.

Table D - 5: Boxplot Statistics for Figure D - 16

Month	$Median_{(last\ 30)} - Median_{(first\ 30)}$	$Median_{(Scen\ C)} - Median_{(last\ 30)}$
Nov	5.9	12.3
Dec	2.1	27.4
Jan	7.9	55.0
Feb	12.4	37.8
Mar	18.2	48.4
Apr	9.5	67.9
Jun	-10.9	-21.6
Jul	3.4	-36.4
Aug	-6.3	-26.1
Sep	-4.0	-6.6

Climate Scenario G

Lastly, Figure D - 17 to Figure D - 19 present the trace plots, envelope plots and boxplots comparing TDA streamflows between the last 30 years of the historical data and the 2020 to 2049 period for scenario G (CNRM GCM).

Figure D - 17: Comparison of Historical vs Climate Scenario G Daily Streamflows at TDA

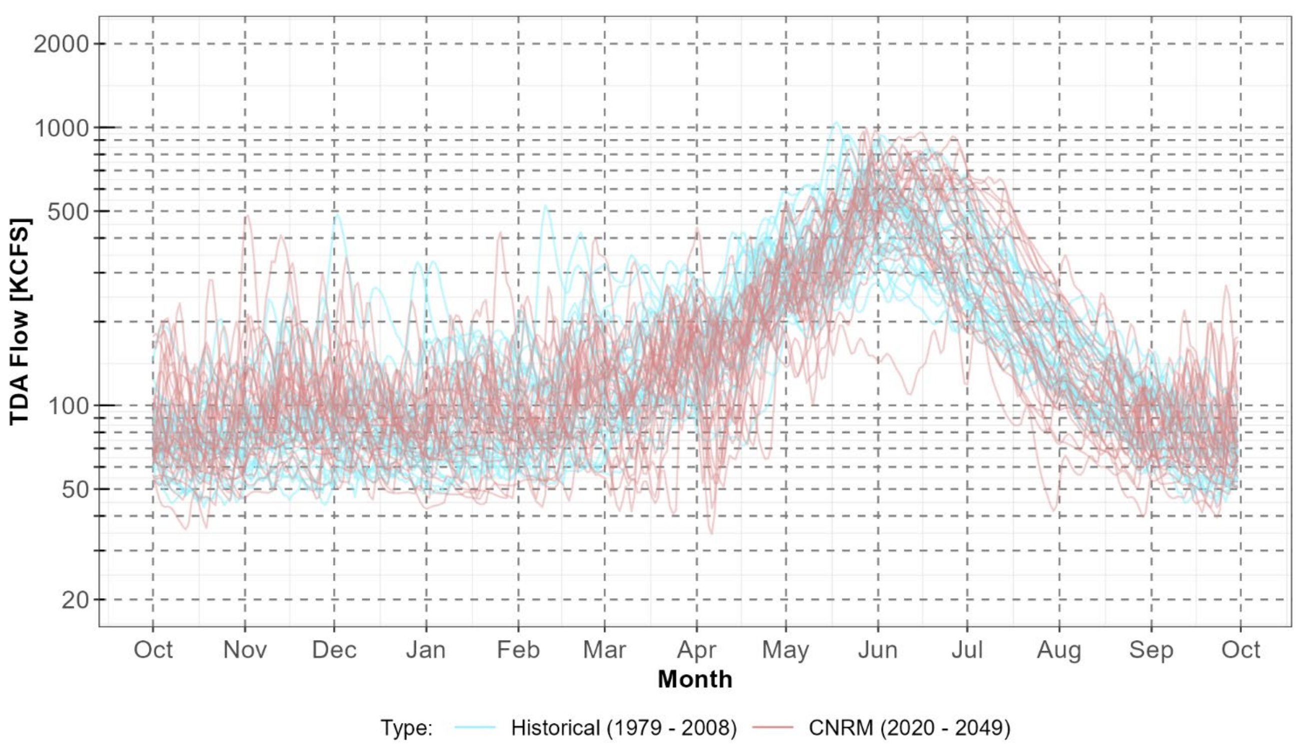

Unlike the clear trends for scenarios A and C presented in Figure D - 11 and Figure D - 14 respectively, in Figure D - 17, the 30 climate scenario G light red traces do not suggest an obvious increase in streamflow for November to April, nor any decrease for June to August. There are however a few climate scenario G traces with low flows for March and April.

Next, the envelopes and averages for the climate scenario G and historical traces are plotted in Figure D - 18, along with the squares indicating the maximum spring average flows. The historical envelope and average are in the light-blue area and dark blue dashed curve while the climate envelope and average are in the light red area and dark red dashed curve.

Figure D - 18: Comparison of Historical and Climate Scenario G Streamflows

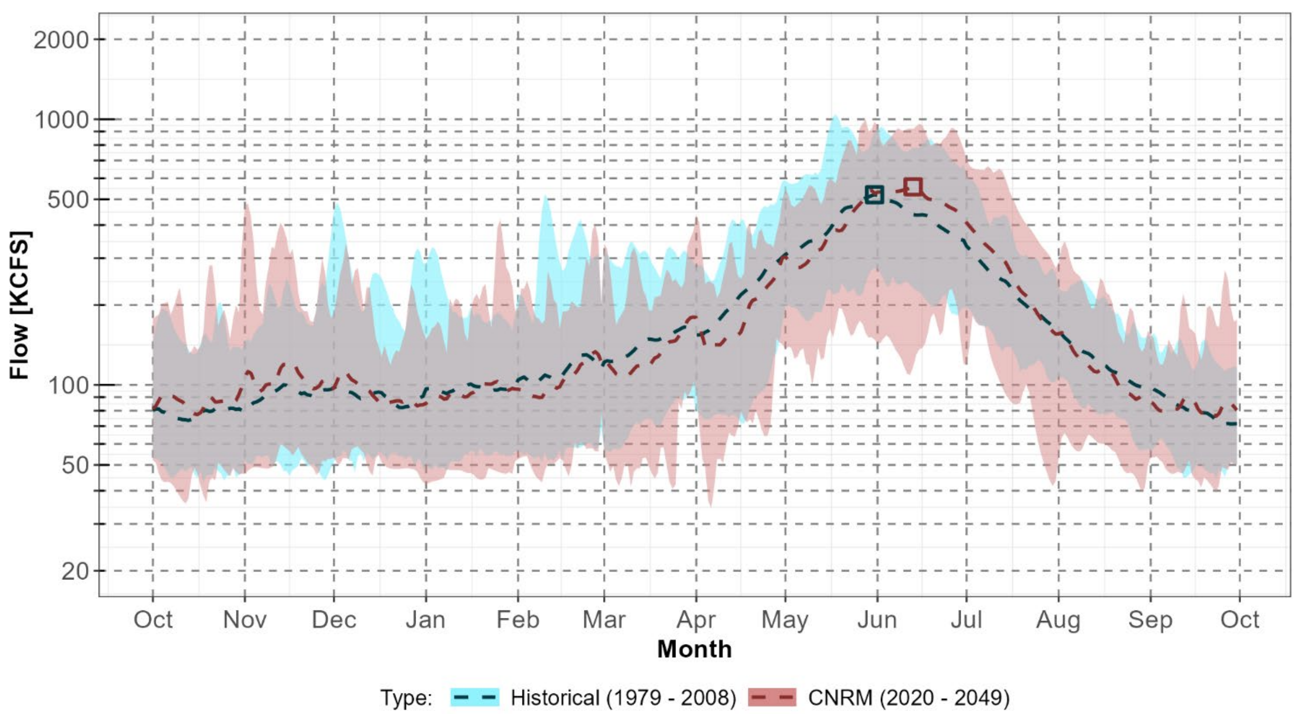

Comparisons of the envelopes and averages in Figure D - 18 show that flows are comparable between the climate scenario and the last 30 historical years for many months. The average flow for scenario G is generally slightly higher from October to December, slightly lower from January to May, but higher for June and July. Furthermore, the climate scenario maximum spring average flow occurs later (than the historical maximum spring average flow in the dark blue square) by 13 days. This is in contrast to those for scenarios A and C which occur earlier.

Thus, climate trends for scenario G are significantly different than those for scenarios A and C. The increase in average streamflow, observed from October to mid-May for climate scenario A and from November to May for climate scenario C, is not apparent in Figure D - 18 where the average streamflow for climate scenario G (in the dark red dashed curve) oscillates about the historical average (in the dark blue dashed curve). Conversely, the decrease in summer flows for June to August observed for climate scenarios A and C is actually reversed where the average for climate scenario G is higher than the historical average (for June and July).

Finally, in Figure D - 19, monthly distributions of the daily TDA streamflows for the first 30 historical years, the last 30 historical years, and the climate scenario G years are plotted in the gray, light blue, and light red boxplots, respectively.

Figure D - 19: Comparison of Monthly Distributions of Historical and Climate Scenario G Daily Streamflows at TDA

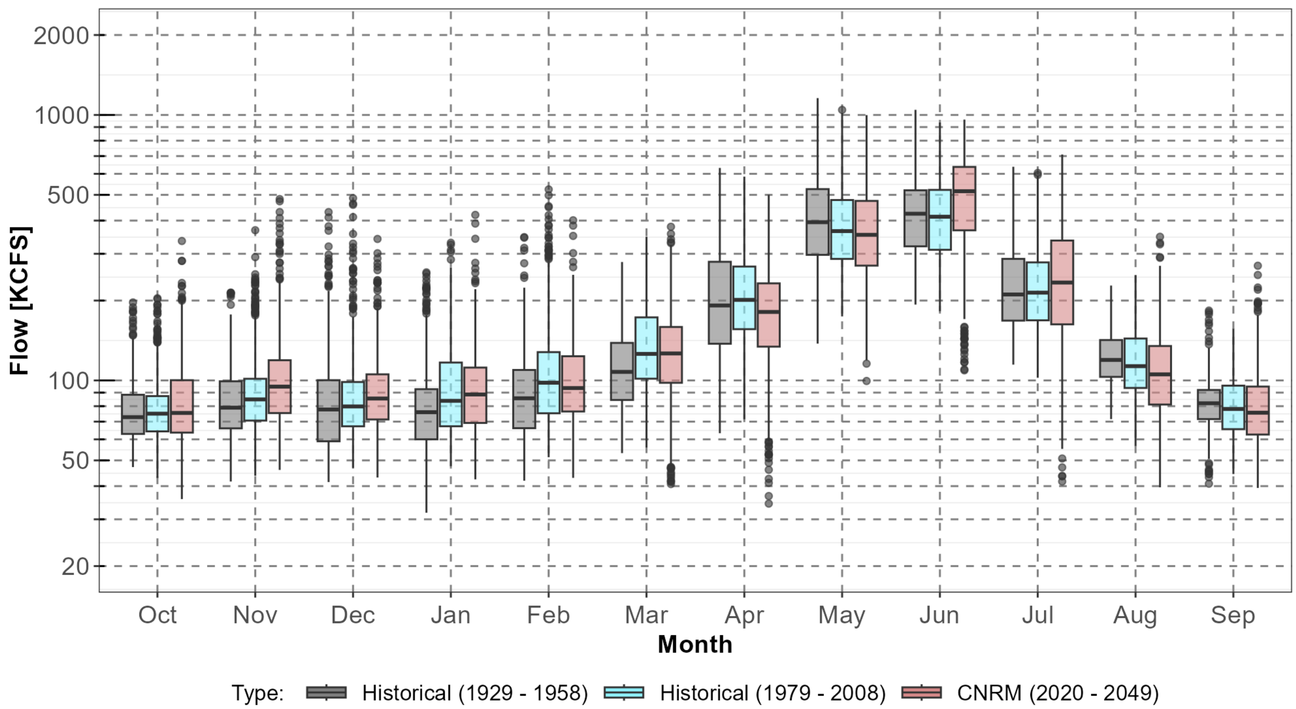

Boxplot comparisons of the monthly distributions show that streamflows for scenario G (light red boxplots) are slightly higher than the historical flows (last 30 years, in light blue) for November to January, where the median climate scenario streamflows are higher by less than 10 KCFS. However, climate scenario G streamflows are generally slightly lower than historical flows for February to May. In contrast, flows for scenarios A and C are significantly higher than historical flows over the same months. In addition, for the summer months the climate median flow is 102 KCFS (or 24.8%) higher for June, and 19.6 KCFS (or 9%) higher for July. The increasing flows in the two summer months for scenario G is opposite to the decreasing flows for scenarios A and C.

A Summary of the Three Climate Scenarios

In summary, all three climate scenarios show increasing TDA streamflows in mid-winter, from November to January, and decreasing streamflows in late summer and early fall, from August to September. In particular, climate scenarios A and C show increasing streamflows in spring, from March to May, and decreasing flows in early summer, from June to July. In contrast, for climate scenario G, streamflows decrease in spring, from March to May, and increase in early summer, from

June to July. These climate trends are consistent with findings in RMJOC report I.[50] Figure D - 20 presents boxplot comparisons of the monthly flows among the three scenarios.

Figure D - 20: Comparison of Monthly Distribution of Daily TDA Streamflows Across Climate Scenarios

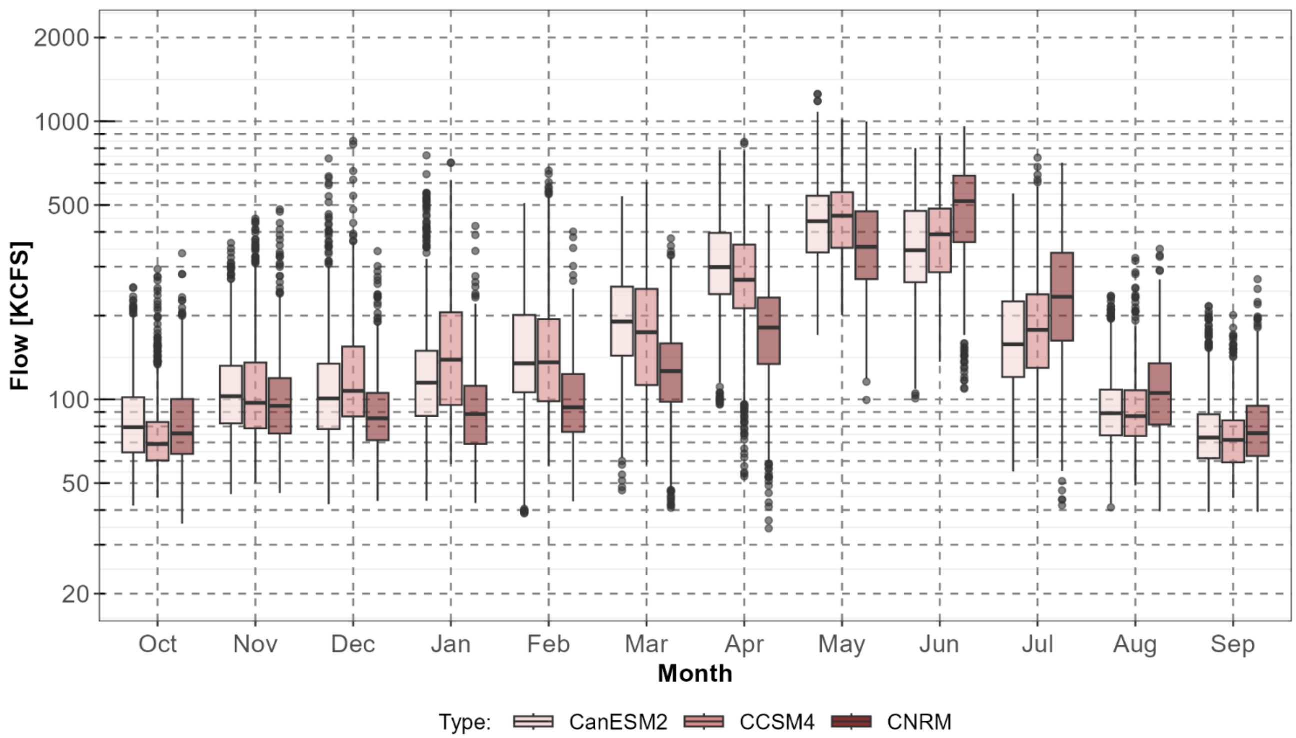

In Figure D - 20, boxplots for scenario A (CanESM2), C (CCSM4), and G (CNRM), are plotted in light pale red, light red, and dark red, respectively. Compared to the flows for scenarios A and C, the flows for scenario G are lower for December to May, and higher for June to August. Flow comparisons between scenarios A and C show scenario A having higher flows in October, March and April, and scenario C having higher flows in December and January, and May to July. For the remaining four months, scenarios A and C have comparable flows where the differences between their median flows are less than 6 KCFS.

A possible explanation for scenario G having opposite climate-driven trends in streamflows than those for scenarios A and C is as follows. The RMJOC report I[51] shows that nearly all outputs from hydrological model VIC-P3, which was used in climate scenario G, show decreasing streamflows in

[50] *Climate and Hydrology Datasets for RMJOC Long-Term Planning Studies: Second Edition (RMJOC-II) Part I: Hydroclimate Projections and Analyses*" at https://www.bpa.gov/-/media/Aep/power/hydropower-data-studies/rmjoc-ll-report-part-l.pdf.

[51] See Figures 54 to 57 in *Climate and Hydrology Datasets for RMJOC Long-Term Planning Studies: Second Edition (RMJOC-II) Part I: Hydroclimate Projections and Analyses*" at https://www.bpa.gov/-/media/Aep/power/hydropower-data-studies/rmjoc-ll-report-part-l.pdf.

spring, from March to May, and increasing streamflows in early summer, from June to July. In contrast, all scenarios that were derived using hydrological model VIC-P1, which include both scenarios A and C, have the opposite seasonal trends of increasing streamflows in spring and decreasing streamflows in early summer. This observation suggests that the opposite climate-driven trends between scenarios G and A or C are primarily due to differences in the hydrological models and not primarily due to the GCMs themselves.

Very High and Very Low Streamflows

In addition to understanding power production from hydro generation, the Council's models also seek to ensure that other requirements for the hydro system are met. This includes fish and wildlife protection, flood control, river navigation, irrigation, and recreation. Regulating the hydro system to meet its many objectives becomes very challenging during time periods with very high or very low streamflows. Therefore, it is of interest to analyze and compare the frequencies of very high and very low streamflows in the historical period and future period as forecasted in the three selected climate scenarios.

Very High Streamflows

In general, high streamflows tend to enhance the hydro-system's ability to achieve its many objectives, among them are power generation, fish and wildlife protection, river navigation, and irrigation.

However, consecutive days of very high modified streamflows over one to two weeks could lead to flooding. For example, in Figure D - 8, the gray trace with very high streamflows from late May to early June, at or greater than 1,000 KCFS, represents the 1948 modified streamflows[52] at the Dalles. These very high flows led to catastrophic flooding at Vanport, Oregon, before some big storage hydro-projects were constructed. Besides 1948, there are three more water-years, 1972, 1974, and 1997, where modified streamflows in May or June also met or exceeded 1,000 KCFS.

With all the storage projects currently available, some hydro-regulation planning studies for these four water-years show that monthly averaged regulated[53] outflows at the Dalles in May or June are between 460 KCFS and 590 KCFS. Even with these lower outflows at the Dalles, the US Army Corps

[52] Since the Council's models use modified streamflows as inputs, therefore, all the TDA streamflows analyzed in this appendix have been modified streamflows. For consistency, analyses of very high and very low TDA streamflows will also be in terms of the modified streamflows. Other organizations also analyze a different type of streamflow, the No-Regulation-No-Irrigation (NRNI) flow.

[53] For example, at BPA, the model used for some long-term hydro-regulation studies uses monthly average modified streamflows as inputs, and the model outputs monthly averaged regulated outflows. Regulated outflow at a reservoir results from the modified flow (which is an inflow into the reservoir) under the influence of operations of the reservoir (i.e., the reservoir storing or discharging various volumes of water) and all upstream reservoirs.

of Engineers nevertheless determined that flooding begins when outflows reach 450 KCFS and flooding becomes significant for outflows reaching 600 KCFS.[54]

In comparison, among the 90 climate water-years from the three climate scenarios, there are just two water-years, 2047 of climate scenarion A (for seven consecutive days) and 2048 of climate scenario C (for one day), where the TDA modified streamflows exceed 1,000 KCFS in mid-May.

Figure D - 21 presents a jitter plot comparing historical and climate scenarios where TDA streamflows have consecutive days with magnitude greater than 1,000 KCFS. The x-axis are the water years, and on the y-axis are the consecutive daily TDA modified flows in KCFS. Historical water years are in green and water years from the climate scenarios are in light red.

Figure D - 21: Comparison of Historical and Climate Scenarios with Very High Streamflows at TDA

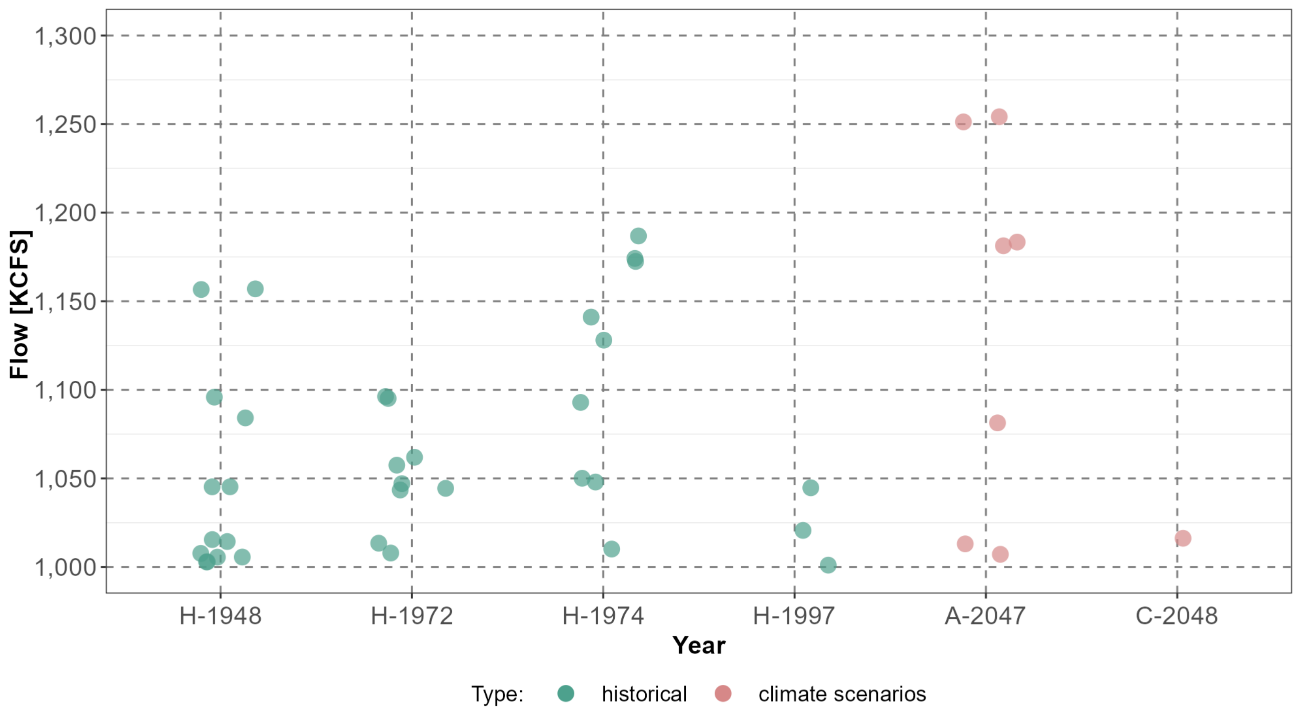

Figure D - 21 shows that for very high TDA daily modified flows, there were three historical water-years, 1948, 1972, and 1974, (ignoring the short three days in 1997). For those three years, there were between 9 to 13 consecutive days with flows greater than 1,000 KCFS. On the other hand, there is just one forecasted climate scenario water-year, 2047 in scenario A (ignoring the one day in climate

[54] *White Paper on COLUMBIA RIVER POST-2024, FLOOD RISK MANAGEMENT PROCEDURE*, U.S. Army Corps of Engineers, Northwestern Division, September 2011.

scenario year 2048 in scenario C). For year 2047 in scenario A, there are seven consecutive days with very high flows, and two of them have even higher flows than the highest historical flow.

Since the number of historical water-years, 80 (from the 2010 Level Modified Flow data set), is slightly smaller than 90, which is the number of climate scenario water-years, it could be concluded that there are fewer climate scenario water-years with many consecutive days of very high flows. This is likely due to smaller snowpacks whose runoffs contriubte significantly to streamflows in May in most climate scenario years.

Very Low Streamflows

On the other hand, very low modified streamflows for couple of weeks in a month might still allow planners to operate the hydro-system to meet its objectives if there is enough streamflow volume in the previous month or the subsequent month. However, very low streamflows over a few months or longer would degrade the hydro-system’s ability to meet many of its objectives.

Although there is no standard definition of very low streamflows, several historical water-years with very low annual or seasonal streamflow volumes had been used in various planning studies. For example, in the Columbia River Treaty,[55] the four consecutive critical water-years from 1929 to 1932 were used for planning treaty hydro-project operations for water years with very low streamflow volumes. In addition, in previous Bonneville Power Administration’s Rate Case studies,[56] the critical water-year 1937 had been used to calculate the Firm Energy Load Carrying Capability (FELCC) of the (mainly hydro) power system. Aside from the planning studies, the historical 2001 water-year had very low annual and seasonal streamflow volumes that along with other factors contributed to the 2001 West Coast Energy Crisis.[57] Thus, the lowest annual and seasonal modified streamflow volumes at TDA for many of these historical water-years and other relevant water-years are presented in the following figures.

First, in Figure D - 22, the lowest TDA annual streamflow volumes are plotted for historical (in green) and climate scenario (in light red) water-years. For example, the historical water-year 1944 is designated as H-1944 on the x-axis, and water-year 2030 for climate scenario A is designated as A-2030 on the x-axis. The y-axis in this figure is the annual streamflow volume in million acre-feet (MAF).

---

[55] See https://share.google/SyoNsNh0gxCBwFf2J.
[56] See https://www.bpa.gov/-/media/Aep/rates-tariff/historic-rate-cases/bp-14/final-proposal/FINAL-BP-14-FS-BPA-03A-Power-Loads-and-Resources-Study-Documentation.pdf.
[57] See https://www.nwcouncil.org/reports/columbia-river-history/energycrisis.

Figure D - 22: Comparison of the Lowest Annual Streamflow Volumes at TDA

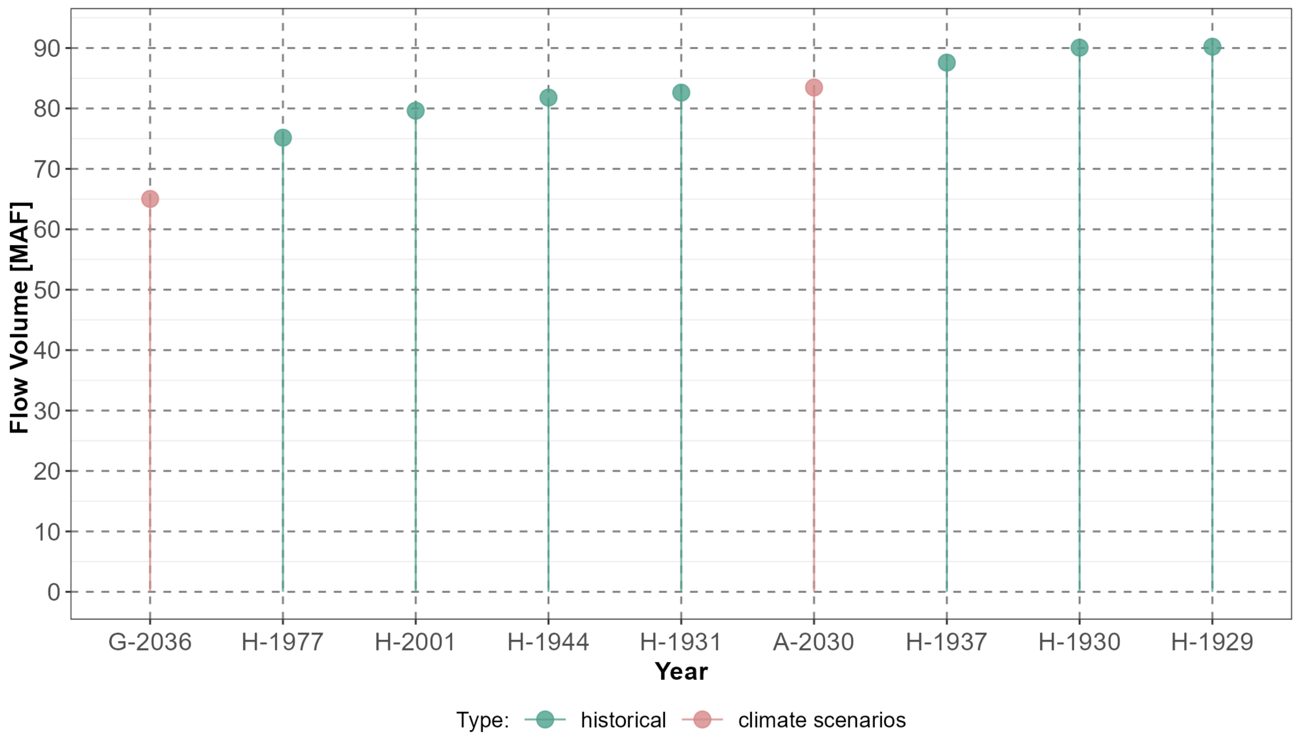

The lowest annual streamflow volumes are plotted in ascending order, where the lowest is the 65.0 MAF for climate water-year 2036 of scenario G. The next lowest volume is 75.2 MAF for the 1977 historical water-year. For convenience, only water-years with volume less than 91 MAF are plotted which include historical critical water-years from 1929 to 1931 and 2001.

Among these lowest annual volumes, there are seven historical water-years and only two climate water years, 2036 of scenario G and 2030 for scenario A. As presented previously, there are slightly fewer historical years (80) than climate scenario years (90), and thus it could be concluded that there are fewer climate water-years with very low annual volumes.

Operating the hydro-system to meet its many objectives is very challenging for these water-years with very low annual volumes. It is also useful to analyze streamflow volumes of seasonal subsets (of a water-year) that are likely to have high loads to further narrow the months during which the hydro-system is under stress to generate power and still meet its other objectives.

The October to February time period covers the beginning of a water-year through the winter months, and its streamflow volume is a significant portion of water available to plan operations of the hydro-system to meet high winter loads and other objectives. Therefore, in Figure D - 23, the lowest TDA October to February seasonal volumes are plotted for historical and climate water-years in ascending order, where the lowest is the 14.4 MAF for the historical year 1937. The next lowest volume is 15.6 MAF for climate water-year 2025 of scenario A. For convenience, only years with volumes less than 18.5 MAF are plotted, which include historical critical water-years from 1929 to 1932.

Figure D - 23: Comparison of Lowest October to February Streamflow Volumes at TDA

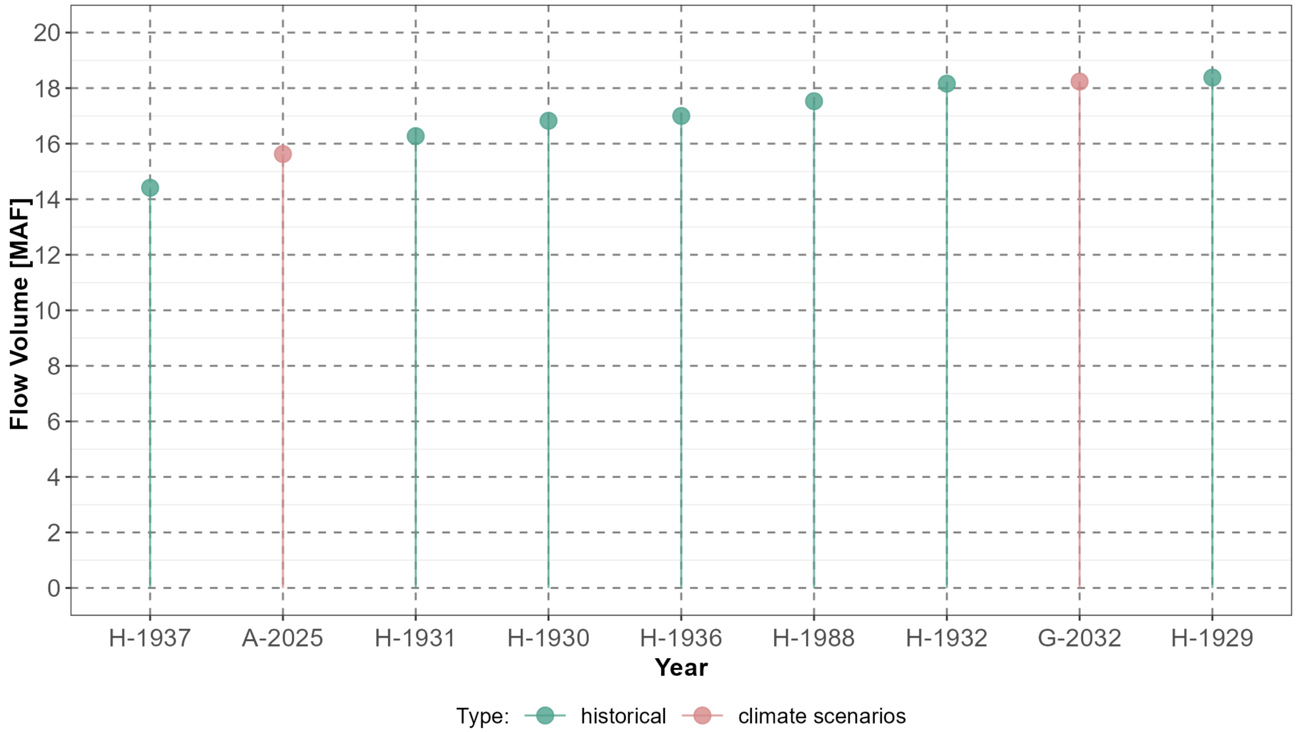

Among these lowest October to February volumes, there are seven historical water-years (in green) and only two climate scenario water years (in light red): 2025 of scenario A and 2032 of scenario G. The lowest volume is 14.4 MAF for historical year 1937 and the next lowest is 15.6 MAF for climate water-year 2025 of scenario A. Since there are slightly fewer historical years (80) than climate scenario years (90), it could be concluded that there are fewer climate water-years with very low October to February volumes.

Finally, the April to September time period covers the usual beginning of snowpack runoff through the summer months, and its streamflow volume is a major portion of water available to plan operations of the hydro-system to meet high summer loads and other objectives. Therefore, in Figure D - 24, the lowest TDA April to September seasonal volumes are plotted for historical (in green) and climate water-years (in light red) in ascending order, where the two lowest are 40.6 MAF and 45.5 MAF for climate water-years 2036 of scenario G and 2030 of scenario A, respectively. The next two lowest are 51.5 MAF and 55.3 MAF for historical years 1977 and 2001, respectively. Only years with volumes less than 69 MAF are plotted, which include historical critical water-years from 1929 to 1931 and 2001.

Figure D - 24: Comparison of Lowest April to September Streamflow Volumes at TDA

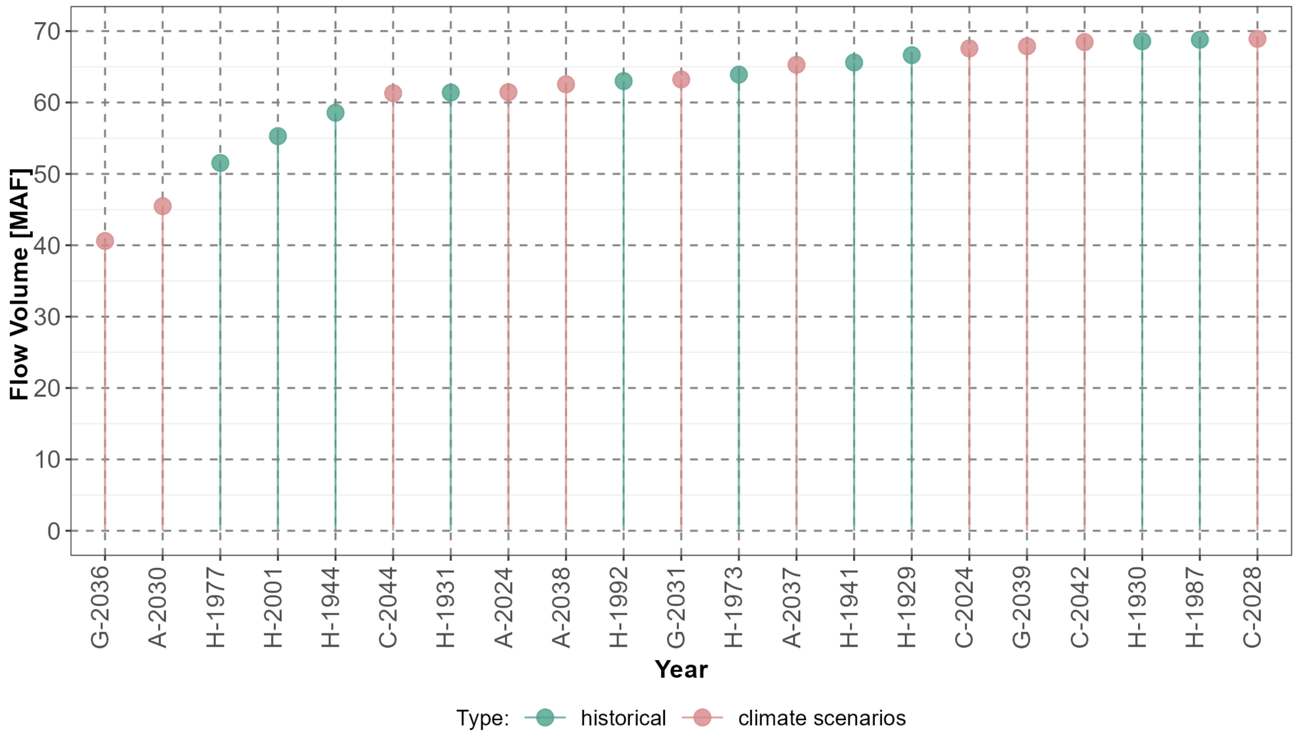

Among these lowest April to September volumes, there are 10 historical water-years and 11 climate water years. Since there are slightly fewer historical years (80) than climate scenario years (90), it could be concluded that there are about the same number of historical and climate water-years with very low April to September volumes.

Trends in Historical and Climate Scenario Temperatures

For the Ninth Plan, the Council has decided to also use temperature data, along with streamflow data, from three of the 19 climate scenarios developed by the RMJOC. The RMJOC temperature data are inputs in the Council's simulation models to forecast loads. They are also used to develop climate scenario wind and solar generations, the details of which are presented in subsequent sections.

For forecasting loads, the Council's simulation model, developed by Itron, produces load forecasts for the 13 regional balancing authorities (BAs).[58] Various combinations of temperatures at 26 locations in the region are used as inputs for the 13 BAs, and plotted in Figure D - 25 below.

[58] See Technical Appendix F - Electricity Demand Forecast in the Ninth Power Plan for more details.

Figure D - 25: RMJOC Temperature Locations

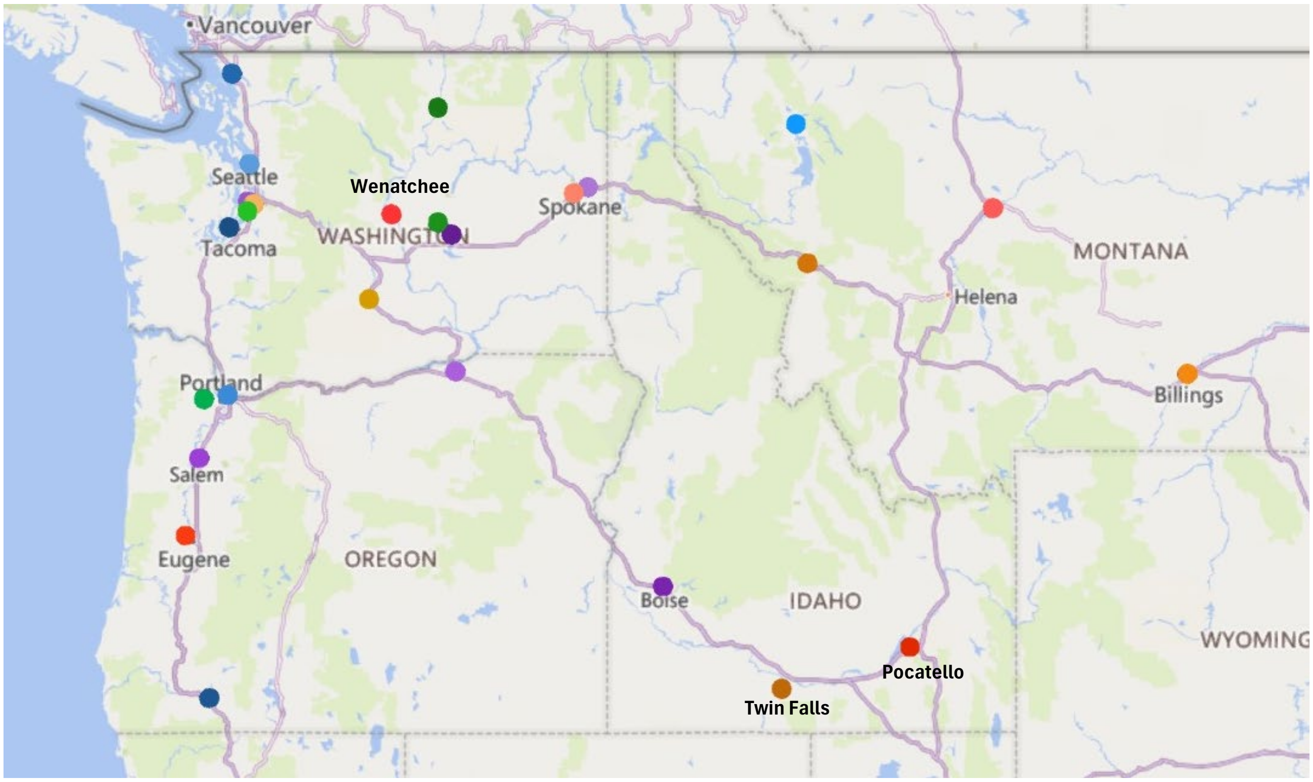

For example, the temperatures of three cities in Idaho are used as inputs for the Idaho Power BA: Pocatello, Twin Falls, and Boise. On the other hand, only one temperature in central Washington is used for the Chelan Public Utility District BA: Wenatchee.

Climate Trends

Since it is not practical to analyze trends in historical or climate temperatures for all 26 locations, only those at the four largest metropolitan areas, in terms of population, are selected for analysis: Boise, Portland, Seattle, and Spokane. Furthermore, the four cities are spread sufficiently far enough from each other that they capture some of the different climate characteristics of the region.

The warming trend of historical temperatures is well known[59] and the forecast of higher warming in the future is also well documented.[60] In this section, warming trends of historical and climate scenario temperatures at the four metropolitan areas are analyzed in detail.

Since the RMJOC climate scenario temperature data are daily minimum and daily maximum temperatures at the airports of the four cities, then historical temperatures at the four airports are

[59] See https://www.climate.gov/news-features/understanding-climate/climate-change-global-temperature
[60] See https://cig.uw.edu/learn/climate-change.

downloaded from the NOAA website[61] for analysis. For simplicity, the airports are abbreviated as follows: BOI for Boise, GEG for Spokane, PDX for Portland, and SEA for Seattle. Although historical data at the four airports are available with different starting dates, nevertheless, they are all available starting on 1/1/1948. Thus, the historical data are 77 years of daily minimum and daily maximum temperatures from 1/1/1948 to 12/31/2024. In contrast, the daily climate scenario temperature data are the 30 years from 1/1/2020 to 12/31/2049 as used in the Power Plan

Before presenting the temperature analyses, it should be noted that the RMJOC climate scenario temperatures used in the Ninth Plan and in this section have been adjusted. The reason is that some climate scientists from the CWAC, based on their research, felt that some climate scenario temperatures at Seattle and Portland are unrealistically low. Specifically, the lowest daily minimum temperature around -4 F at SEA and -15 F at PDX from climate scenario G are too low. Some of the climate scientists believe that the original grid size of scenario G, about 1 to 2 degrees longitude and latitude, is too large to accurately model the Rocky Mountain range, and thus not able to prevent very cold temperatures from the interior east moving to the coastal west region.[62] As a solution, they suggested that these unrealistically low temperatures be substituted with the corresponding lowest historical observed temperatures, which are listed in Table D - 6.

Table D - 6: The Lowest Historical Temperatures in [F] at the Four Airports

BOI	GEG	PDX	SEA
-25	-25	-3	0

There are nine days out of the 90 climate scenario years where some of the climate temperatures at the four airports are below their corresponding historical lowest temperatures in Table D - 6 above: two days at BOI (-27, -29); three days at GEG (-27, -32, -34); one day at PDX (-15); and three days at SEA (-1, -1 and -4).

Even though climate scientists from the CWAC suggested changing only the two specific airports, at SEA and PDX, for consistency of analysis in this section, all climate scenario temperatures from those nine days at the four airports that are below their corresponding lowest historical temperatures listed in Table D - 6 are substituted with their corresponding historical temperatures.

Similarly, for consistency as inputs into the load forecast model, climate scenario temperatures at all 26 locations are also adjusted so that if their daily minimum temperatures are below their corresponding lowest historical temperatures, they are then substituted with the corresponding lowest historical temperatures.

[61] https://www.ncei.noaa.gov/cdo-web/search.
[62] Climate and Weather Advisory Meeting on 12/4/2024: https://www.nwcouncil.org/meeting/climate-and-weather-advisory-committee-2024-12-04.

Overall Trends

There are 77 years of historical temperature data, from 1948 to 2024, and as used in the Power Plan, 30 years of forecasted temperature data, from 2020 to 2049, from each of the three climate scenarios. To analyze the warming trends in a systematic way, three sets of temperature data, each consisting of 30-years of temperatures, are used. The data sets are as follows: the *first historical 30-years*, designated as H_1 which begins in 1948 and ends in 1977; the *next historical 30-years*, designated as H_2, which begins in 1984 and ends in 2013; and finally, the *climate scenario 30-years* which begins in 2020 and ends in 2049, for each of the three climate scenarios. The years in H_1, H_2, and the climate scenario 30-years, are selected such that there is an equal gap of 37 years for warming trend to evolve between the sets. Specifically, there are 37 years between the first year of H_1 (1948) and the first year of H_2 (1984), and between the first year of H_2 (1984) and the first year of the climate scenario years (2020). Having an equal time gap between $H_1$and H_2, and between H_2 and the climate scenario years, allows an equal amount of time for the warming temperatures to develop between between the three time periods, and comparison of changes in temperatures among the three time periods would be fair.

Therefore, if the increase in temperature between $H_1$and H_2 is less than that between H_2 and the climate scenario 30-years, then it could be concluded that the warming trend has increased over time. On the other hand, if the increase in temperature between $H_1$and H_2 is greater than that between H_2 and the climate scenario 30-years, then the warming trend has decreased over time. These conclusions are possible due to the equal time gap of 37 years among the three time periods.

Boxplots of the distributions of the daily maximum and daily minimum temperatures of the two historical sets H_1 and H_2, and climate scenarios A, C, and G, at the four cities are plotted in Figure D - 26.

Figure D - 26: Distributions of Daily Maximum and Minimum Temperature at the Four Cities

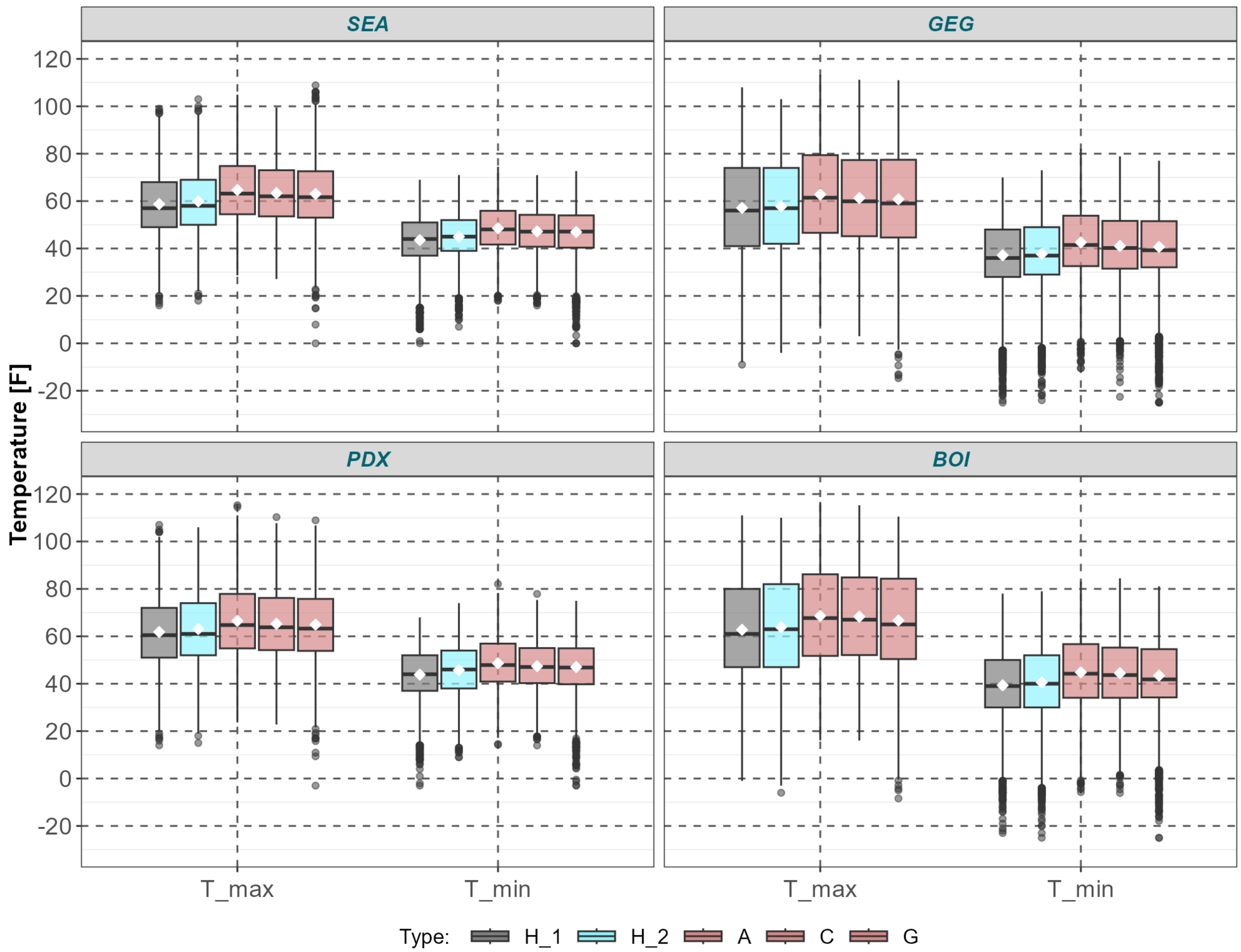

In Figure D - 26, the distributions of daily temperatures at the four cities are plotted in four separate panels arranged in their relative geographical locations: SEA at top left; GEG at the top right; PDX at the bottom left; and BOI at the bottom right. Furthermore, in each panel, the daily maximum temperatures are on the left while the daily minimum temperatures are on the right. In addition, the historical and climate temperatures are plotted in different color boxplots: gray for H_1, light blue for H_2, and light red for the three climate scenarios. Specifically, the left red boxplot represents A, the middle red boxplot represents represents C, and the right red boxplot represents G. Finally, the white diamond inside each boxplot represents the average of the distribution.

It could be seen that (except for the daily minimum temperatures at PDX) both the daily maximum and minimum temperature distributions for H_2 have *not increased significantly* from those for H_1. On the other hand, both the daily maximum and minimum temperature distributions of all three climate scenarios are *higher* than those for H_2. Since the gap between H_1 and H_2, and between H_2 and the climate scenario years are the same at 37 years, then the warming trends have increased over time (except for the daily minimum temperatures at PDX). Furthermore, among the three climate scenarios, A has the highest warming and G has the lowest warming. In addition, the variances of the daily minimum temperatures are less than the corresponding variances of the daily maximum temperatures.

To quantify the warming trends of the daily maximum temperatures T_{max}, differences of the averages of the five distributions (the white diamonds inside the boxplots) are tabulated in Table D - 7 for the four cities.

Table D - 7: Differences of the Averages of the Daily Maximum Temperature Distributions in [F]

T_{max}	H_2 vs H_1	A vs H_2	C vs H_2	G vs H_2
BOI	+ 1.1	+ 4.8	+ 4.4	+ 2.8
GEG	+ 0.6	+ 5.0	+ 3.5	+ 3.0
PDX	+ 1.2	+ 3.4	+ 2.2	+ 1.9
SEA	+ 1.2	+ 4.8	+ 3.4	+ 3.1

Similarly, for the daily minimum temperatures T_{min}, differences of the averages of the five distributions are tabulated in Table D - 8 for the four cities.

Table D - 8: Differences of the Averages of the Daily Minimum Temperature Distributions in [F]

T_{min}	H_2 vs H_1	A vs H_2	C vs H_2	G vs H_2
BOI	+ 1.2	+ 4.2	+ 3.9	+ 2.9
GEG	+ 0.6	+ 4.9	+ 3.4	+ 3.0
PDX	+ 1.9	+ 2.9	+ 1.7	+ 1.3
SEA	+ 1.5	+ 3.5	+ 2.2	+ 1.9

Both Table D - 7 and Table D - 8 support the following qualitative climate trends in Figure D - 26:

- The distributions of both daily maximum and daily minimum temperatures for H_2 are only slightly higher that those for H_1 (except for the daily minimum temperatures at PDX).
- The distributions of daily maximum and daily minimum temperatures for the three climate scenarios are higher than those for H_2.
- The warmings of the three climate scenario temperatures relative to H_2 are higher than the corresponding warmings of H_2 of relative to H_1 (except for the daily minimum temperatures at PDX). Therefore, the warming trends have increased over time excluding the noted exception at PDX.

However the following trend holds for both types (daily maximum and daily minimum) of temperature distributions at all four cities:

- Among the three climate scenarios, A has the highest warming and G has the lowest warming.

Because very low temperatures in the winter months and very high temperatures in the summer months are likely to contribute to very high loads, then it is also useful to analyze climate trends for the winter, and summer subsets of the overall distributions already analyzed in this section. For completeness, climate trends for other seasonal subsets are also analyzed.

In addition, further analyses show that the daily maximum temperatures and daily minimum temperatures are highly correlated for the five data sets plotted in Figure D - 26 . Specifically, the correlation coefficients are, at BOI, at or greater than 0.92; at GEG, also at or greater than 0.92; at PDX, between 0.80 and 0.88; and at SEA, between 0.84 and 0.89. Because of the high correlation between the daily maximum and daily minimum temperatures, in the next four sections, for simplicity, climate trends for the seasons are analyzed using either the daily maximum or the daily minimum temperatures as appropriate. For example, for the winter months, the daily minimum temperatures are analyzed, while for the summer months, the daily maximum temperatures are analyzed.

Analyses in subsequent sections also include discussions of heating degree-days (HDDs) and cooling degree-days (CDDs), and their calculations, by definition, involve both the daily maximum and daily minimum temperatures. However, because of the high correlation between the daily maximum and minimum temperatures, analyses of HDDs are simplified to involve only the daily maximum temperatures, and conversely, analyses of CDDs are simplified to involve only the daily minimum temperatures.

Trends in the Winter Months

For the Northwest region, the winter months are usually defined as December, January, and February, and loads during these months are generally the highest. In Figure D - 27 are the boxplots of the distributions of the daily minimum temperatures for the winter months of the two historical sets H_1 and H_2, and climate scenarios A, C, and G, for the four cities. This figure shows winter months showing the same climate trend as presented in the previous section: warming temperatures from H_1 to H_2 to the climate scenario years as presented in the previous section. Therefore, the distribution of HDDs of the climate scenario temperatures will be lower than the distribution of HDDs of the historical temperatures in H_2, which in turn will be lower than the distribution of HDDs of the historical temperatures in H_1.

The forecasted loads follow the trends in the HDDs and thus, the distribution of forecasted loads using the climate scenario temperatures is lower than using historical temperatures in H_2, which in turn is lower than using historical temperatures in H_1.

Figure D - 27: Distributions of Winter Daily Maximum and Minimum Temperature at the Four Cities

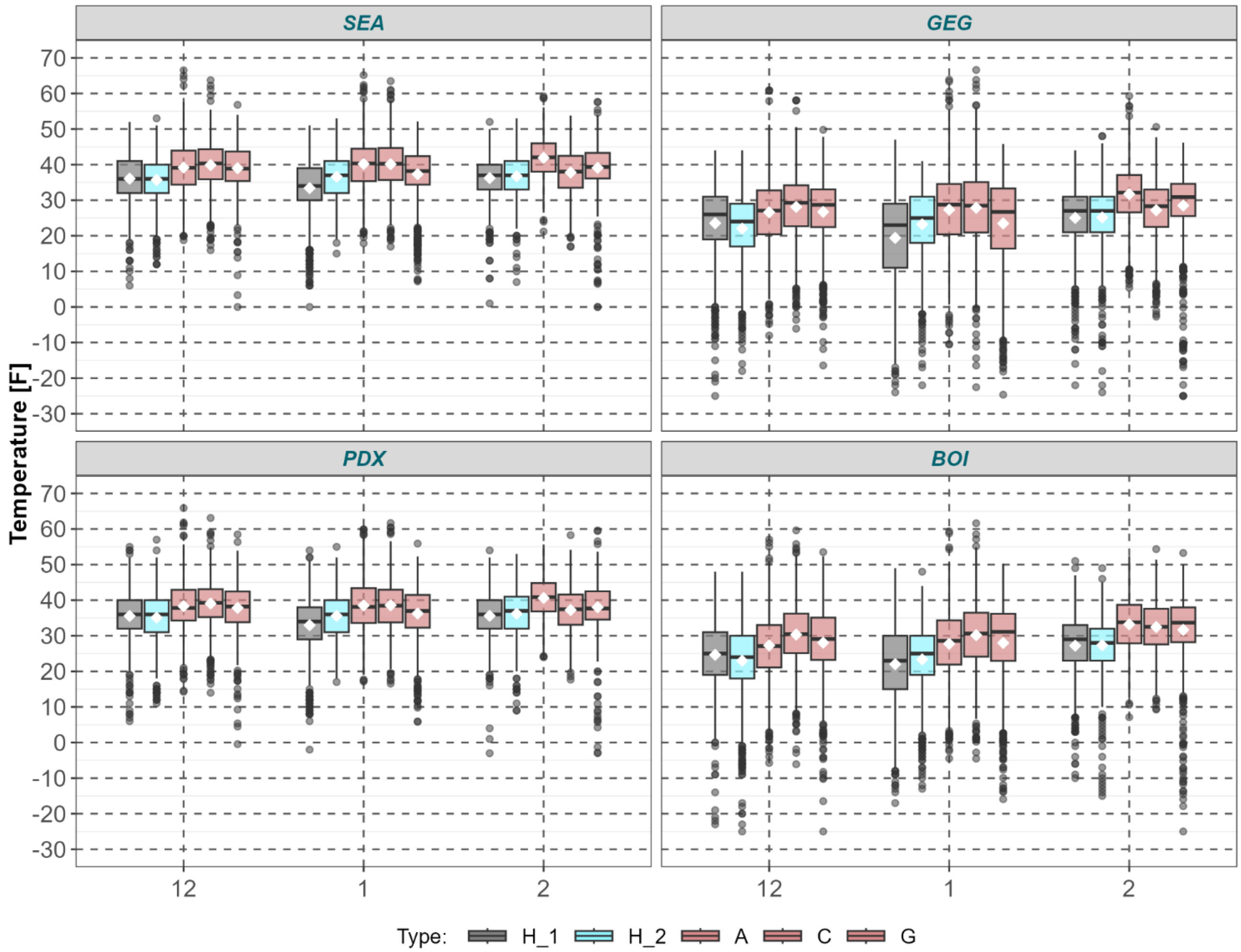

From Figure D - 27, the distributions of daily minimum temperatures at the near coastal cities, SEA and PDX, are higher than those at the inland cities, GEG and BOI. Furthermore, the aggregate warmings of the daily minimum temperatures for all 12 months in Figure D - 26 are not spread uniformly over the three months in Figure D - 27. The differences of the averages between the five distributions are tabulated in Table D - 9 to Table D - 12 for the four cities. In each of the four Tables, the the highest warmings by month are bolded.

It is interesting that in the historical data that December has cooled for H_2 compared to H_1. Otherwise, over all three months at all four cities, it is the expected climate trend of warming temperatures from H_1 to H_2 to the climate scenario years. Therefore, it could be deduced that the forecasted loads using climate scenario temperatures on average will be lower than those forecasted using historical temperatures in H_1 and H_2.

Table D - 9: Differences of the Averages of the Daily Minimum Temperature Distributions in [F] for BOI for Months 12, 1, 2

$BOI/Month$	H_2 vs H_1	A vs H_2	C vs H_2	G vs H_2
12	- 1.7	+ 4.3	**+ 7.4**	**+ 5.1**
1	**+ 1.3**	+ 4.4	+ 6.8	+ 4.6
2	+ 0.1	**+ 5.9**	+ 5.1	+ 4.3

Table D - 10: Differences of the Averages of the Daily Minimum Temperature Distributions in [F] for GEG for Months 12, 1, 2

$GEG/Month$	H_2 vs H_1	A vs H_2	C vs H_2	G vs H_2
12	- 1.5	+ 4.6	**+ 6.1**	**+ 4.7**
1	**+ 3.8**	+ 4.1	+ 4.6	+ 0.2
2	+ 0.1	**+ 6.6**	+ 2.0	+ 3.4

Table D - 11: Differences of the Averages of the Daily Minimum Temperature Distributions in [F] for PDX for Months 12, 1, 2

$PDX/Month$	H_2 vs H_1	A vs H_2	C vs H_2	G vs H_2
12	- 0.5	+ 3.2	**+ 4.0**	**+ 2.7**
1	**+ 2.6**	+ 2.9	+ 3.0	+ 0.7
2	+ 0.6	**+ 4.4**	+ 1.0	+ 1.8

Table D - 12: Differences of the Averages of the Daily Minimum Temperature Distributions in [F] for SEA for Months 12, 1, 2

$SEA/Month$	H_2 vs H_1	A vs H_2	C vs H_2	G vs H_2
12	- 0.4	+ 3.5	**+ 4.2**	**+ 3.3**
1	**+ 3.2**	+ 3.6	+ 3.5	+ 0.7
2	+ 0.5	**+ 5.2**	+ 1.1	+ 2.4

Moreover, from H_1 to H_2, the month with the highest warming is January. However, for climate scenario A, the month with the highest warming is February, while for scenarios C and G, the month with the highest warming is December. Overall, all three winter months and at all four cities, it is the usual climate trend that climate scenario A has the highest warming and scenario G has the lowest warming, with one exception: at BOI, climate scenario C that has the highest warming.

However, as plotted in Figure D - 27, climate scenario G, despite on average, having warmer (daily minimum) temperatures than both historical data sets, still on occasions has comparatively very low temperatures as compared to the historical sets at all four cities. It should be reminded that some of the lowest temperatures in G that are below the lowest historical temperatures have been adjusted to be equal to those lowest historical temperatures. A more detailed analysis of these very cold temperatures of the four cities are presented in a subsequent section.

Trends in the Summer Months

Next, the summer months for the Northwest are usually defined as June, July, and August, and loads during these months are generally also the highest. In Figure D - 28 are the boxplots of the distributions of the daily maximum temperatures for the summer months of the two historical sets H_1 (in gray) and H_2 (in light blue), and climate scenarios A, C, and G (in light red), for the four cities.

In Figure D - 28, over all three summer months at all four cities, it is the same overall climate trend of warming temperatures from H_1 to H_2 to the climate scenario years. Therefore, the distribution of cooling degree-days (CDDs) of the climate scenario temperatures will be higher than the distribution of CDDs of the historical temperatures in H_2, which in turn will be higher than the distribution of CDDs of the historical temperatures in H_1. The forecasted loads follow the trends in the CDDs and thus, it could be deduced that the distribution of forecasted loads using the climate scenario temperatures will be higher than that using historical temperatures in H_2 which in turn will be higher than that using historical temperatures in H_1.

Putting summer and winter together, it could be deduced that the distribution of forecasted loads in the climate scenarios will be higher than historicals for the summer months and lower than historicals for the winter months.

Figure D - 28: Distributions of Summer Daily Maximum and Minimum Temperature at the Four Cities

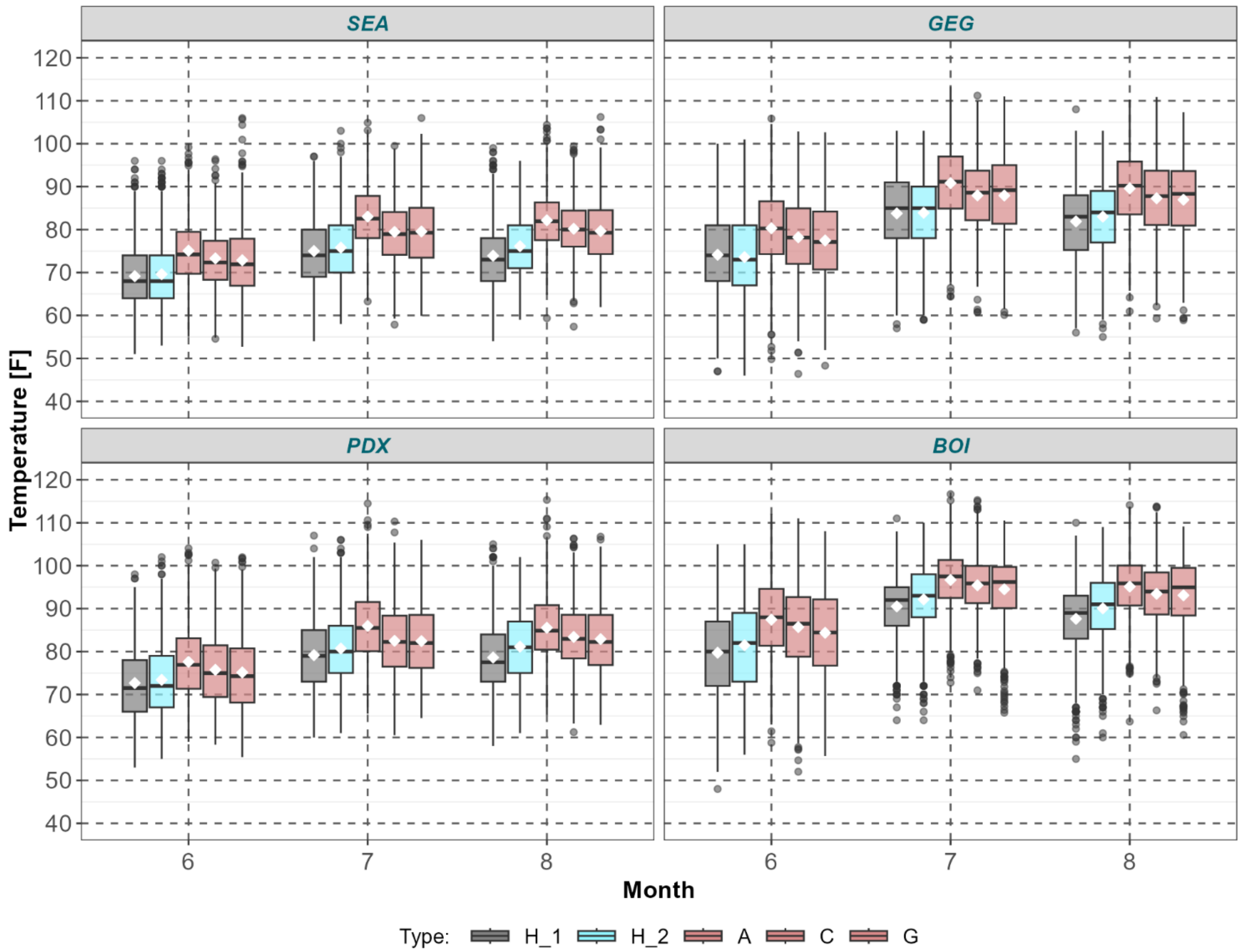

It should be noted that the highest historical temperatures were achieved at GEG at 109 F, PDX at 116F, and SEA at 108 F on several days in and around the 2021 heat dome event. However, historical year 2021 is not among the years in historical data H_1 or H_2. Therefore, these highest historical temperatures for the three cities are not plotted in Figure D - 28. However, a more detailed analysis of very high climate scenario temperatures as plotted in Figure D - 28, and very high historical temperatures from 1948 to 2024, which do include those of the 2021 heat dome, are presented in a subsequent section.

In addition, in Figure D - 28, for each of the three summer months respectively, the distributions of daily maximum temperatures at the near coastal cities, SEA and PDX, are lower than those at the inland cities, GEG and BOI. Furthermore, the aggregate warmings of the daily maximum temperatures for all 12 months in Figure D - 26 are not spread uniformly over the three months in Figure D - 28. The differences of the averages between the five distributions are tabulated in Table D - 13 to Table D - 16 for the four cities. In each of the four Tables, the the highest warming by month in bold text.

Table D - 13: Differences of the Averages of the Daily Maximum Temperature Distributions in [F] for BOI for Months 6, 7, 8

$BOI/Month$	H_2 vs H_1	A vs H_2	C vs H_2	G vs H_2
6	+ 1.7	**+ 6.0**	**+ 4.2**	+ 2.9
7	+ 1.6	+ 4.5	+ 3.3	+ 2.4
8	**+ 2.4**	+ 5.1	+ 3.4	**+ 3.0**

Table D - 14: Differences of the Averages of the Daily Maximum Temperature Distributions in [F] for GEG for Months 6, 7, 8

$GEG/Month$	H_2 vs H_1	A vs H_2	C vs H_2	G vs H_2
6	- 0.5	+ 6.7	**+ 4.6**	+ 3.9
7	+ 0.1	**+ 6.9**	+ 4.1	**+ 4.0**
8	**+ 1.1**	+ 6.6	+ 4.3	**+ 4.0**

Table D - 15: Differences of the Averages of the Daily Maximum Temperature Distributions in [F] for PDX for Months 6, 7, 8

$PDX/Month$	H_2 vs H_1	A vs H_2	C vs H_2	G vs H_2
6	+ 0.8	+ 4.2	**+ 2.3**	+ 1.7
7	+ 1.6	**+ 5.2**	+ 1.8	+ 1.7
8	**+ 2.5**	+ 4.4	+ 2.3	**+ 1.8**

Table D - 16: Differences of the Averages of the Daily Maximum Temperature Distributions in [F] for SEA for Months 6, 7, 8

$SEA/Month$	H_2 vs H_1	A vs H_2	C vs H_2	G vs H_2
6	+ 0.5	+ 5.5	+ 3.7	+ 3.3
7	+ 0.8	**+ 7.2**	+ 3.6	**+ 3.8**
8	**+ 2.2**	+ 6.0	**+ 4.1**	+ 3.5

From H_1 to H_2, the month with the highest warming is August for all four cities. However, from to H_2 to the climate scenario years, there is no set pattern in the city or the month with the highest warming. Nevertheless, over all all three summer months and at all four cities, it is the usual climate trend that climate scenario A has the highest warming and scenario G has the lowest warming.

Trends in the Other Months

In addition to the winter and summer months are the spring months, from March to May, and the fall months, from September to November. For the spring and fall months, for simplicity, only the daily maximum temperatures are analyzed. Boxplots of the distributions of the daily maximum temperatures at the for cities are plotted for the spring months in Figure D - 29, and for the fall months in Figure D - 30.

For each of the four cities, the distributions of daily maximum temperatures for the spring and fall months plotted in Figure D - 29 and Figure D - 30, are lower than those of the summer months plotted in Figure D - 28, which lead to their CDDs being lower than those of the summer months. On the other hand, their distributions of daily minimum temperatures (not presented for simplicity) are higher than those of the winter months, and thus, their HDDs will be lower than those of the winter months. Because of the lower HDDs than those of winter months and lower CDDs than those of the summer months, it could be deduced that the distributions of the forecasted loads for the spring and fall months will be lower than those for the winter and summer months.

In Figure D - 29 below, over all three spring months at all four cities, is also the overall climate trend of warming from H_1 (in gray boxplots) to H_2 (in light blue boxplots) to the climate scenario years (in light red boxplots). The warmer climate scenario temperatures will lead to lower HDDs and higher CDDs than those of the historical temperatures, which will lead to the forecasted loads for the climate scenarios being lower (than historical) for the cooler days but higher (than historical) for the warmer days.

As discussed previsouly, for the winter and summer months, the warming climate scenario temperatures lead to simple deductions of lower winter loads but higher summer loads when compared to historical winter and summer loads. However, for the spring months, there is not a simple deduction on how climate scenario loads compare to historical loads.

Figure D - 29: Distributions of Spring Daily Maximum and Minimum Temperature at the Four Cities

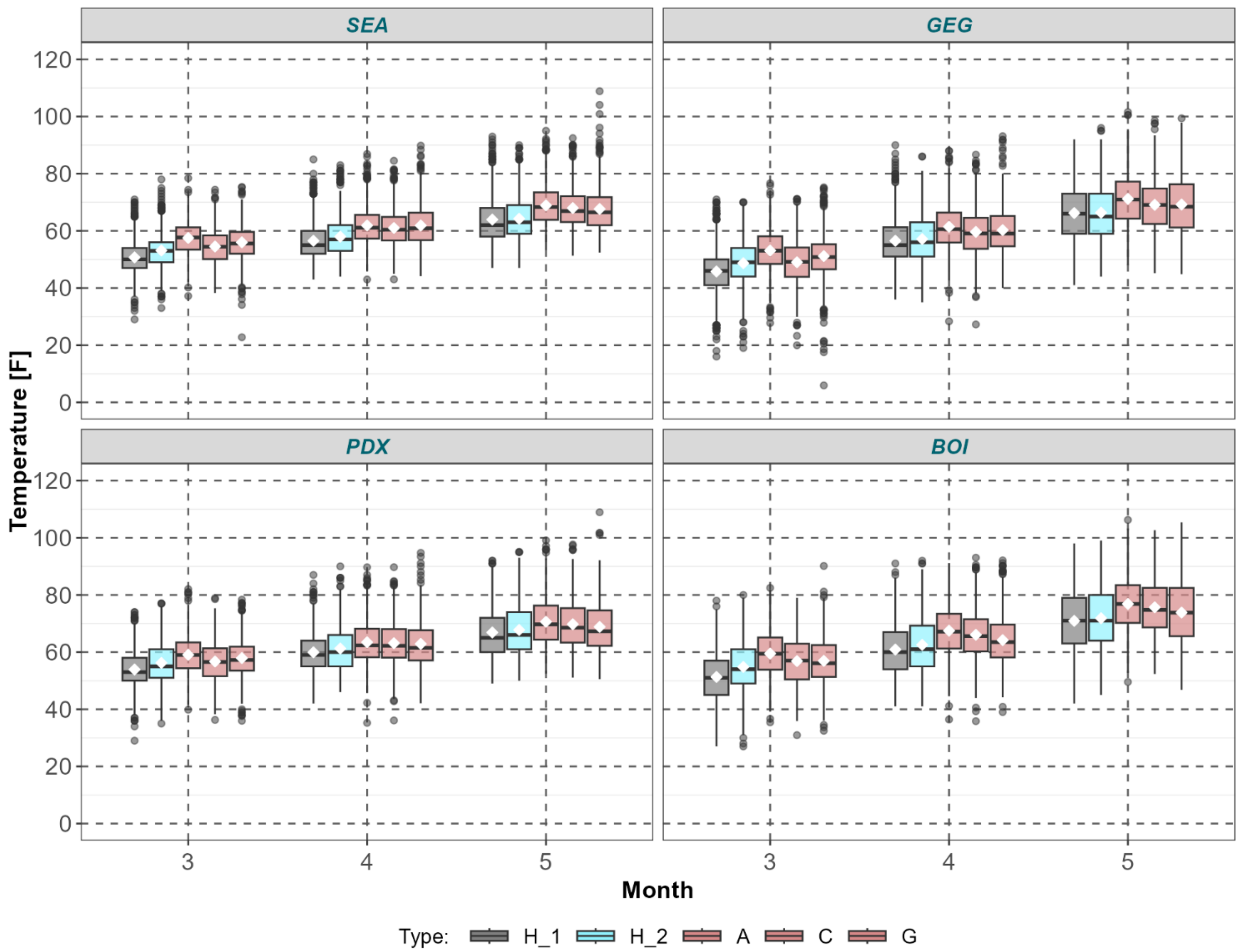

In general, for the spring months, some of the climate trends are similar to those discussed previously for the winter and summer months:

- the temperatures are getting warmer over the years, from H_1 to H_2, and from H_2 to the climate scenario years;
- for the climate scenarios at all four cities, climate scenario A has the highest warming while G has the lowest warming.

Moreover, from H_1 to H_2, the month with the highest warming is March for all four cities. However, from to H_2 to climate scenarios A and C, the month with the highest warming is May. But for scenario G, there is no pattern for the month with the highest warming over the four cities.

It should be noted that for the “shoulder” summer month of May, there are some days where the daily maximum temperatures are at or greater than 100 F at the four cities, and the forecasted loads on these days are expected to be particularly high.

Finally, in Figure D - 30 below, for all three fall months at all four cities, is once again the ovearll climate trend of warming from H_1 (in gray boxplots) to H_2 (in light blue boxplots) to the climate scenario years (in light red boxplots). Following the same analyses as performed for the spring months: the warmer climate scenario temperatures lead to lower HDDs and higher CDDs than those of the historical temperatures, which lead to the forecasted loads for the climate scenarios being lower (than historical) for the cooler days but higher (than historical) for the warmer days. Therefore, for the fall months, there is not a simple deduction how climate scneario loads compare to historical loads, just as for the spring months.

Figure D - 30: Distributions of Fall Daily Maximum and Minimum Temperature at the Four Cities

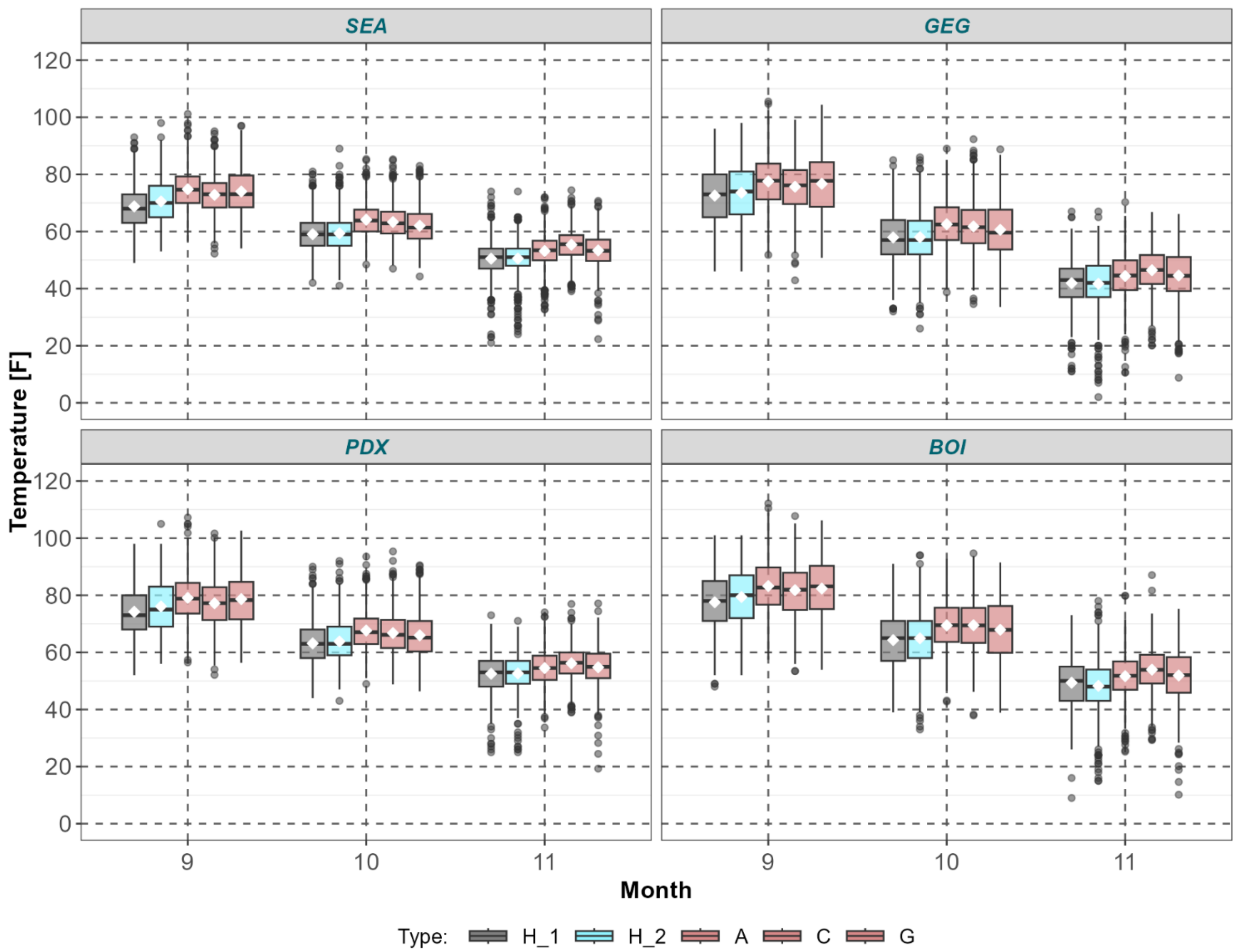

In general, for the fall months, some of the climate trends are similar to those discussed previously for the winter, summer, and spring months:

- the temperatures are getting warmer over the years, from H_1 to H_2, and from H_2 to the climate scenario years;

- for the climate scenarios at all four cities, climate scenario A usually has the highest warming while G has the lowest warming with one exception: at BOI, it is climate scenario C that has the highest warming.

Moreover, from H_1 to H_2, the month with the highest warming is September. However, for climate scenario A, the month with the highest warming is October, while for scenarios C and G, the month with the highest warming is November.

Trends in Cold Snaps and Heat Waves

A regional cold snap or heat wave is generally defined as three or more consecutive days of very low or very high temperatures, respectively, across the region. Since temperatures in coastal areas such as PDX or SEA are milder than those in interior regions such as BOI or GEG, then temperatures that are considered very high or very low in coastal areas might be considered merely high or low in interior regions. Conversely, temperatures that are considered very high or very low in interior regions are likely to be very rare in coastal areas that it is unlikely to have three or more consecutive days of such temperatures there. Therefore, for the entire region, there is not a standard definition of the very low temperatures for a cold snap or the very high temperatures for a heat wave. Nevertheless, for the example very high and very low temperatures defined in this section, the regional power system is likely to be under stress to serve the high loads during the multi-day durations of the cold snaps and heat waves.

This analysis uses temperatures at the four regional population centers: BOI, GEG, PDX, and SEA. The Council defines a regional heat wave as any event where the daily maximum temperatures of all four cities are at or greater than a threshold temperature of 95 F for three or more consecutive days, as there are two historical events in 2021 and 2022 that meet this threshold.

The climate trend of heat waves are presented in Figure D - 31 below, where the historical and climate scenario data are plotted in the green circles and light red circles, respectively. Also, the historical and climate scenario years in which the heat waves occur are listed along the x-axis. More specifically, the two historical heat waves are listed as H_2021 (the heat dome event) and H_2022 at the left side of the figure. In contrast, there are 14 climate scenario heat waves starting with A_2022, representing climate year 2022 of climate scenario A, and ending with G_2039, at the right side, representing climate year 2039 of scenarion G. Also, it could be seen that there are two heat waves for climate years 2041 and 2029 of scenario A, and climate year 2039 of scenario G.

Figure D - 31: Daily Heat Wave Maximum Temperatures at Four Cities

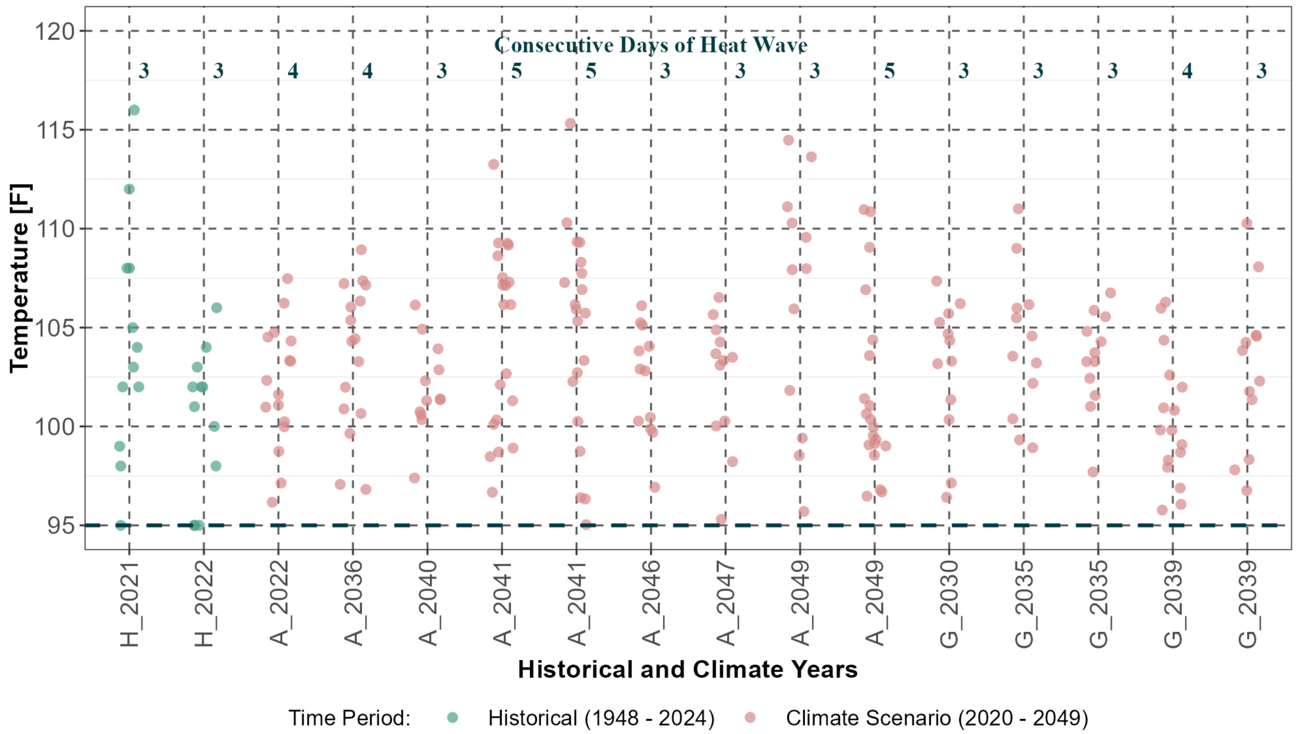

In Figure D - 31, the durations of the heat waves are listed in the dark green numbers near the top. For example, for the H_2021 heat wave at the left side, the duration was three consecutive days. Therefore, the daily maximum temperatures at the four cities for the three days are plotted in 12 green circles, with one at 95 F, which is the heat wave threshold temperature, plotted in the horizontal dark green dashed line. There are three climate scenario heat waves with longer durations of five consecutive days: the two in A_2041 and the second in A-2049. For these, there are 20 light red circles plotted.

The climate trend in Figure D - 31 is clear: there are many more heat waves in the climate scenario years, totaling 14, than in the historical years, totaling two. In addition, many of the climate heat waves have longer durations. However, for a fair comparison of the number of heat waves, the populations of the two data sets should be the same. But in this analysis there are more years of climate scenario data (90) than years of historical data (77), which leads to the population of climate data having a ratio of $90/77 \cong 1.17$ relative to the population of historical data. In other words, the climate data is about 17% larger than the historical data, and thus, the number of heat waves in the historical data should be adjusted due to the smaller population of the historical data. For a very rough estimate, increasing the population of the historical data by 17% should increase the number of heat waves to $(1.17) \times 2 = 2.34$. However, even with the population adjustment, there are still many more heat waves in the climate scenario years than in the historical years.

Next, it is useful to disaggregate temperatures at the four cities, which leads to Figure D - 32 below.

Figure D - 32: Daily Heat Wave Maximum Temperatures at Four Cities

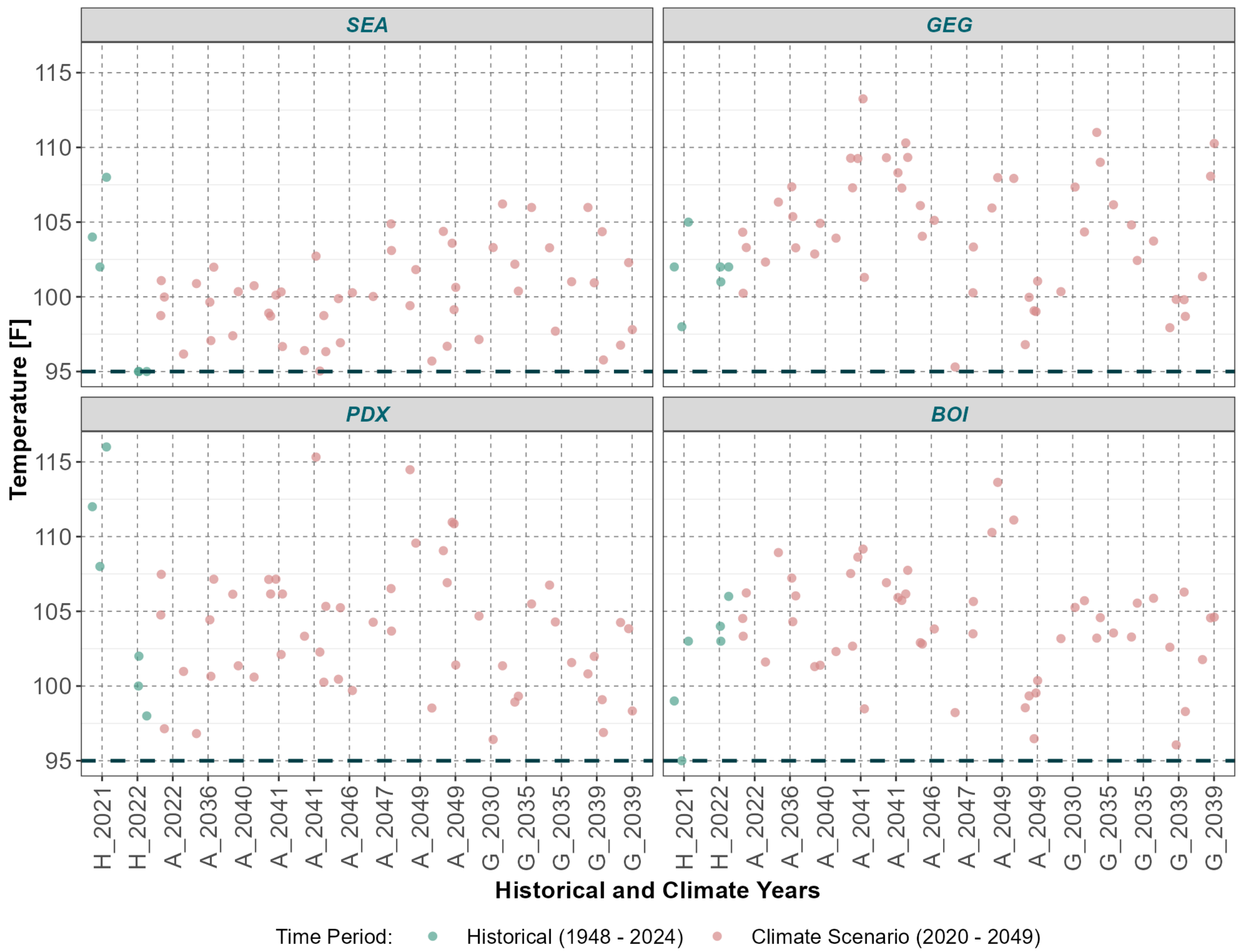

In Figure D - 32, the SEA heat-wave temperatures are plotted in the top left panel. It could be seen that they are, as a distribution, lower than those of the other three cities plotted in the remaining panels. There are only five days where the SEA temperatures are at or above 105 F compared to the many more days in the other three panels. Furthermore, for all three days of the H_2022 heat wave, the SEA daily maximum temperatures were at 95 F, the heat wave threshold temperature. In addition, there are no climate scenario heat-wave temperatures higher than highest historical temperature of 108 F during the 2021 heat dome. However, for temperatures outside of heat-waves, there is one climate scenario temperature slightly higher than 108 F.

Furthermore, for the PDX (bottom left panel) heat-wave temperatures, there are two climate scenario temperatures, in years 2041and 2049 of climate scenario A, that are just slightly below the highest historical temperature of 116 F during the 2021 heat dome. For temperatures outside of heat-waves, there is no climate scenario temperature higher than the highest historical temperature of 116 F.

In addition, for the inland cities, BOI (bottom right panel) and GEG (top right panel), there are many climate scenario heat-wave temperatures significantly higher than the historical heat-wave temperatures as plotted in Figure D - 32. Outside of temperatures during heat-waves, the highest historical temperatures at BOI and GEG were 111 F and 109 F, respectively. It should be noted the 109 F GEG temperature occurred on the day after the historical 2021 regional heat-wave ended. On that same day, the PDX and SEA temperatures were at 93 F and 85 F, respectively, which were below the threshold heat-wave temperature of 95 F. There are 41 and 24 climate scenario daily maximum temperatures higher than the highest historical temperature at BOI (111 F) and GEG (109 F), respectively.

Next, cold snaps are analyzed. For this analysis, the Council defined a cold snap as any event such that the daily minimum temperatures of all four cities are at or lower than a threshold temperature of 18 F for three or more consecutive days.

The climate trend of cold snaps is presented in Figure D - 33 below, where the historical and climate scenario data are plotted in the green circles and light red circles, respectively. Also, the historical and climate scenario years in which the cold snaps occur are listed along the x-axis. More specifically, there were 10 historical cold snaps compared to four climate scenario cold snaps all from scenario G.

Figure D - 33: Daily Cold Snap Minimum Temperatures at Four Cities

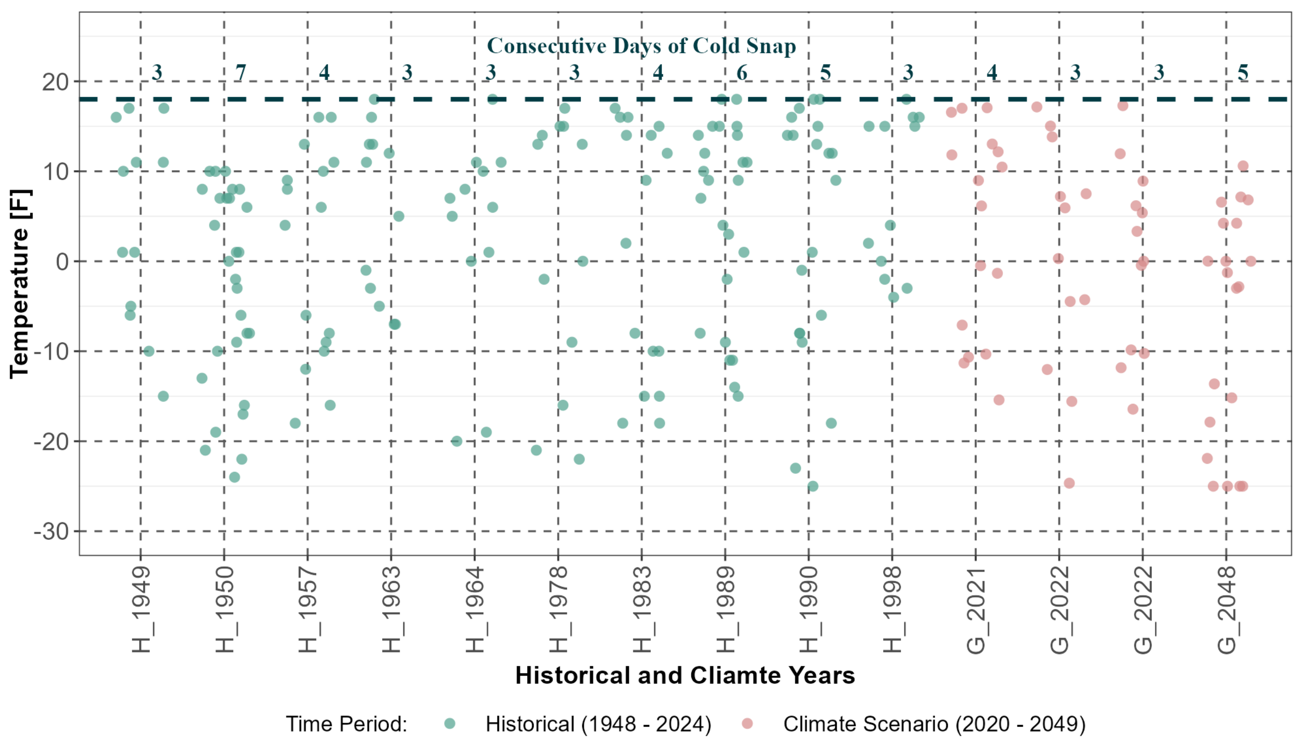

In Figure D - 33, the durations of the cold snaps are listed in the dark green numbers listed near the top. For example, during the H_1950 cold snap near the left side, the duration was very long and lastedseven consecutive days. Therefore, the daily minimum temperatures at the four cities for the seven days are plotted in 28 green circles, where most of them are at or below 10 F. The longest duration of a climate scenario cold snap is five consecutive days, in G_2048. The cold snap daily minimum threshold temperature of 18 F is plotted in the horizontal dark green dashed line.

It should be noted in January 2024, there were five consecutive days with very cold temperatures at the four cities. However, among the five days, there were three days at PDX and SEA with daily minimum temperatures higher than the threshold temperature of 18 F. Thus, this cold event in 2024 is not a cold snap as defined in this analysis.

The climate trend presented in Figure D - 33 is also clear, namely, there are fewer cold snaps in the climate scenario years than in the historical years: four versus ten. However, the number of cold snaps in the historical years should be adjusted due to the historical data being 17% smaller than the climate data. Therefore, the adjusted number of historical cold snaps is $(1.17) \times 10 \cong 11.7 \approx 12$ which is even higher than before, being nearly 3 times the number of climate scenario cold snaps.

Finally, disaggregating temperatures in Figure D - 33 into those at the four cities result in Figure D - 34 below.

Figure D - 34: Daily Cold Snap Minimum Temperatures at Four Cities

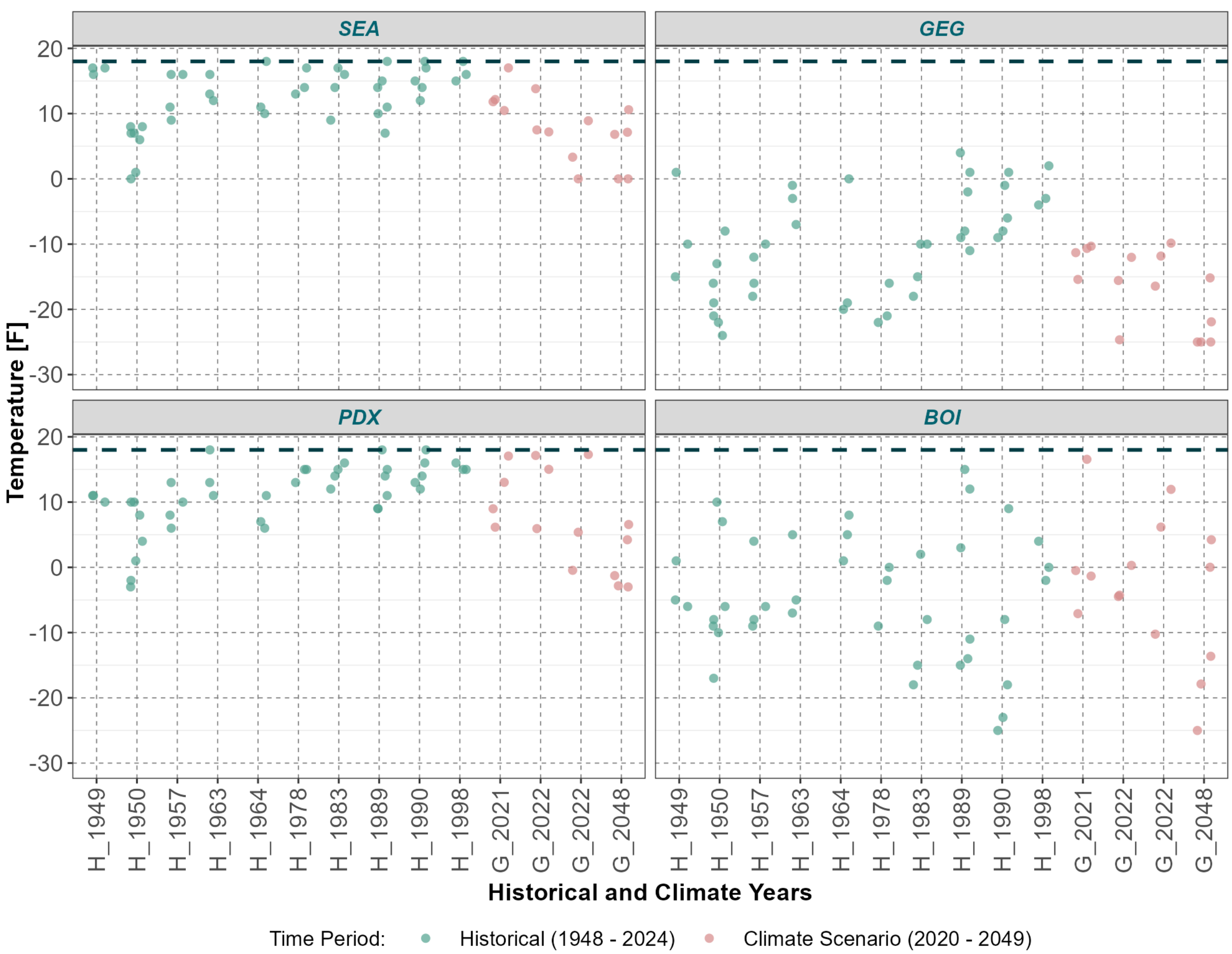

In Figure D - 34, the SEA and PDX cold snap temperatures are plotted in the top left panel and bottom left panel respetively. As distributions, they are significantly higher than those at GEG and BOI. There are no days below 0 F at SEA, and only six days slightly below 0 F at PDX. It should be noted that the climate scenario temperatures have been adjusted such that at each city, those that are below its lowest historical temperature have been set equal to the lowest historical temperature.

Thus, in the climate scenario years, there are fewer cold snaps but many more heat waves (than in the historical years) during which the regional power system would be under stress to serve these very high loads.

Climate Scenario Wind Generation Profiles

As discussed in a previous section, climate scenario wind speed data are not included in the RMJOC data sets; fortunately, wind data from compatible scenarios are available from the Climatology Lab (CL) at the University of California, Merced.[63]

The climate models and downscaling methods of the three selected RMJOC climate scenarios A, C, and G are listed in the left column of Table D - 17 below. It's evident that the BCSD downscaling method was used to develop A and C while MACA was used to develop G. Unfortunately, all climate scenarios from the Climatology Lab (CL) were developed using MACA, as shown in the right column of Table D - 17. Thus, CL has an exact match for scenario G that also used MACA. However, there is not an exact match for either A or C. Nevertheless, since both the RMJOC and CL scenarios originate from the same climate models, it is assumed here that differences between the RMJOC and CL scenarios are small.

Even though the Climatology Lab Scenarios for the CanESM2 and CCSM4 GCMs are not exactly the same as RMJOC scenarios, for simplicity, they will still be referred to as A and C, respectively, in subsequent sections.

Table D - 17: Selected RMJOC Climate Scenarios and Compatible Climatology Lab Scenarios

RMJOC Scenarios	Climatology Lab Scenarios
A: CanESM2_RCP85_**BCSD**	CanESM2_RCP85_**MACA**
C: CCSM4_RCP85_**BCSD**	CCSM4_RCP85_**MACA**
G: CNRM-CM5_RCP85_**MACA**	CNRM-CM5_RCP85_**MACA**

The downloaded CL scenario daily average wind speeds undergo further calculations that result in a set of future hourly wind generation at various locations considered as in-region for the Ninth Plan, which then become inputs into the Council's models. The details are described in this section.

[63] Climatology Lab: *https://www.climatologylab.org/maca.html*.

In-Region Wind Fleets

For the Ninth Plan, the Council used five in-region locations to develop wind generation profiles[64] plotted in Figure D - 35 below.

Figure D - 35: In-Region Wind Fleet Generation Locations for the Ninth Plan

For simplicity, the five simulated wind fleets at the Gorge, Southeast Washington, Idaho, Montana, and Wyoming are abbreviated as GO, WA, ID, MT, and WY, respectively. In addition, the latitude and longitude coordinates of the five wind fleet locations are listed in Table D - 18.

Table D - 18: The Five In-Region Wind Fleet Generation Locations

Locations	Latitude	Longitude
The Gorge (GO)	45.601	-120.602
Southeast Washington (WA)	46.399	-117.578
Idaho (ID)	43.320	-112.007
Montana (MT)	47.166	-110.501
Wyoming (WY)	41.683	-107.200

[64] See Technical Appendix G - New Generating Resources in the Ninth Power Plan for more details.

CL Scenario Wind Speed Data

The CL scenario wind data are at 10-m height ("near-surface") and need to be extrapolated to two hub-heights, 80-m and 100-m, for wind turbine models GE 1.5 SLE and Vestas v112-30, respectively, that were selected for the simulations in the Power Plan. The extrapolation formulas analyzed were taken from the chapter "*Methodologies Used in the Extrapolation of Wind Speed Data at Different Heights and Its Impact in the Wind Energy Resource Assessment in a Region*" by Bañuelos-Ruedas et al. in the book *Wind Farm - Technical Regulations, Potential Estimation and Siting Assessment* (DOI: 10.5772/20669). The authors presented several formulas that relate wind speeds at different heights under certain conditions. One of the formulas is the exponential law:

$$\frac{V_2}{V_1} = \left[\frac{H_2}{H_1}\right]^{\alpha}$$

where V_1 and V_2 are the wind speeds at heights H_1 and H_2 respectively, and α is the friction coefficient or the Hellman exponent. The equation above has a slightly different expression than the one in the reference material. Since many existing wind turbines are located around farmlands, values for α could be selected based on landscape types listed in Table 1 in the reference. For example, $\alpha = 0.15$ for grasslands, while $\alpha = 0.2$ for tall crops, hedges and shrubs. In addition, a commonly used value for α is $(1/7) \approx 0.143$.

Another formula presented in the reference is the logarithmic law:

$$\frac{V_2}{V_1} = \frac{ln\left[\frac{H_2}{H_0}\right]}{ln\left[\frac{H_1}{H_0}\right]}$$

where H_0 is the roughness coefficient length, in meters. Similarly, the equation above has a slightly different expression than the one in the reference. To model wind turbines around farmland, the landscape type "*farming land dotted with some houses and 8-meter-tall sheltering hedgerows within a distance of some 1,250 meters*" was selected from Table 4 in the reference with a corresponding coefficient $H_0 = 0.055$ meters.

Let V_1 represent the CL scenario wind speeds at 10-m height, then $H_0 = 10$ meters. In Figure D - 36 below are plots of the ratio (V_2/V_1) on the y-axis as a function of height H_2 (in meters) on the x-axis. The two green curves represent the exponential law with parameter $\alpha = 0.2$ for the upper dotted curve and $\alpha = (1/7)$ for the lower dashed curve. The light red curve represents the logarithmic law with parameter $H_0 = 0.055$ meters.

Figure D - 36: Wind Speed Ratio vs Height

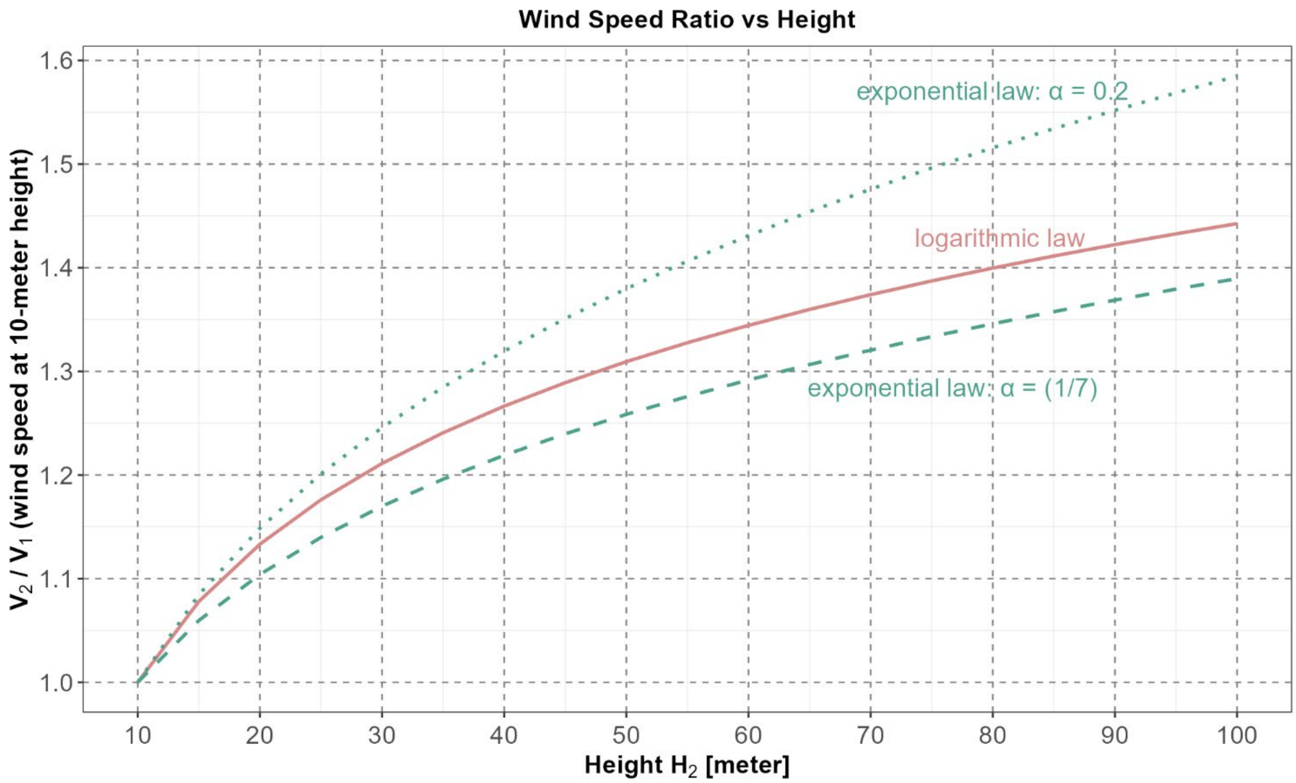

Figure D - 36 shows that all three wind speed ratios start correctly at 1 at a height of 10 meters. For the logarithmic law, the 80-meter and 100-meter wind speeds are respectively 40% and 44% higher than the 10-meter wind speed. Because the log-function increases more slowly for larger values, the 100-meter wind speed is only 3% higher than the 80-meter wind speed. All three curves are relatively close together in the Figure: the upper and lower green curves are about 9% higher and 4% lower, respectively than the red curve for $H_2 = 80$ meters and 100 meters. For simplicity, the red curve, or the logarithmic law, is used to extrapolate climate scenario wind speeds at a 10-meter height to wind speeds at 80 meters and 100 meters, which are then used to simulate wind fleet generation in the Ninth Plan.

However, before using the climate wind data, it should be reminded that in developing the downscaled climate scenario streamflow data for the Northwest region, the RMJOC had to perform bias-corrections in the process.[65] The bias-corrections are developed to transform the climate scenario wind data to resemble historical data in a common historical time period.

[65] *Climate and Hydrology Datasets for RMJOC Long-Term Planning Studies: Second Edition (RMJOC-II) Part I: Hydroclimate Projections and Analyses*" at https://www.bpa.gov/-/media/Aep/power/hydropower-data-studies/rmjoc-ll-report-part-l.pdf.

The climate data used in the Power Plan covers the 30 water-years from 2020 to 2049, or 31 calendar years from 2019 to 2049 (except for several months). The historical data set, the ERA5[66] 100-m wind speed data, are available for years from 1980 to 2018 in the renewable energy simulation model, Time Series Lab (TSL).[67] Therefore, the CL climate 100-m wind data are bias-corrected to resemble the ERA5 100-m wind speed data for the common 31 historical years from 1988 to 2018. However, it turns out that even the ERA5 data themselves require bias-corrections which are discussed in the next section.

The TSL model can be used to generate historical re-analysis data for any coordinate available in the ERA5 datasets, for both wind and solar resources. While a feature of TSL is the ability to extract the embedded ERA5 data (for years 1980 to 2023) for given coordinates and resource types, its main feature is generating historical and future synthetic hourly capacity factors (CFs). The TSL model output of hourly CF profiles for a set of years are then used as inputs in the Council's production-cost model and capital-expansion model to calculate the shares of wind and solar resources in generation portfolios.

The ERA5 Wind Data

The ERA5 wind dataset covers the years from 1940 to the present. It is a blend of observed data (if they are available), and synthetic data calculated using re-analysis (if observed data are not available). However, even the historical ERA5 data needed to be bias-corrected before being used in the Power Plan. The details are discussed in this section.

Although the ERA5 data is widely used, it can contain forecast errors and biases due to different weather modeling errors. Furthermore, the spatial resolution of 0.25 by 0.25 degrees of latitude and longitude in ERA5 data may not fully distinguish finer topography at a particular location. And lastly, different wind and solar-related meteorological observations may have their own data collection sensitivity and limitations. All these factors lead to systemic errors that could result in overestimation or underestimation of capacity factors. A study examining ERA5-derived capacity factors across the continental United States found that broadly, ERA5-derived solar CFs may be biased high, and wind CFs biased low.[68] For example, in winter, the ERA5 solar CF is on average 23% higher than observed data, while annually, ERA5 wind CF is 20% lower than observed data.

To mitigate the inherent biases in ERA5 data, TSL uses observed or "better" synthetic CF data to generate bias-correction profiles. These correction profiles force the average of the distribution of the ERA5 CFs to align with the average of the correction profiles. The correction profiles can be annual

[66] The ERA5 historical climate data is developed by the Copernicus Climate Change Service at the European Centre for Medium-Range Weather Forecasts (ECMRW). See https://www.ecmwf.int/en/forecasts/dataset/ecmwf-reanalysis-v5 for more details.

[67] See https://www.timeserieslab.com for more details.

[68] See https://www.mdpi.com/1996-1073/17/7/1667.

(single value, expected annual CF), monthly (12 values, expected CF for each month), or hourly (288 values, the expected hour in a day in every month).

For the five in-region wind fleet locations (GO, WA, ID, MT, and WY), their hourly bias correction profiles are based on available historical synthetic wind speed data at 100-m hub height for years 2007-2014 from the National Wind Toolkit developed by the National Laboratory of the Rockies (NLR).[69] For selected wind turbine types, their wind CFs are then calculated by the NLR System Advisor Model (SAM)[70,71] which are then used by TSL[72] to bias-correct the ERA5 wind CFs and wind speeds at 100-m hub height.

The bias-corrected ERA5 100-m wind data resemble the corresponding NLR 100-m wind data at the five wind fleet locations plotted in Figure D - 35 and listed Table D - 18. The bias-corrected ERA5 80-m wind data are calculated from the ERA5 100-m data using the logarithmic law formula discussed in the previous section. For simplicity, these bias-corrected ERA5 wind data in subsequent sections will be referred to as just the ERA5 wind data.

Since the NLR data themselves are also synthetic, it would be prudent to assess how well the bias-corrected ERA5 data compare with any available observed historical data. Fortunately, there are some observed historical wind generation data around the Gorge area available from the Bonneville Power Administration (BPA).[73] The wind generation data tabulated by BPA is from a collection of wind farms within its balancing area which are plotted in Figure D - 37 below.

[69] The National Laboratory of the Rockies is formerly known as the National Renewable Energy Laboratory. Its Wind Toolkit is: https://www.nlr.gov/grid/wind-toolkit.
[70] NLR's System Advisor Model: https://sam.nlr.gov.
[71] See Technical Appendix G - New Generating Resources in the Ninth Power Plan for more details.
[72] Reference the TSL manual.
[73] See https://transmission.bpa.gov/Business/Operations/Wind.

Figure D - 37: BPA Wind Generation[74]

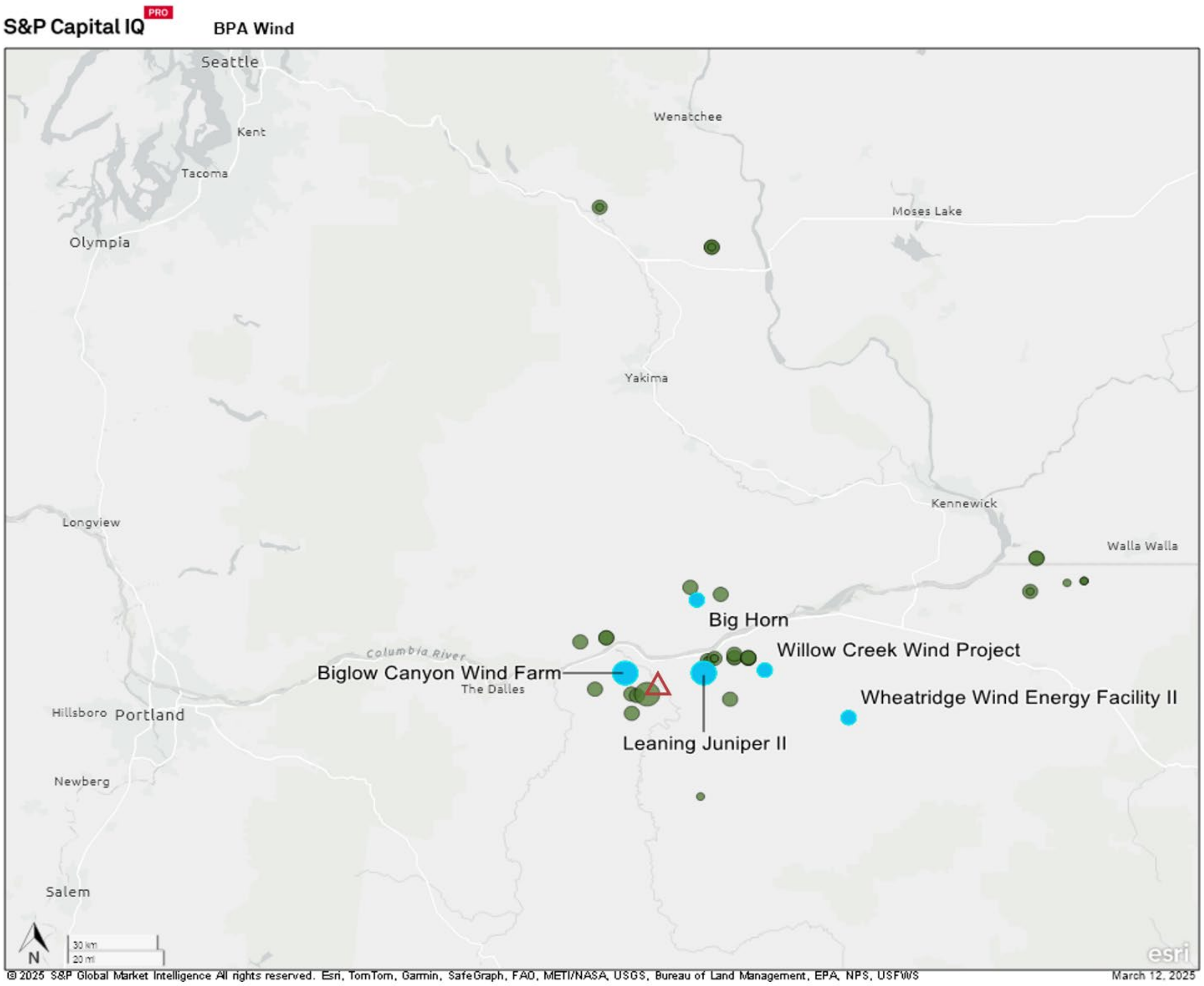

The wind farms in the BPA BA are plotted in the blue and green circles where a few are widely spread out in Figure D - 37. In contrast, the climate scenario wind data at “The Gorge,” one of the five representative wind fleets used in the Ninth Power Plan, is at a single location, plotted in the red triangle.

The various wind farms in BPA’s BA were developed over 25 years starting from 1998 to 2022, and their aggregate nameplates are listed in Table D - 19.[75] It should be noted that a few wind farms left the BPA BA between 2014 and 2022, and thus in the Aggregate Nameplate column in Table D – 19, the 2022 aggregate nameplate is less than the 2014 aggregate nameplate.

[74] S&P Global Database for 2025.
[75] See https://transmission.bpa.gov/Business/Operations/Wind/Solar_and_Wind_Nameplate_LIST.pdf.

Table D - 19: Aggregate Namplate Wind Generation in the BPA BA

Year	Aggregate Nameplate (MW)
1998	25
2006	721
2007	1,303
2014	4,782
2022	2,827

Many of the wind turbines in the various wind farms in the BPA BA were developed over the 25 years and are of different technology types and have different ages where turbines of higher ages would be less efficient in generation.[76]

The BPA aggregated wind generation capacity factors (CFs) are available from 2007 to 2024.[77] For the bias-corrected ERA5 historical wind data from 1988 to 2018, their generation CFs are calculated by the TSL model using the reference 80-m wind turbine GE 1.5 SLE,[78] which by default has no aging effect.

In Figure D - 38 below are comparisons of the distributions of capacity factors (CFs) by month between the BPA (in the light blue boxplots), historical ERA5 (light gray boxplots), and historical ERA5 with aging turbines (medium gray boxplots) for the years they have in common, from 2007 to 2018. CFs of the ERA5 with aging turbines are calculated by multiplying the CFs of ERA5 by a roughly estimated aging factor of 0.74 to reflect BPA wind turbines having higher ages and older technology. The factor 0.74 is the ratio of average BPA CF to average ERA5 CF, where the averages are calculated from their corresponding entire (or annual) distributions.

[76] See the article "*How does wind farm performance decline with age?*" in Renewable Energy 66 (2014) 775 – 786
[77] See https://transmission.bpa.gov/Business/Operations/Wind
[78] See Technical Appendix G - New Generating Resources in the Ninth Power Plan for more details.

Figure D - 38: Comparison of Bonneville and ERA5 Daily Average Wind Capacity Factors

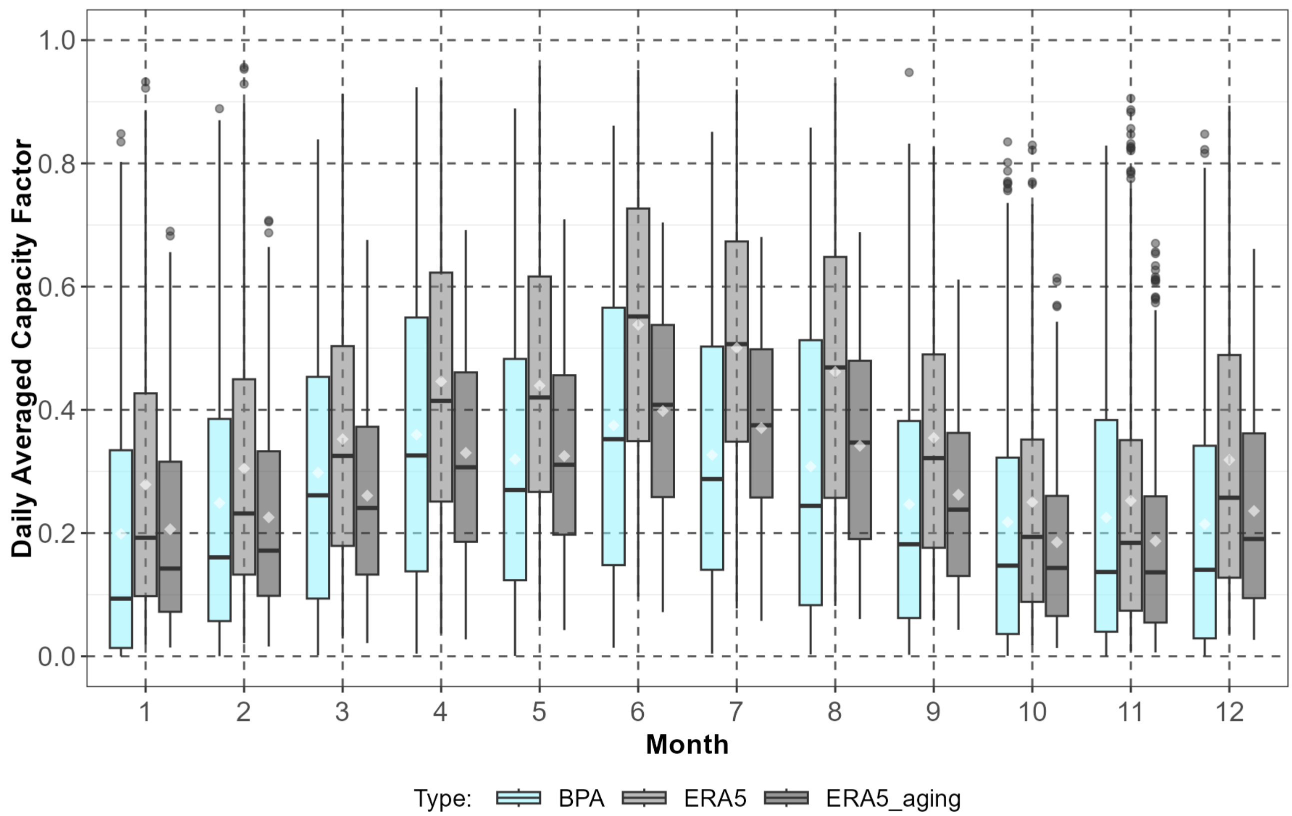

It seems that with the aging factor applied to the ERA5 CFs, their monthly distributions, plotted in the medium gray boxplots, are comparable to the BPA monthly distributions, plotted in the light blue boxplots. Furthermore, both BPA and ERA5 distributions share the seasonal shapes of having higher spring and summer CFs and lower fall and winter CFs.

For the four remaining wind fleet locations, WA, ID, MT, and WY, (see Figure D - 35 and Table D - 18), there is no publicly available observed wind data for comparison to the bias-corrected ERA5 wind data. Therefore, there is no further modification to the bias-corrected ERA5 wind data at the four locations.

Bias-Corrections of the Extrapolated CL Wind Data to the ERA5 Wind Data

There are 30 different bias-corrections of the CL climate 80-m and 100-m wind data to resemble the corresponding historical ERA5 80-m and 100-m wind data, respectively. The number of bias-corrections result from taking all combinations of the two hub-heights, five wind fleet locations, and the three climate scenarios. However, for simplicity, bias-corrections for the combination of only the 80-m hub-height, the Gorge location, and climate scenario A are presented in this section since bias-corrections for the remaining 29 combinations follow the same processes.

At the Gorge, it has been observed that for some consecutive very cold days or very warm days, wind speeds were very low, leading to lower wind generation. Moreover, if the very cold or very warm temperatures are widespread throughout the region, then the loads were also very high. These periods with very high loads but very low wind are challenging for the power system. Therefore, it is important that in the common historical years, 1988 to 2018, the CL climate wind-temperature correlations resemble those correlations in the historical ERA5 data.

Furthermore, at the Gorge, it has also been observed that the monthly wind speeds have seasonal patterns: higher during late spring and summer months, but lower during late fall and winter months. The CL wind data from 1988 to 2018 should also follow similar seasonal patterns as exhibited in the ERA5 wind generation data in Figure D - 38.

As an example, in Figure D - 39 below, at the Gorge, for the historical years 1988 to 2018, the 80-m ERA5 wind and temperature correlations are plotted in the top panel, and the wind seasonal shapes are plotted in the bottom panel.

Figure D - 39: ERA5 Wind Speed and Temperature Data at the Gorge

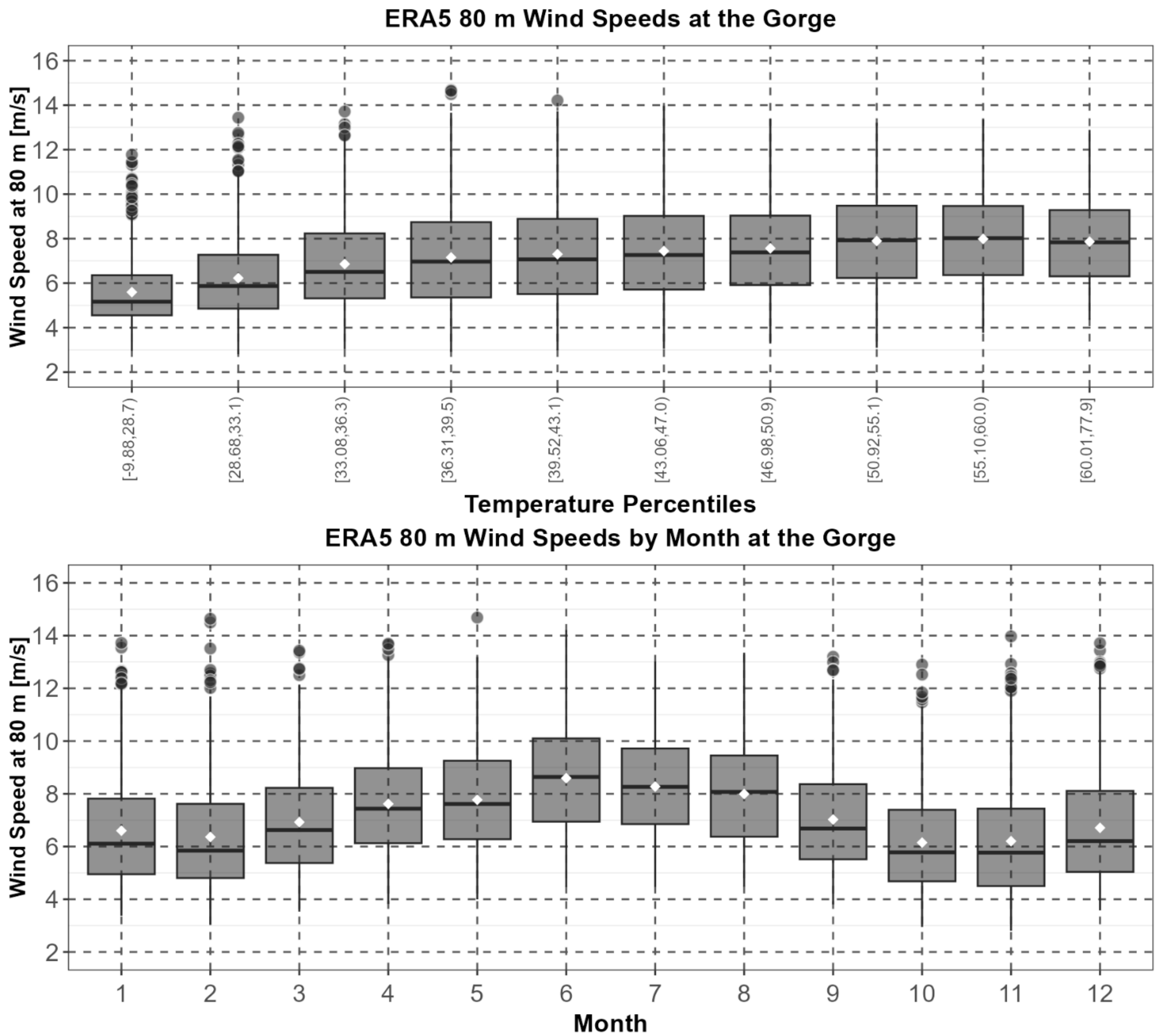

For the ERA5 wind-temperature correlations data plotted in the top panel in Figure D - 39, along the x-axis, the daily minimum temperature (a part the ERA5 climate data set embedded in the TSL model) distribution at the Gorge for 1988 to 2018 has been divided into ten equal population percentile subsets. For example, the lowest 10th percentile of the temperature distribution is inside the interval [-9.88 F, 28.7 F). On the other hand, the highest 10th percentile is inside the interval [60.01 F, 77.9 F]. The remaining eight sorted percentile subsets are in between the lowest and the highest percentile subsets. These ten percentile groups of daily minimum temperatures are plotted along the x-axis.

It is quite clear from the wind-temperature correlation plot that wind speeds for the lowest 10th percentile temperatures (at the left most boxplot) are significantly lower than the other percentile groups. On the other hand, it does not seem that wind speeds for the highest 10th percentile temperatures (at the right most boxplot) are lower than adjacent percentile groups.

For the ERA5 monthly wind speed distributions plotted in the bottom panel, the seasonal patterns are clear: higher wind speeds for late spring to summer months, and lower wind speeds for late fall to winter months.

For climate scenario A whose GCM is CanESM2, the 10-m wind speed and temperature at the Gorge were both downloaded from Climatology Lab[79] for historical years 1988 to 2018, and climate scenario years 2019 to 2049 for the Power Plan. As comparisons to the ERA5 data in Figure D - 39, the extrapolated 80-m wind and temperature correlations for climate scenario A in the historical years are plotted in the top panel of Figure D - 40, and its wind seasonal shapes are plotted the bottom panel Figure D - 40.

[79] Climatology Lab: *https://www.climatologylab.org/maca.html*.

Figure D - 40: Climate Scenario A Wind Speed and Temperature Data for the Gorge

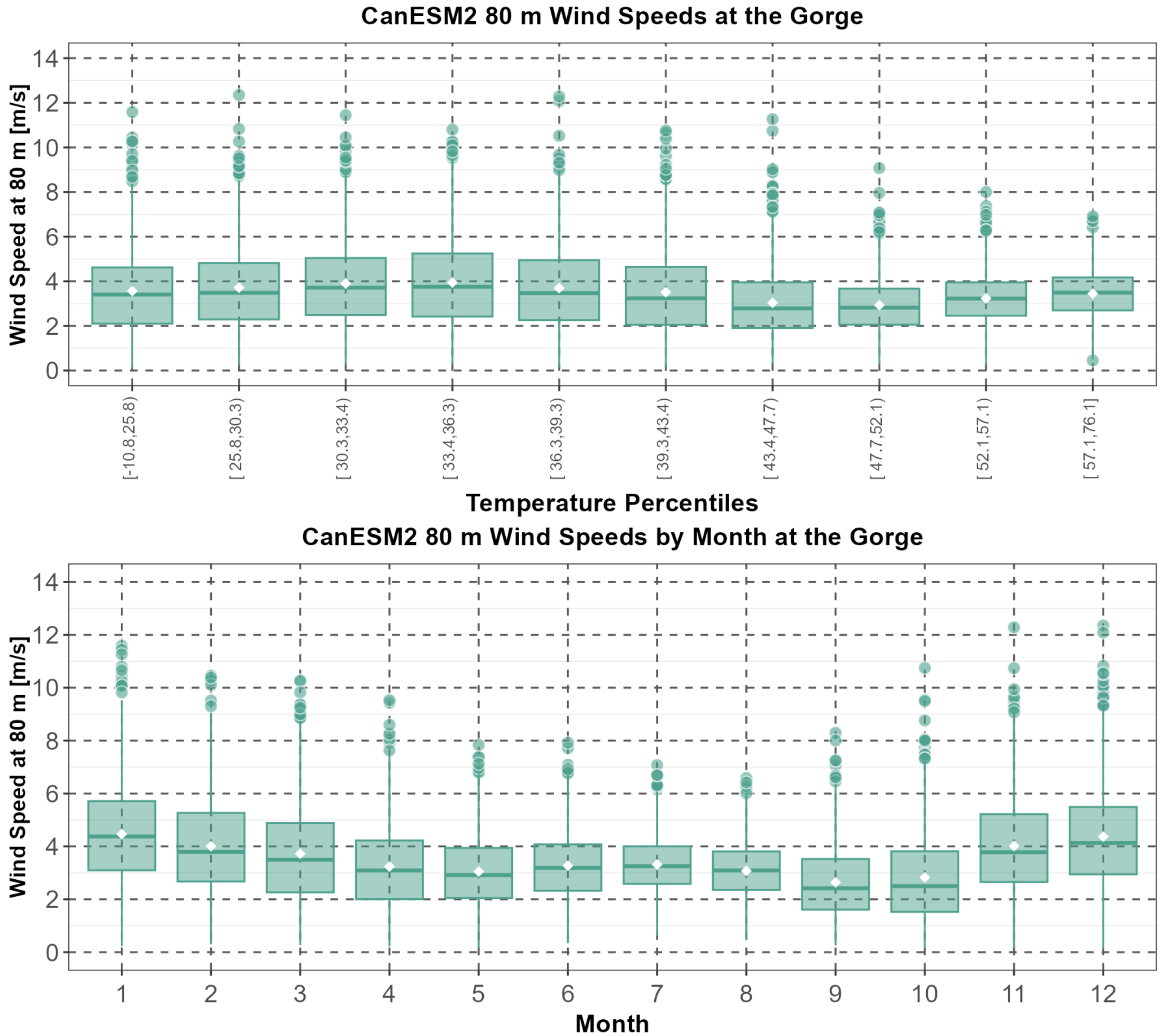

The climate scenario A wind-temperature correlations data are plotted in the top panel in Figure D - 40. They are plotted similarly to the ERA5 wind-temperature correlations data plotted in the top panel in Figure D - 39. The scenario A daily minimum temperatures along the x-axis have been divided into ten equal population percentile subsets. For example, the lowest 10th percentile of the temperature distribution is inside the interval [-10.8 F, 25.8 F). On the other hand, the highest 10th percentile is inside the interval [57.1 F, 76.1 F]. Scenario A's temperature percentiles are a couple of degrees lower than those of ERA5.

It's evident that the climate wind speed distributions in Figure D - 40 are significantly lower than those of ERA5 in Figure D - 39. Furthermore, for scenario A, the wind speed distribution at the lowest 10th percentile of temperature is not significantly lower than the other percentile groups, which does not match the correlations of ERA5.

Therefore, the wind-temperature distributions in the top panel of Figure D - 40 were bias-corrected as described in the next section to resemble those of ERA5 data.

For scenario A monthly wind speed distributions plotted in the bottom panel of Figure D - 40, its seasonal patterns seem to be opposite to those of ERA5 plotted in the bottom panel of Figure D - 39: lower wind speeds for late spring to summer months, and higher wind speeds for late fall to winter months.

Thus, the monthly wind speed distributions for scenario A were also bias-corrected to resemble those of ERA5. However, this monthly bias-correction was performed *after* the wind-temperature correlations bias-correction.

In summary, there were two bias-corrections to the climate scenario wind speed distribution, the first one to resemble the ERA5 wind speed-temperature correlations, and afterward a second one to resemble the ERA5 monthly wind speed distributions.

Bias-Correction of Climate Scenario Wind-Temperature Correlations

For the historical years 1988 to 2018, the bias-corrections of climate scenario A wind-temperature correlations to resemble the ERA5 wind-temperature correlations are performed for each of the ten temperature percentile groups separately. For example, for the lowest 10th percentile of scenario A temperatures at the left-most boxplot where the daily minimum temperatures are in interval [-10.8 F, 25.8 F) in the top panel of Figure D - 40, the scenario A wind speed distribution is bias-corrected to the corresponding ERA5 wind speed distribution for the lowest 10th percentile of ERA5 temperatures inside the interval [-9.88 F, 28.7 F) in the top panel of Figure D - 39.

The bias-correction method for the distributions is quantile delta mapping[80] (QDM) as recommended by a climate scientist consulting with the Council. The bias-corrected climate scenario A wind-temperature correlations are plotted in the bottom left panel of Figure D - 41.

The ten sets of QDM parameters used to bias-correct the scenario A wind-temperature correlations to resemble the ERA5 wind-temperature correlations for the historical years 1988 to 2018 were saved and then used to bias-correct the scenario A wind-temperature correlations for the climate scenario years 2019 to 2049, plotted in the bottom right panel of Figure D - 41.

[80] See https://medium.com/@juanmi.gutierrez/quantile-mapping-bias-correction-63ed01d5a618 for an introduction.

Figure D - 41: Comparison on Wind Speeds and Temperatures of ERA5 and Climate Scenario A Data (with and without Bias-Correction) at the Gorge

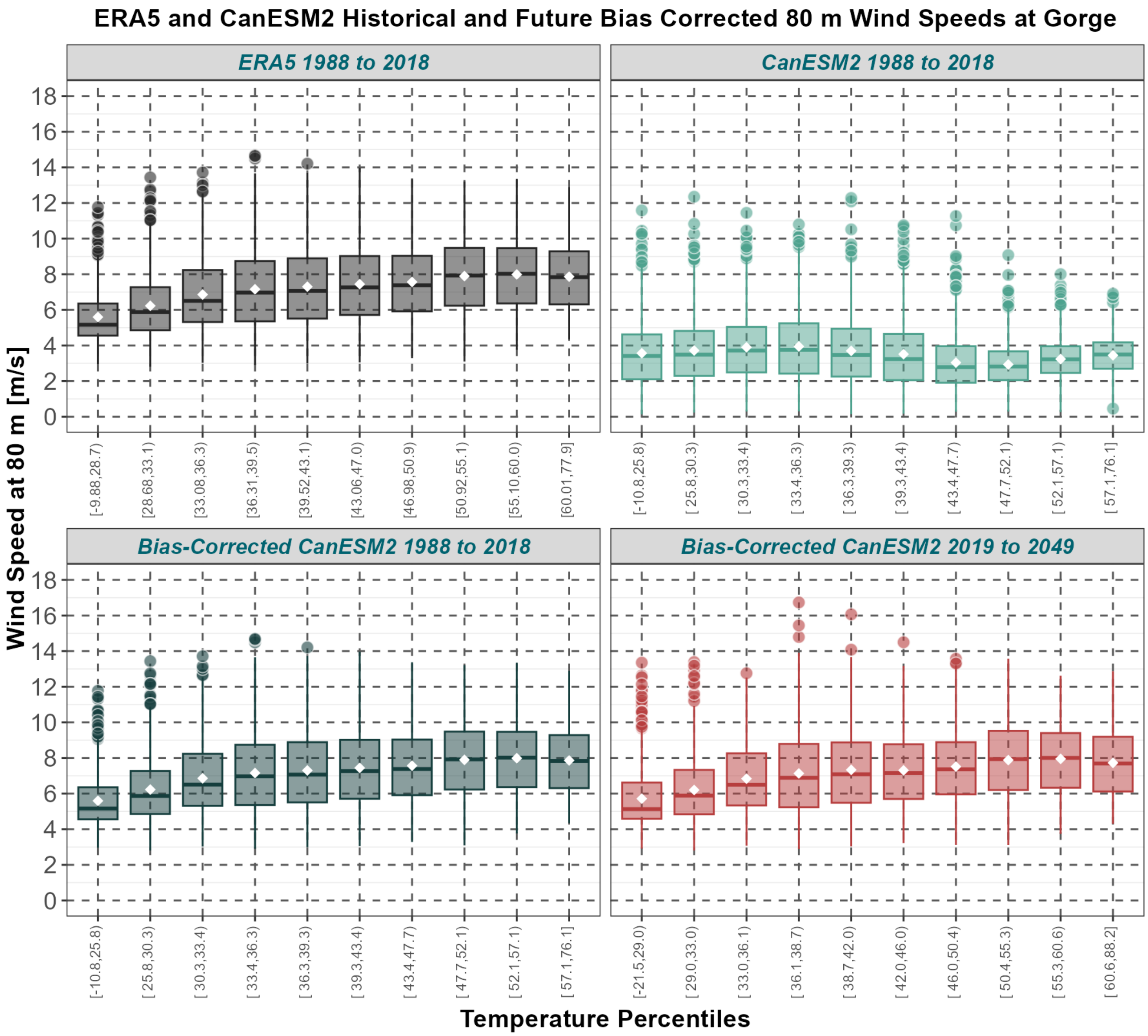

All four plots in Figure D - 41 are wind-temperature correlations. The wind speed distributions are along the y-axis versus ten daily minimum temperature percentile groups along the x-axis. The top-left panel is the ERA data for 1988 to 2018 from the top panel of Figure D - 39; the top-right panel is the (un-bias-corrected) scenario A data for climate scenario years 1998 to 2018 from the top panel of Figure D - 40. The bottom-left panel is the bias-corrected scenario A data for climate scenario years 1998 to 2018. It's evident that the bias-corrected wind-temperature correlations excellently match those of the ERA5 data in the top-left panel.

Finally, the bottom right in Figure D - 41 is the bias-corrected scenario A data for climate scenario years 2019 to 2049. Since these bias-corrected wind-temperature correlations use bias-correction parameters developed for scenario A data for climate scenario years 1998 to 2018, they do not match perfectly to the ERA5 data in the top-left panel, which is expected. The difference could be attributed to effects of climate change. Nevertheless, the ERA5 wind-temperature correlations are well preserved, especially for the lowest 10th percentile of temperatures, where the wind speed distribution is significantly lower than all other percentile groups.

Bias-Correlation of Seasonal Patterns

In Figure D - 42, the monthly ERA5 wind speed distributions in the gray boxplots are plotted with the bias-corrected (for wind-temperature correlations) scenario A for climate scenario years 1988 to 2018 in the green boxplots, and the bias-corrected scenario A for climate scenario years 2019 to 2049 in the red boxplots.

Figure D - 42: Monthly ERA5 and Bias-Corrected Climate Scenario A Wind Speeds at the Gorge

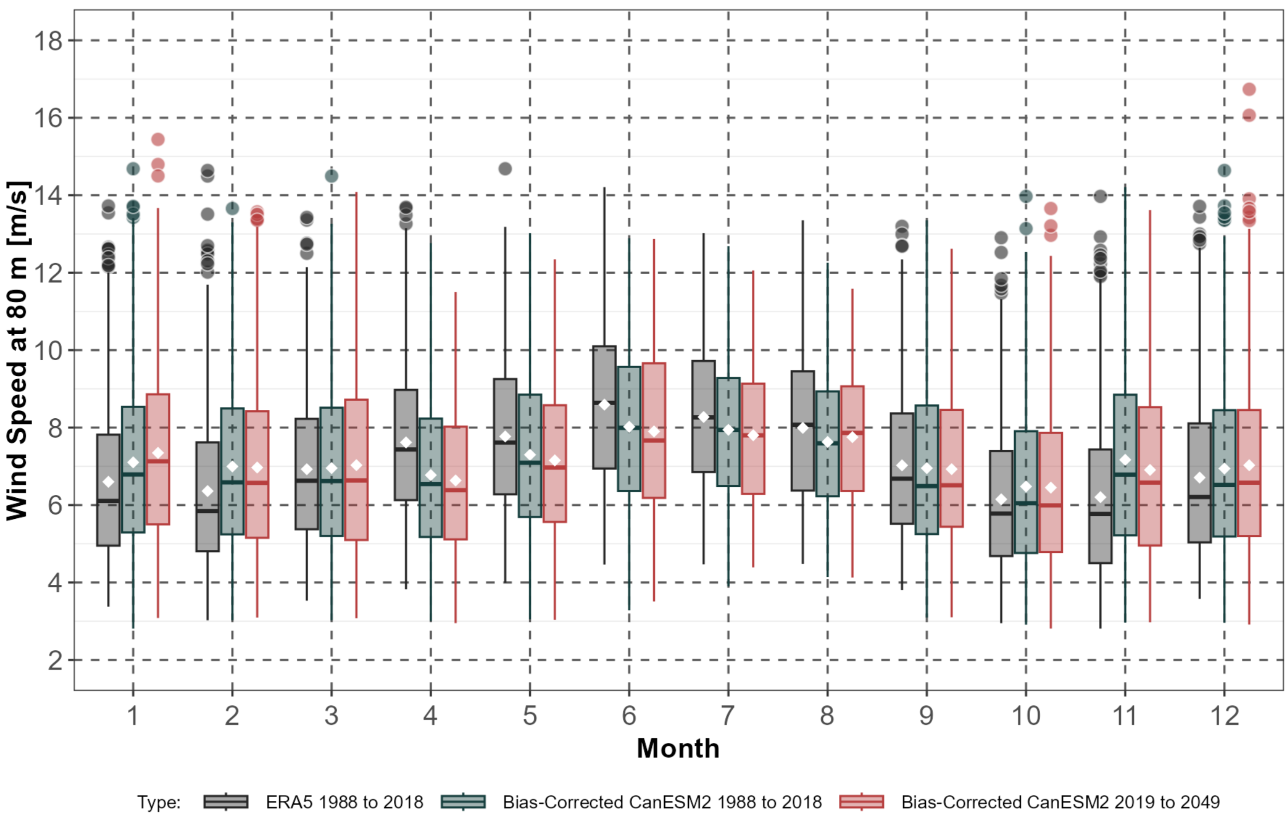

In In Figure D - 42, the bias-corrected scenario A wind speed data for the historical years 1988 to 2018 (in green boxplots) were bias-corrected to resemble the ERA5 wind speed-temperature correlations. However, after that (first) bias-correction they do not resemble the ERA5 monthly wind speeds distributions (in gray boxplots). Therefore, the bias-corrected scenario A data undergo a second bias-correction to resemble the ERA5 monthly distributions.

This monthly bias-correction was performed on each of the 12 monthly distributions separately, using a simpler method. For example, for month 1, in unit of meter/sec, the averages (e.g., the white diamonds in Figure D - 42) of the ERA5, scenario A (1988 – 2018), and scenario A (2019 – 2049) are

6.60, 7.10, and 7.35 respectively. Then the ratio of the ERA5 average to the scenario A (1988 – 2018) average is calculated, which results in the ratio $6.60/7.10 \cong 0.930$.

The (second) bias-corrections of both scenario A (1988 – 2018) and scenario A (2019 – 2049) for month 1 consist of multiplying all wind speeds in both distributions by the ratio 0.93. Similarly, bias-corrections of scenario A data for other months are performed using the same method: multiplication by the ratio of averages. Table D - 20 lists the relevant average wind speeds and ratios for all 12 months.

Table D - 20: Monthly Average Wind Speeds in [m/s] and Bias-Correction Ratios

Month	Avg ERA5 Wind Speed	Avg Scen A (1988 – 2018) Wind Speed	Ratio
1	6.60	7.10	0.93
2	6.36	7.00	0.91
3	6.93	6.95	1.00
4	7.62	6.77	1.12
5	7.77	7.30	1.06
6	8.59	8.02	1.07
7	8.27	7.94	1.04
8	7.99	7.63	1.05
9	7.02	6.95	1.01
10	6.15	6.48	0.95
11	6.20	7.17	0.87
12	6.71	6.94	0.97

The final bias-corrected monthly wind speed distributions for scenario A are plotted in Figure D - 43 below.

Figure D - 43: Final Bias-Corrected Climate A Wind Speeds at the Gorge

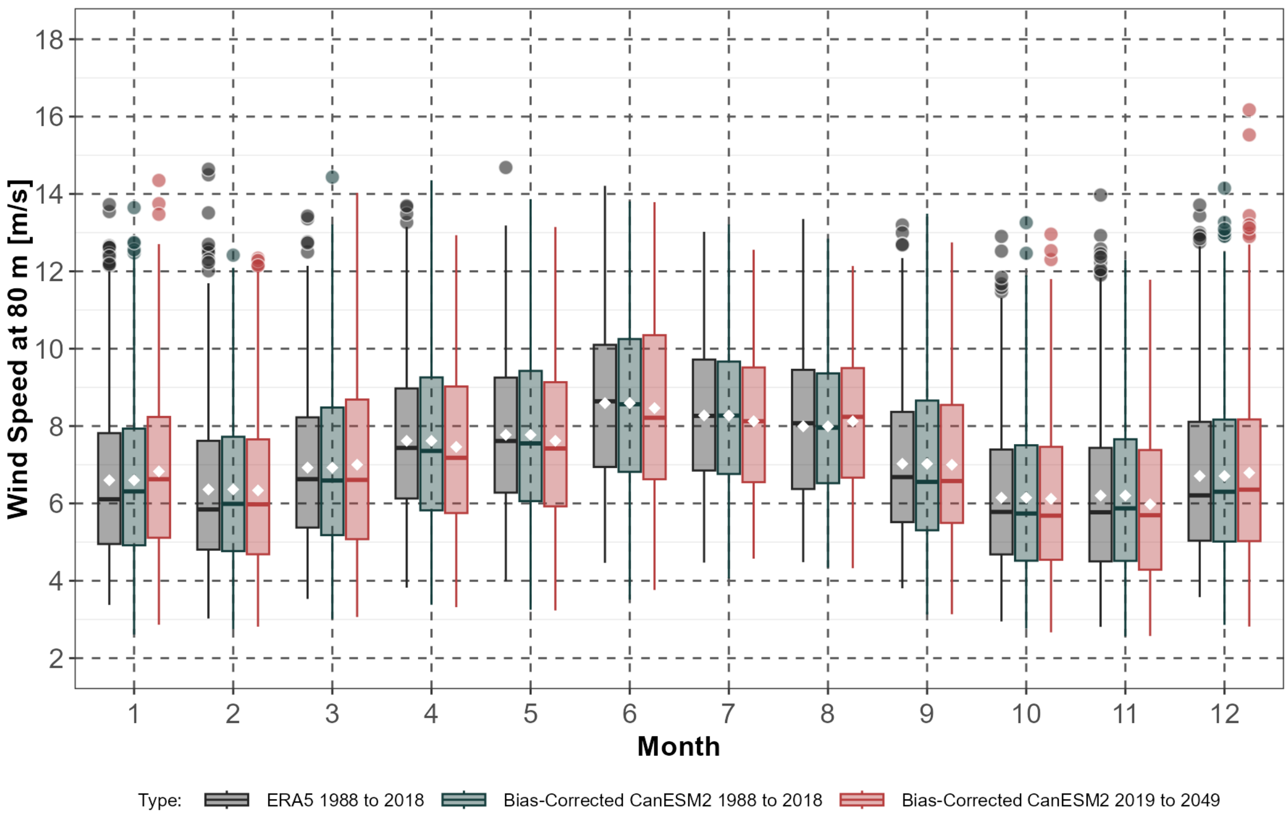

In Figure D - 43, the final bias-corrected scenario A data for the historical years 1988 to 2018 in the green boxplots resemble the ERA5 data in the gray boxplots, with their averages being exactly the same. Furthermore, the seasonal patterns in the scenario A wind speeds match the ones in the ERA5 data: lower speeds for the late fall and winter months, and higher speeds for the late spring and summer months.

Moreover, the final bias-corrected scenario A data for climate scenario years 2019 to 2049 in the red boxplots have larger differences relative to the ERA5 data in the gray boxplots. The differences could be attributed to climate change. Nevertheless, the scenario A data still retain the ERA5 seasonal patterns, and have monthly averages close to those of ERA5.

It should be noted that the additional monthly bias-corrections would degrade the excellent matching of the wind-temperature correlations of the bias-corrected scenario A data to those of ERA5, as presented in the bottom panels in Figure D - 41.

Therefore, after first undergoing wind-temperature correlation bias-correction and then monthly wind speed bias-correction, the final wind-temperature plots are presented in the bottom panels of Figure D - 44.

Figure D - 44: Wind Speed and Temperature Correlations for Final Bias-Corrected Climate A Data at the Gorge

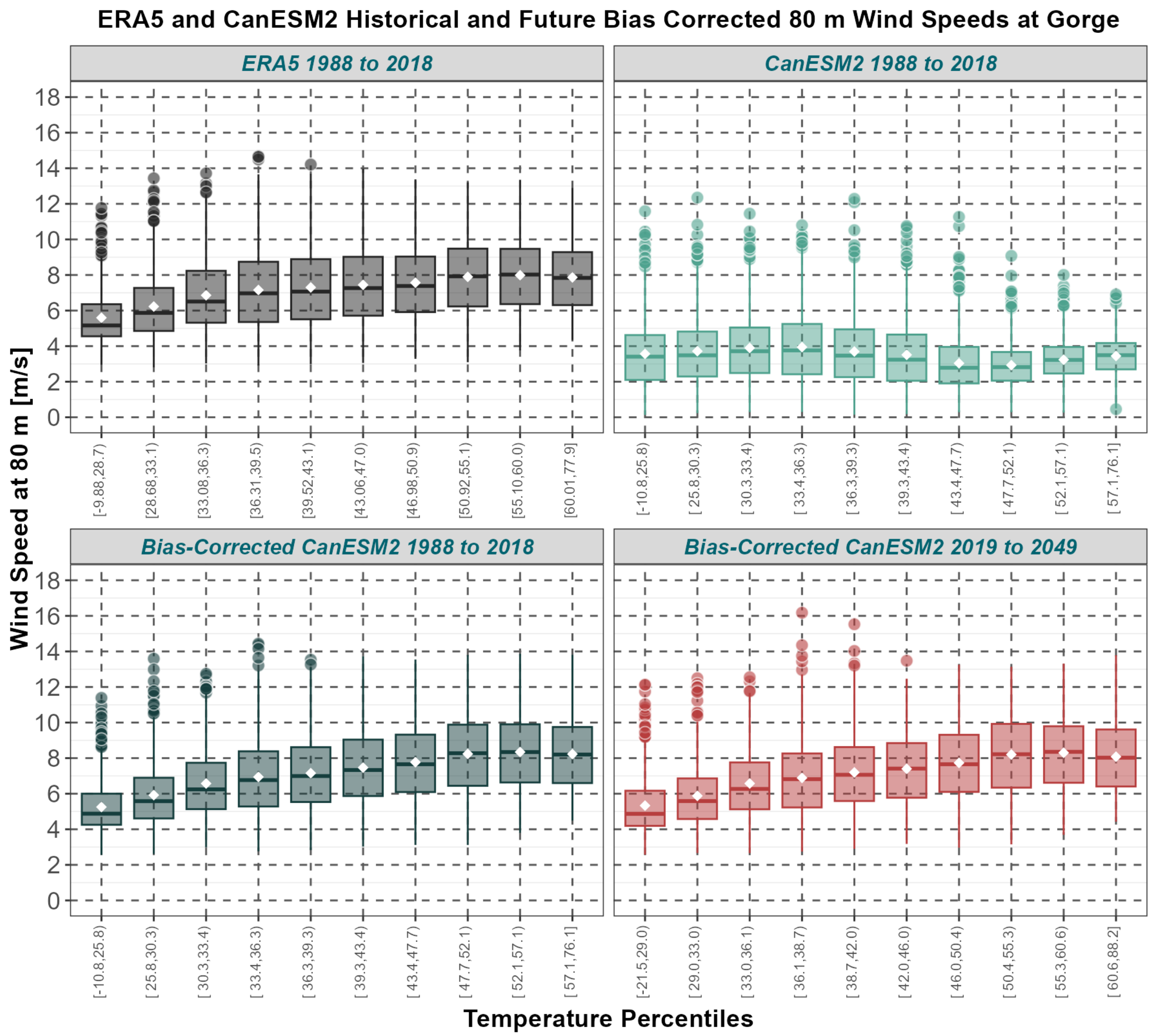

In Figure D - 44, both the scenario A (1988 to 2018) data, in the bottom-left panel, and scenario A (2019 to 2049) data in the bottom-right panel, have been bias-corrected twice: first for wind-temperature correlations, and then second for monthly wind speeds. Since the scenario A data plotted in the bottom panels of Figure D - 41 have undergone just the wind-temperature correlation bias-correction, those distributions are slightly different (and somewhat difficult to notice) than the corresponding ones in the bottom panels of Figure D - 44.

Calculating Hourly Shapes for the Bias-Corrected Daily CL Wind Data

The bias-corrected CL wind data for climate scenario years 2019 to 2049 developed in the previous section are daily averaged wind speeds. The next step is to derive hourly shapes for the daily data which then become inputs into the TSL model that calculates and outputs hourly wind generation. The hourly wind generation in turn becomes an input in the Council's models.

Given a climate calendar date and its daily averaged wind speed, its hourly shapes are derived from pairing the climate calendar date with a selected ERA5 historical calendar date that has hourly wind speeds. The hourly shape derivations are illustrated in the following two figures.

Figure D - 45: Example Wind Speeds for a Day

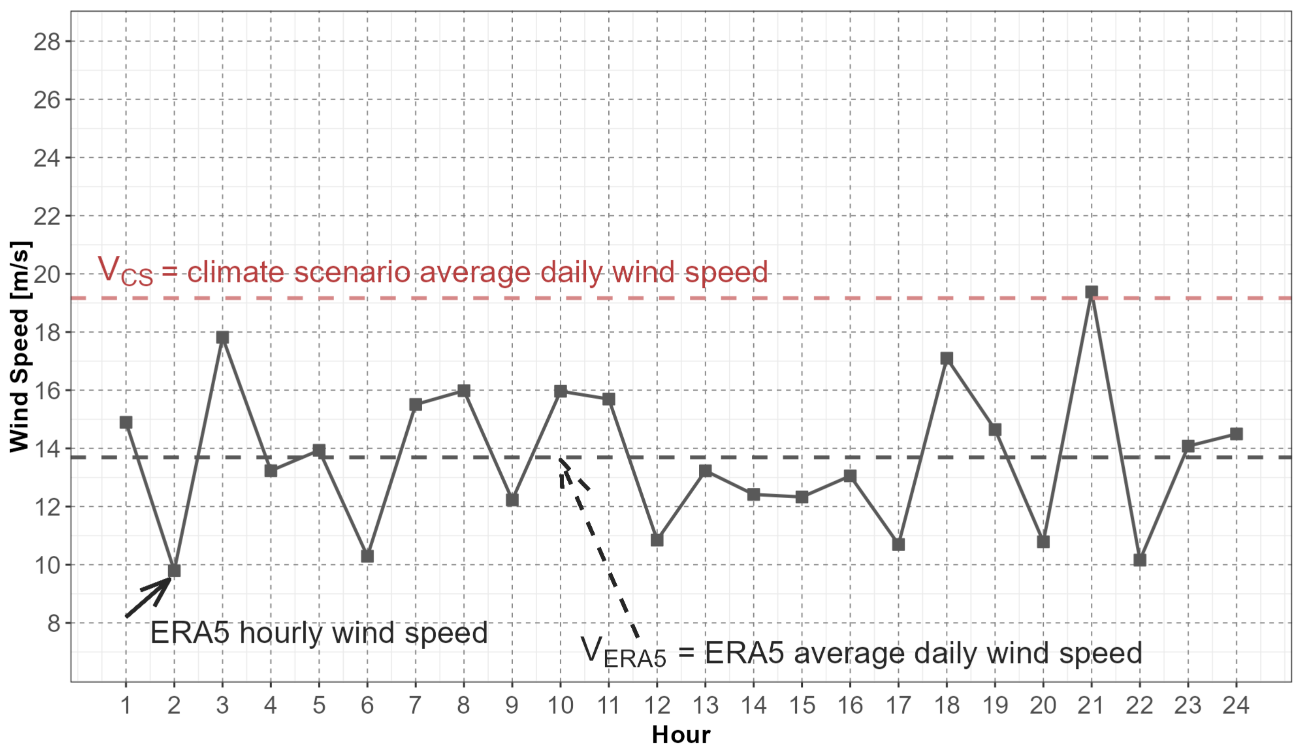

In Figure D - 45, the example climate scenario daily averaged wind speed V_{CS} is plotted as a light red horizontal dashed line. The example ERA5 24 hourly wind speeds are plotted as gray squares connected by a solid gray curve, and their daily averaged wind speed V_{ERA5} is plotted as a gray horizontal dashed line.

The ratio of the climate scenario daily averaged wind speed to the ERA5 daily averaged wind speed is defined as ratio $= V_{CS}/V_{ERA5}$. Therefore, the climate scenario 24 hourly wind speeds are calculated by multiplying this ratio to the 24 hourly ERA5 wind speeds (in the gray squares). This is illustrated in Figure D - 46 below.

Figure D - 46: Calculating Climate Scenario A Hourly Wind Speeds for an Example Day

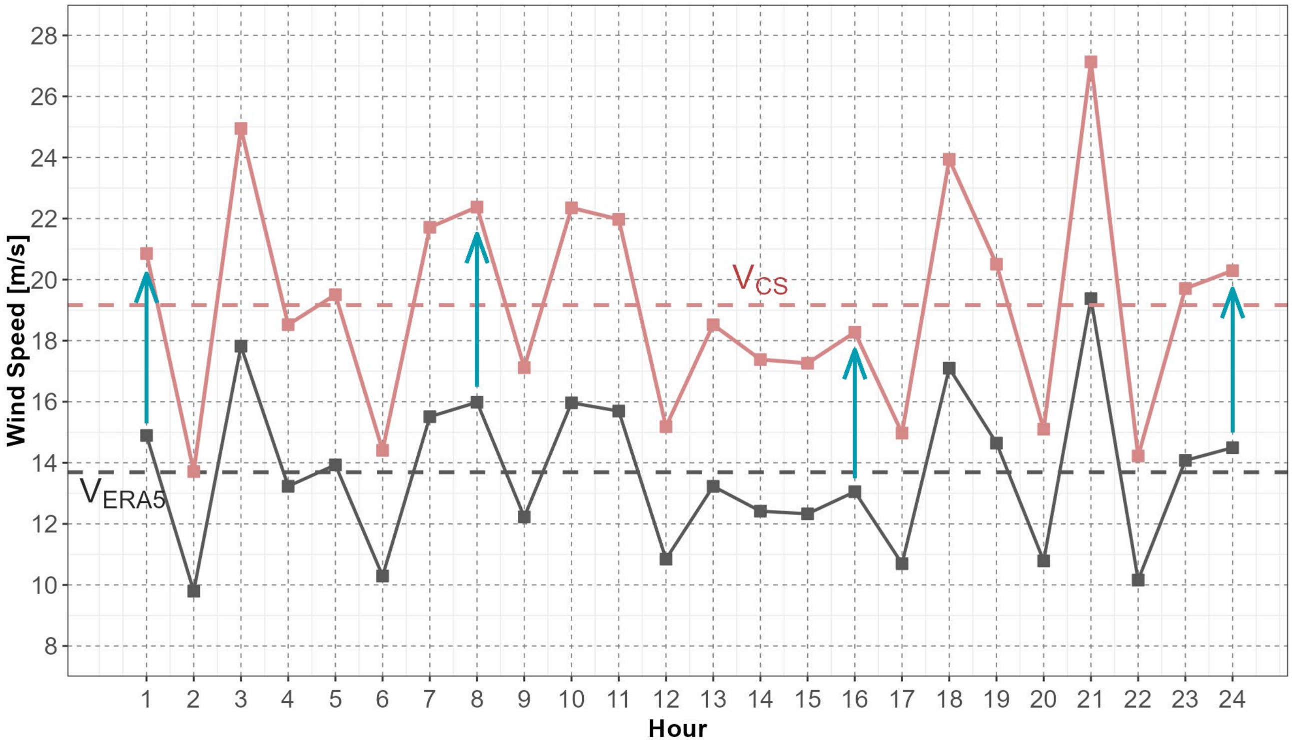

In Figure D - 46, the climate scenario 24 hourly wind speeds in the red squares are derived by multiplying the ERA5 24 hourly wind speeds in the gray squares by the ratio of the average wind speeds, V_{CS}/V_{ERA5}.

Therefore, to enable calculations of climate scenario hourly wind speeds as illustrated here, a method was developed to select an ERA5 historical date (with its corresponding 24 hourly wind speeds) to pair with a given climate scenario calendar date. Given that the climate scenario wind data used in the Ninth Plan cover climate scenario years 2019 to 2049, and the recent ERA5 historical data cover years 1988 to 2018, a few methods were considered.

Ultimately, a method suggested by a climate scientist consulting with the Council is adopted based on assuming the hourly wind shapes could be correlated to properties of the daily averaged wind speeds. The first assumption is that since the daily average wind speeds are correlated with temperature percentiles as presented in Figure D - 44, then perhaps the hourly wind shapes could also be correlated to the temperature percentiles. In Figure D - 47 below the ERA5 and scenario A (2019 to 2049) wind-temperature correlation plots are copied from Figure D - 44.

Figure D - 47: ERA5 and Final Climate Scenario A Wind Speeds at the Gorge

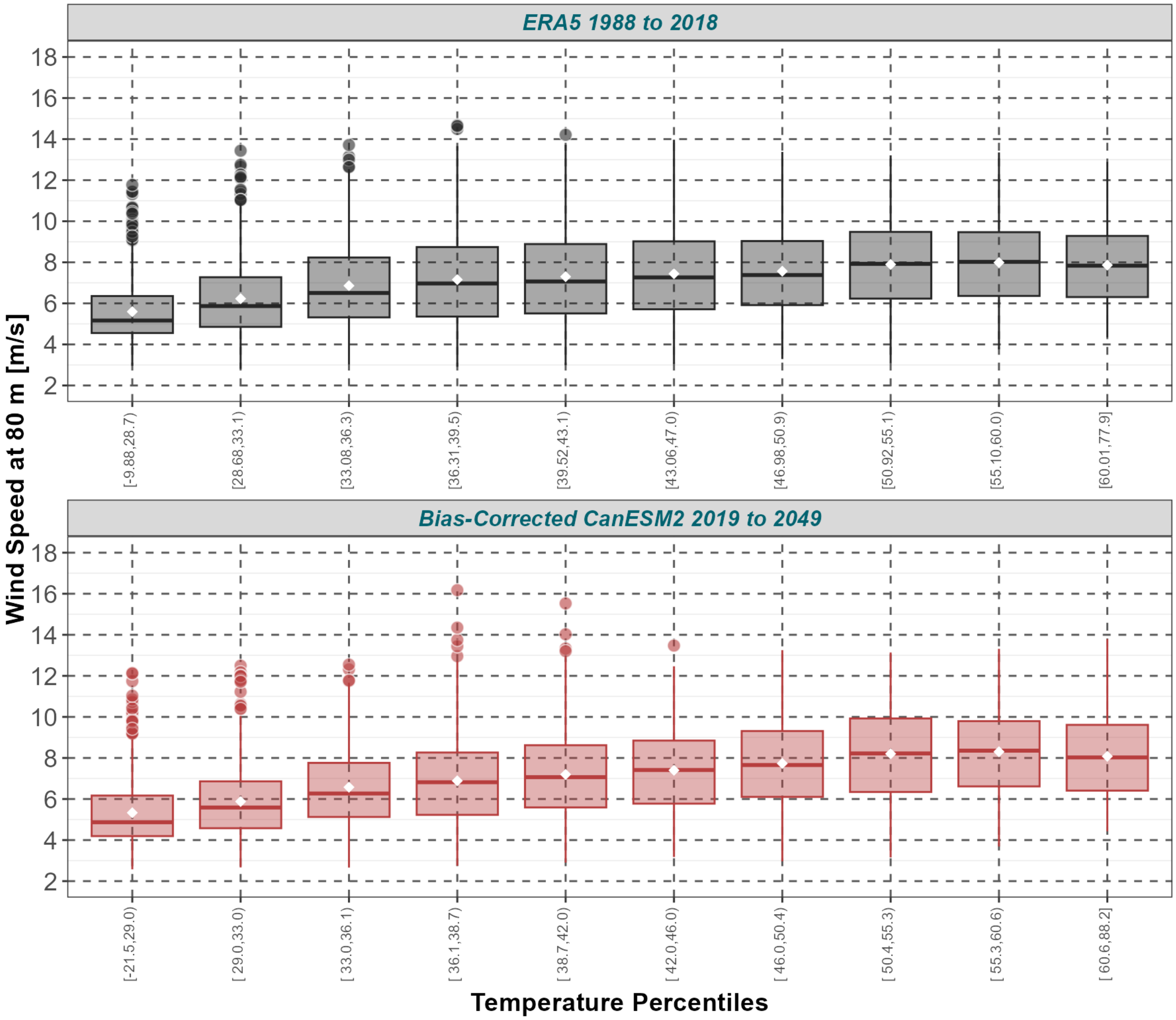

Figure D - 47 shows that daily average wind speeds are lower for the very low temperature percentiles on the left side of the plots. Then perhaps hourly wind shapes for those low temperature percentiles could be different than those for the higher temperature percentiles. Therefore, pairing a climate scenario date with a selected ERA5 historical date is done for each of the ten temperature percentile groups separately.

For example, climate scenario dates in the left-most red boxplot where the climate scenario temperatures are in the interval [-21.5 F, 29.0F) are paired only with the ERA5 historical dates in the left-most gray boxplot where the ERA5 temperatures are in the interval [-9.88 F, 28.7 F). Within the left-most red boxplot and gray boxplot, the distributions of daily averaged wind speeds range from a maximum of around 12 m/s to a minimum of around 2 m/s.

The second assumption is that perhaps the higher and lower wind speeds of the distributions could have different hourly shapes. Therefore, for these two left-most boxplots, pairing a climate scenario date with a selected ERA5 historical date is done by the rank of the wind speeds. More specifically, the climate scenario date with the highest wind speed is paired with the ERA5 historical date with the highest wind speed. Next, the climate scenario date with the second highest wind speed is paired with the ERA5 historical date with the second highest wind speed, and so on. Figure D - 48 below illustrates the date-pairing process.

Figure D - 48: Wind Speed Pairing Process for Developing Hourly Shapes

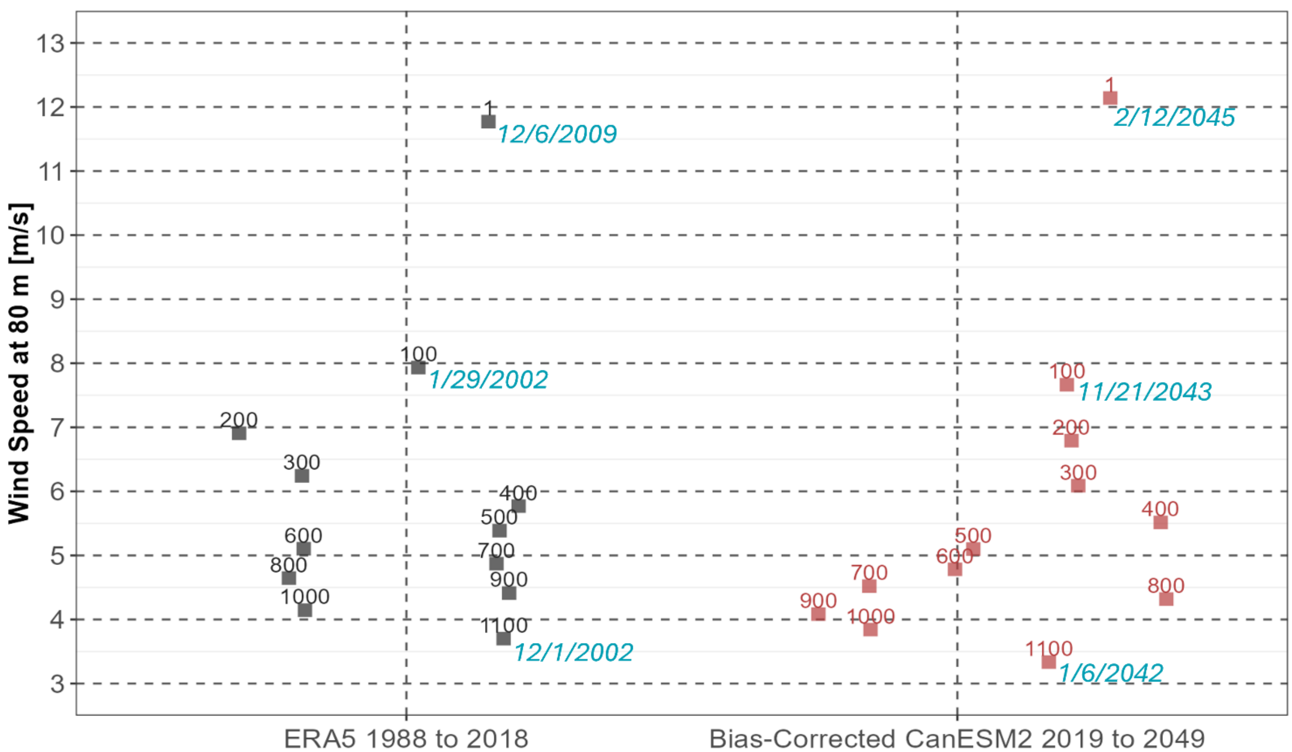

For the 31 years of ERA5 (1988 to 2018) data and scenario A (2019 to 2049) data, there are 11,323 daily average wind speed data. Therefore, the lowest 10th percentile of the daily minimum temperatures has 1,133 daily data, which are still too many to be plotted in a figure.

Thus, in Figure D - 48, only 12 sample ranks (out of a total of 1,133 ranks) of wind speeds are plotted for the ERA5 and scenario A (2019 to 2049) data. The sample ranks are (1, 100, 200, ..., 1100) where rank-1 represents the highest wind speed, and rank-1100 represents wind speed near the minimum. The rank number is plotted on top of the corresponding square. For example, the rank-1, rank-100, and rank-1100 ERA5 wind speeds in units of m/s are 11.8, 7.9, and 3.7 respectively, and plotted in the gray squares on the left side. The rank-1, rank-100, and rank-1100 scenario A (2019 to 2049) wind speeds are 12.1, 7.7 and 3.3 respectively, and plotted in the red squares on the right side.

Furthermore, for the ERA5 data on the left side, the historical dates corresponding to rank-1, rank-100, and rank-1100 wind speeds are 12/6/2009, 1/29/2002, and 12/1/2002 respectively. For the scenario A (2019 to 2049) data, the climate scenario dates corresponding to rank-1, rank-100, and rank-1100 wind speeds are 2/12/2045, 11/21/2043, and 1/6/2042, respectively. Of course, historical and climate scenario dates exist for other wind speeds in Figure D - 48, but only these few dates are plotted to avoid over-crowding.

Thus, for the rank-1 speeds, climate scenario date 2/12/2045 is paired with ERA5 historical date 12/6/2009; for the rank-100 speeds, climate scenario date 11/21/2043 is paired with ERA5 historical date 1/29/2002; and for the rank-1100 speeds, climate scenario date 1/6/2042 is paired with ERA5 historical date 12/1/2002. Date pairings between climate scenario dates and ERA5 dates are also performed for the remaining wind speeds in Figure D - 48, and furthermore, for all remaining 1,127 ranks of wind speeds in the left-most boxplots of Figure D - 47 that are not explicitly plotted in the Figure D - 48.

The same pairing process is also applied to the remaining 9 temperature percentile boxplots in Figure D - 47, and thus completing the pairings of all scenario A climate scenario dates with specific ERA5 historical dates. Moreover, by pairing a scenario A climate scenario date with a selected ERA5 historical date, it enables the 24 hourly ERA5 wind speeds (on that ERA5 date) to be used to calculate the 24 hourly scenario A wind speeds on that paired climate scenario date, as discussed previously.

At the end of this process, hourly winds for all scenario A (2019 to 2049) data are calculated.

This methodology for estimating climate scenario hourly wind speed was presented to CWAC. While some members suggested a few analyses to evaluate how well the GCMs simulate climate scenario wind speed data, they did not have any objection to the methodology.

Climate Scenario Hourly Wind Generation

Although examples in the previous sections are for the combination of only the 80-m hub-height, the Gorge location and climate scenario A, the same bias-correction and hourly wind speed calculation processes have also been applied to all remaining combinations of two hub-heights, five in-region locations, and three climate scenarios.

Therefore, the CL climate scenario hourly wind speed data for 2019 to 2049 at turbine hub-heights of interest are available as inputs into the TSL model to calculate wind generation for a set of specified turbine parameters. The monthly aggregate (A, C, G) climate scenario hourly wind generation CFs for the five in-region locations, the Gorge (GO), southeast Washington (WA), Idaho (ID), Montana (MT) and Wyoming (WY) are plotted in Figure D - 49 for the reference 100-m wind turbine, Vestas v112-30.

1 **Figure D - 49: Final Monthly Aggregate Wind Speeds for 100 M Wind Turbine**

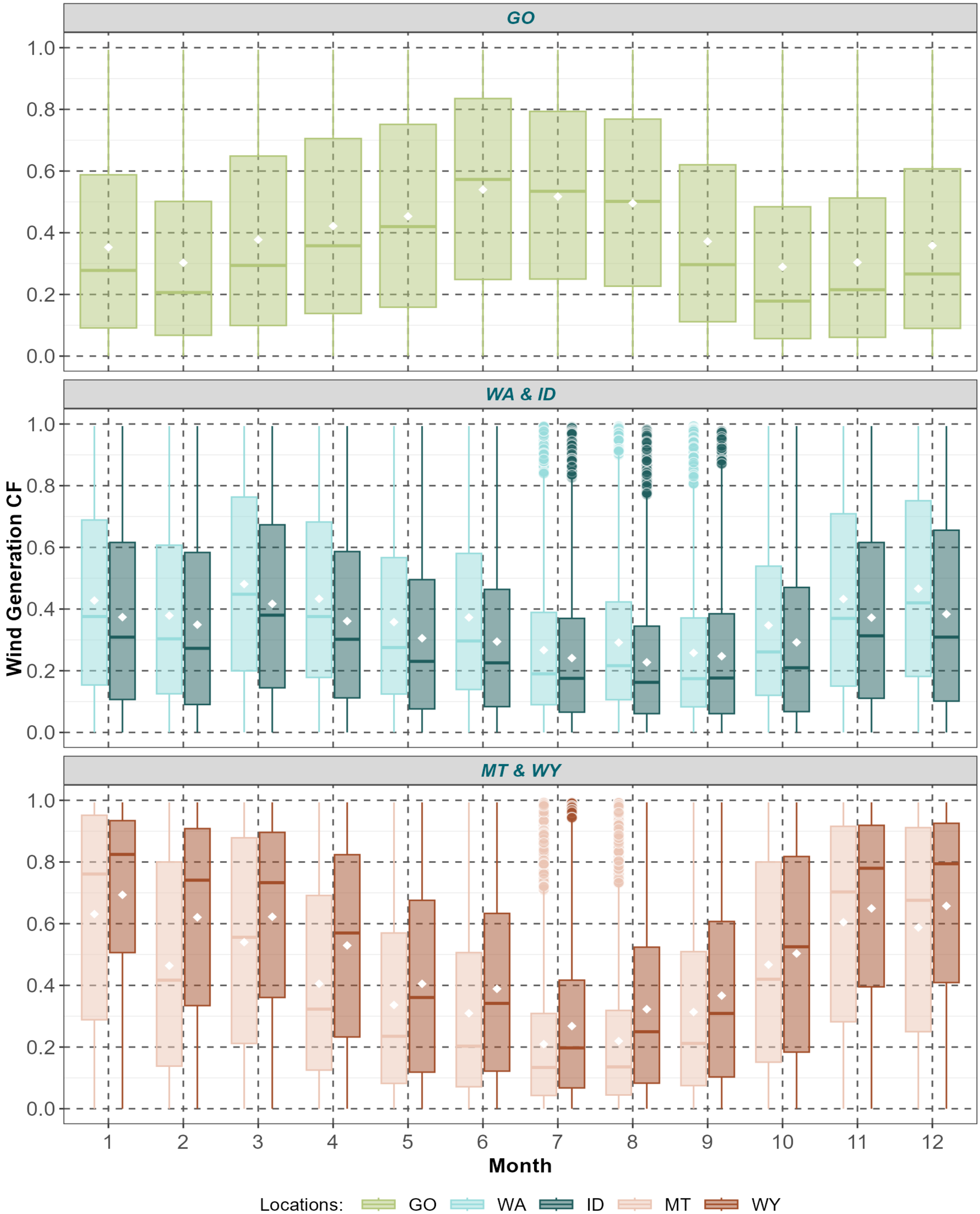

2

In Figure D - 49, the aggregate (A, C, G) climate scenario wind generation CFs for the 100-m hub height Vestas v112-30 turbine are plotted along the y-axis as boxplots with the months along the x-axis. CFs for the five in-region wind fleet locations, the Gorge (GO), southeast Washington (WA), Idaho (ID), Montana (MT) and Wyoming (WY), have different seasonal patterns and thus are plotted in different panels.

In the top panel, the Gorge (GO) CFs are plotted in the light green boxplots and they reflect the same seasonal patterns of scenario A (2019 to 2049) in the red boxplots of Figure D - 43: lower for the late fall and winter months, and higher for the late spring and summer months.

In the middle panel, the southeast Washington (WA) and Idaho (ID) CFs are plotted in the light teal and green boxplots respectively. Their seasonal patterns are lower for months of July, August, and September, and higher for other months.

Finally, in the bottom panel, the Montana (MT) and Wyoming (WY) CFs are plotted in the light red and darker red boxplots respectively, and the seasonal patterns seem to be opposite to those of the Gorge (plotted in the top panel): higher for the late fall and winter months, and lower for the late spring and summer months. In general, the complementary seasonal patterns of the Gorge, and the Montana and Wyoming group are beneficial for the power system since it is less likely to have low seasonal wind generation region wide.

Table D - 21 below lists the averages (i.e., the white diamonds inside the boxplots) of the wind CFs for the 100-m hub height Vestas v112-30 turbine for the five wind fleet locations.

Table D - 21: Monthly Average Aggregate Climate Scenario (A, C, G) Wind CFs

Month	1	2	3	4	5	6	7	8	9	10	11	12
GO	0.35	0.30	0.38	0.42	0.45	0.54	0.52	0.50	0.37	0.29	0.30	0.36
WA	0.43	0.38	0.48	0.43	0.36	0.37	0.27	0.29	0.26	0.35	0.43	0.47
ID	0.37	0.35	0.42	0.36	0.31	0.29	0.24	0.23	0.25	0.29	0.37	0.38
MT	0.63	0.46	0.54	0.41	0.34	0.31	0.21	0.22	0.31	0.47	0.60	0.59
WY	0.69	0.62	0.62	0.53	0.41	0.39	0.27	0.32	0.37	0.50	0.65	0.66

In Table D - 21, the maximum monthly average wind CF is 0.69 for the WY wind fleet for January. The minimum monthly average wind CF is 0.21 for the MT wind fleet for July.

The annual average wind CFs for the five wind fleet locations are listed in
Table D - 22 below.

Table D - 22: Annual Average Aggregate Climate Scenario (A, C, G) Wind Capacity Factors

Wind Fleet Locations	Annual Average
GO	0.399
WA	0.376
ID	0.322
MT	0.424
WY	0.502

The highest and lowest overall wind CFs are the WY wind fleet at 0.502 and the ID wind fleet at 0.322, respectively.

The wind CFs for all three climate scenarios, A, C, and G were plotted in aggregate in Figure D - 49. Nevertheless, the CFs for each separate climate scenario look very similar to these aggregates. The reason is that, at each of the five wind fleet locations for each of the three climate scenarios, the various bias-corrections discussed previously are applied to the climate wind speed data in the historical time-period, the years 1988 to 2018, to resemble the ERA5 historical wind data. Therefore, all three bias-corrected climate scenario wind data for years 1988 to 2018 resemble very closely the same ERA5 historical wind data. Furthermore, the same bias-correction parameters developed for the historical time-period are also applied to climate scenario wind data for years 2019 to 2049. Thus, the three bias-corrected climate scenario wind speed data for years 2019 to 2049 also somewhat resemble the same ERA5 historical wind data, just not to the same degree as the climate data in the historical period, from 1988 to 2018. As an example, see Figure D - 43 and Figure D - 44 for data at the Gorge location for climate scenario A.

Very Low Wind Generation

It is prudent to analyze the frequency and duration of very low wind generation since power system planners would have to develop a program to acquire sufficient and economical generation from other sources to meet load. Even though there is no standard definition of very low wind generation, this analysis assumes wind generation is low when the daily average capacity factor (CF) is less than or equal to the 10th percentile of the distribution of all daily average CFs.

For simplicity, let the 10th percentile of all daily average CFs be represented by CF_{10}, and let those days where their CFs $\leq CF_{10}$ be referred to as low-CF days. For the five wind fleet locations, their CF_{10}'s are listed in Table D - 23 below.

Table D - 23: The 10th Percentiles of the Distributions of Daily Average Wind CFs Calculated from The Hourly CFs for the GO, WA, ID, MT, and WY Wind Fleet locations

10th Percentiles of CFs	GO	WA	ID	MT	WY
$\boldsymbol{CF_{10}}$	0.085	0.111	0.069	0.089	0.129

For the aggregate 93 climate scenario years, resulting from the three climate scenarios each having 31 climate scenario years, there are a total of 33,945 days of daily average CFs. Therefore, the number of days where their daily average CFs $\leq CF_{10}$ is about 3,395, depending on the number of ties. Furthermore, for each of the five wind fleet locations, there are about the same number of low-CF days, 3,395. However, there are only 11 low-CF dates common to all five wind fleets, where on those common dates, the daily average CFs of all five wind fleets are less than or equal to their respective CF_{10}'s listed in Table D - 23. Therefore, the probability for a day where the entire in-region daily average wind generation is very low is $11/33{,}945 \cong 0.00032$, which is quite small.

However, instead of analyzing the total number of low-CF days or dates for all 93 climate scenario years, a more interpretable quantity could be the average number of low-CF days per year. For example, for all five wind fleet locations, the average number of low-CF days is $(3{,}395\ \text{days})/(93\ \text{years}) \cong 36.5$ days per year (where the daily average CF $\leq CF_{10}$). Furthermore, the average number of low-CF days common to all five wind fleets farm is $(11\ \text{days})/(93\ \text{years}) \cong 0.12$ days per year.

Since 0.12 days per year is less than 1 day per year, then the reciprocal is, $1/(0.12\ \text{days per year}) \cong 8.45$ years per low-CF day. In other words, for all five wind fleets simultaneously having one common low-CF day, the frequency is on average once every 8.45 years.

In the top panel of Figure D - 50 below, the average number of low-CF days per year for the five wind fleet locations are plotted.

Figure D - 50: Low Wind Events in Climate Scenario Wind Profiles

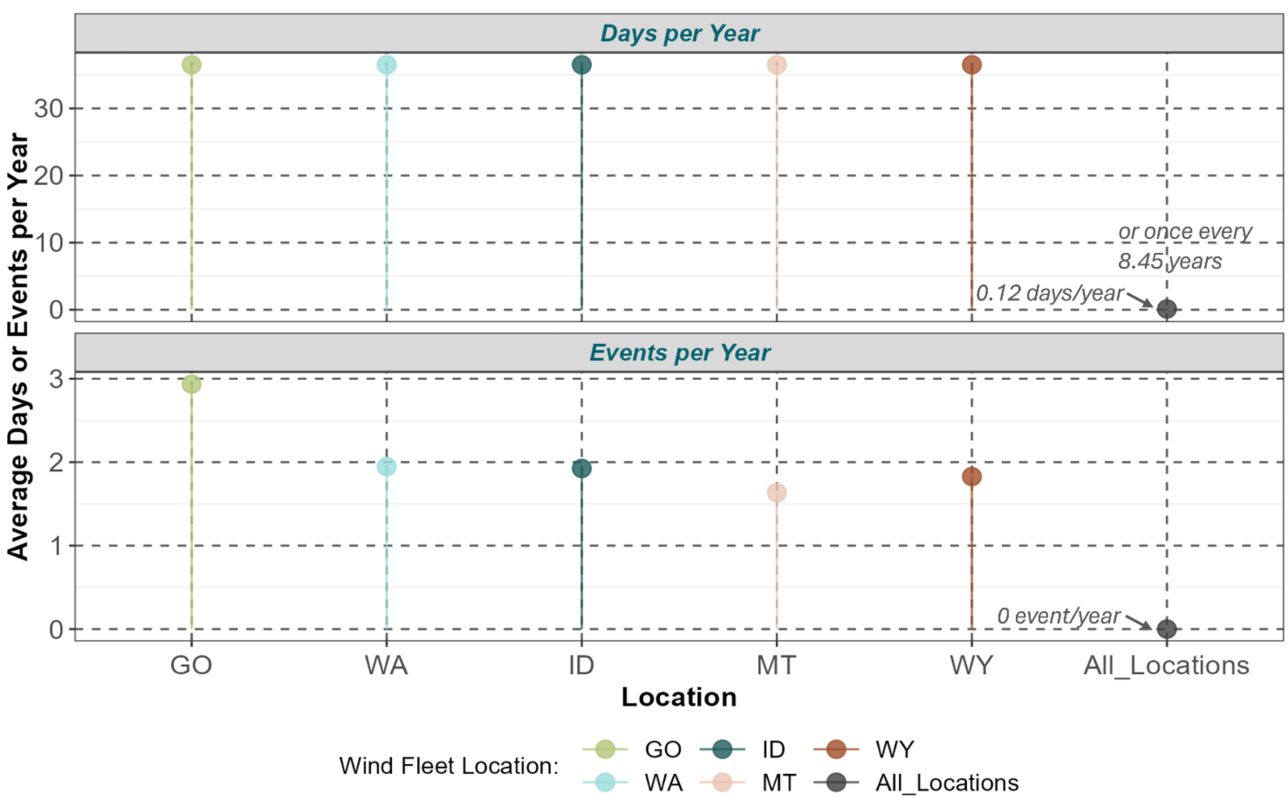

There are on average 36.5 low-CF days per year for each of the five wind fleet locations: GO (light green circle), WA (blue circle), ID (dark green circle), MT (light red circle) and WY (dark red circle), listed from left to right on the x-axis. Furthermore, on average only around 0.12 common low-CF days per year for all five wind fleet locations, plotted in the gray circle on the right side.

Among these low-CF days could be subsets of three-or-more consecutive low-CF days, which are conditions under which it is even more challenging to operate the power system to meet load. Let each set of three-or-more consecutive low-CF days be referred to as a low-CF event. For example, for the GO wind fleet, among the 3,395 total low-CF days, there are 273 low-CF events.

In terms of average number of low-CF events per year, for the GO wind fleet, it is $(273 \text{ events})/(93 \text{ years}) \cong 2.94$ average number of events per year. In the bottom panel of Figure D - 50 above, the average number of low-CF events per year for the five wind fleet locations and for All-Locations are plotted. Going from left to right on the x-axis, the values are: GO (light green circle) 2.94; WA (blue circle) 1.95; ID (dark green circle) 1.92; MT (light red circle) 1.63; WY (dark red circle) 1.83; All-Locations (gray circle) 0. Therefore, the entire (in-region) wind fleet does not have very low generation that lasts for 3 or more days.

Climate Scenario Solar Generation Profiles

Climate scenario solar radiation data, like the climate scenario wind speed data, are not included in the RMJOC data sets, but climate solar data from compatible scenarios are also available from the Climatology Lab (CL) at the University of California, Merced.[81]

However, during the Climate and Weather Advisory Committee meeting,[82] climate scientists suggested that the GCMs, due to the coarse grid size, could not model very well cloud cover over a fine spatial-scale area such as those occupied by solar farms. Because of this limitation, the climate scenario solar radiation data, specifically the Surface Downwelling Shortwave Radiation equivalent to the global horizontal irradiance (GHI), should not be used to calculate solar generation. Instead, some climate scientists suggested using historical solar radiation data to calculate solar generation.

The historical solar data readily available is the 44 years of ERA5 climate data, from 1980 to 2023, embedded in the Time Series Lab (TSL) model. For the solar farm locations selected for the Ninth Power Plan, the synthetic historical solar GHI data are downloaded from the National Solar Radiation Database (NSRDB).[83] Then for selected reference solar panels, their solar CF profiles are calculated by NLR's SAM and used by TSL to bias-correct the ERA5 solar CFs and solar GHI data.

[81] Climatology Lab: *https://www.climatologylab.org/maca.html*.
[82] Discussions during the Climate and Weather Advisory Committee Meeting on 12/04/2024: https://www.nwcouncil.org/meeting/climate-and-weather-advisory-committee-2024-12-04.
[83] See https://nsrdb.nrel.gov/data-viewer.

In-Region Solar Generation Profiles

For the Ninth Power Plan, the Council developed in-region solar generation profiles based on three locations[84] plotted in Figure D - 51 below.

Figure D - 51: Solar Locations for Developing Generation Profiles Assumed in Ninth Power Plan

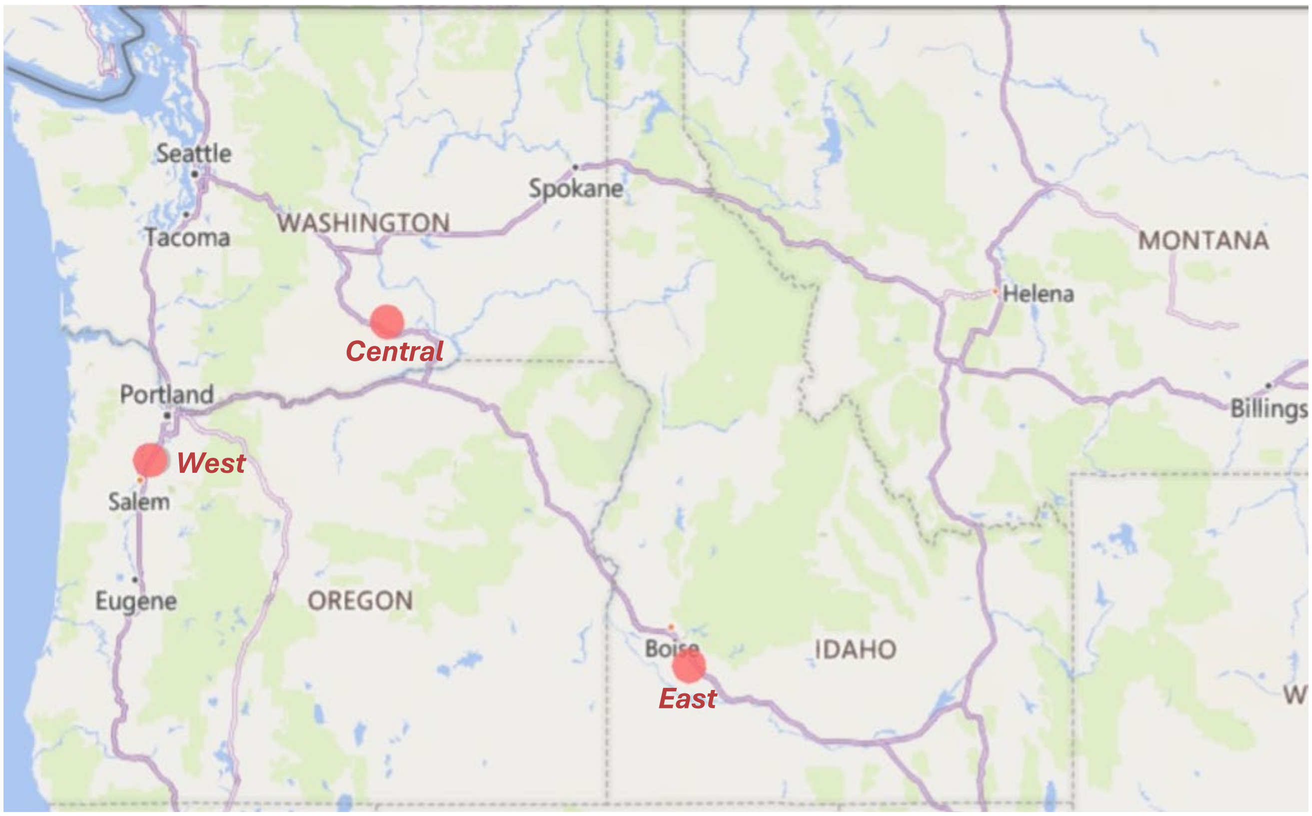

For simplicity, the three simulated solar farms are referred to as the "West", which is located near Portland; the "Central", which is in south central Washington; and the "East", which is located near Boise. More specifically, the latitude and longitude coordinates of the three locations are listed in Table D - 24.

Table D - 24: The Three In-Region Solar Farm Locations Simulated in the Power Plan

Locations	Latitude	Longitude
West	45.128	-122.828
Central	46.324	-119.822
East	43.304	-115.989

[84] See Technical Appendix G - New Generating Resources in the Ninth Power Plan for more details.

There are two types of solar panels used in the Power Plan modeling: the fixed-axis and 1-axis, both with the same "DC to AC" ratio of 1.4.[85] Furthermore, at each of the three locations, both types of solar panels have the same tilt parameter which is the latitude.

Methodology for Developing In-Region Solar Generation Profiles

As discussed in a previous section, the daily climate scenario streamflow, temperature, and wind data are coincident, since they are outputs from the same climate models, and thus represent the same weather system taking place in the region on the same climate scenario dates. However, the ERA5 historical solar GHI data, which is collected from historical observed data or estimated using climate models, does not represent the same weather systems as the three types of climate scenario data, since it is not an output of global climate models (GCMs).

Nevertheless, some climate scientists think that solar data and a type of temperature data (to be discussed) are correlated. The correlations are first analyzed using the ERA5 historical data. It is then assumed that the same ERA5 correlations also exist between the climate scenario solar data and temperature data. Finally, a method is developed to apply the ERA5 correlations to the climate scenario temperature data to estimate synthetic climate scenario solar data.

On the same calendar date of a year (i.e., January 1st, April 18th, etc.), it is believed that the ERA5 GHI data should be correlated to diurnal temperature range, which is defined as the difference between the daily maximum temperature and the daily minimum temperature. A couple of examples are presented below.

As a first example, in Figure D - 52 , at the "West" solar farm, the ERA5 daily average GHI are plotted against the daily diurnal temperature range for the set of 44 January 1st's, a winter day, from 1980 to 2023. However, for correlation analysis, more data should be included. Therefore, to increase size of the data, the five days surrounding January 1st are plotted: December 30th and 31st, January 1st, 2nd, and 3rd, from 1980 to 2023, resulting in $5 \times 44 = 220$ data points. Since these five days are consecutive, they have almost the same daylight hours, and thus almost the same amount of "blue sky" solar irradiance (defined as the solar energy radiation reaching the Earth's surface on a clear, cloudless day). Therefore, differences in GHI among the five consecutive days should be due to different cloud cover, and not due to the small differences in daylight hours or solar elevation angles of the five days.

[85] See Technical Appendix G - New Generating Resources in the Ninth Power Plan for more details.

Figure D - 52: ERA5 Daily Average GHI vs Diurnal Temperature on December 30-January 3 for the West Solar Location

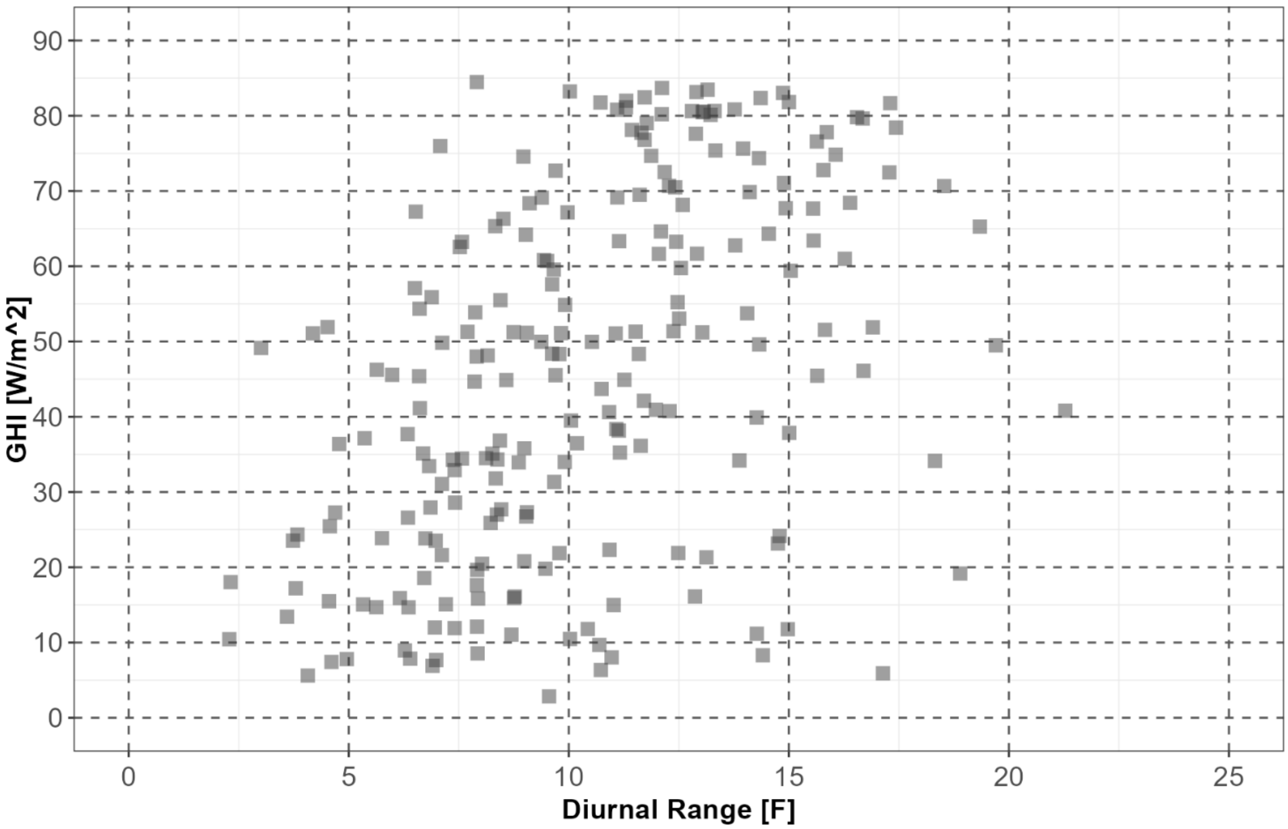

In Figure D - 52 above, there seems to be some correlation in the scatter-plot between the ERA5 daily average GHI (plotted along the y-axis) and diurnal temperature range (plotted along the x-axis). However, for a given diurnal temperature range, there is significant variance in the GHI. Nevertheless, it seems that as the diurnal temperature range increases the solar GHI tends to increase as well. The correlation coefficient is small, about 0.46.

Next, also at the "West" solar farm, the correlation between the 44 years of ERA5 daily average GHI and diurnal temperature range is analyzed for a summer day, July 1st. Similarly, the five days surrounding July 1st are plotted: June 29th, June 30th, July 1st, July 2nd, and July 3rd. The scatter plot of the ERA5 data is presented in Figure D - 53 below.

Figure D - 53: ERA5 Daily Average GHI vs Diurnal Temperature on June 29-July 3 for the West Solar Location

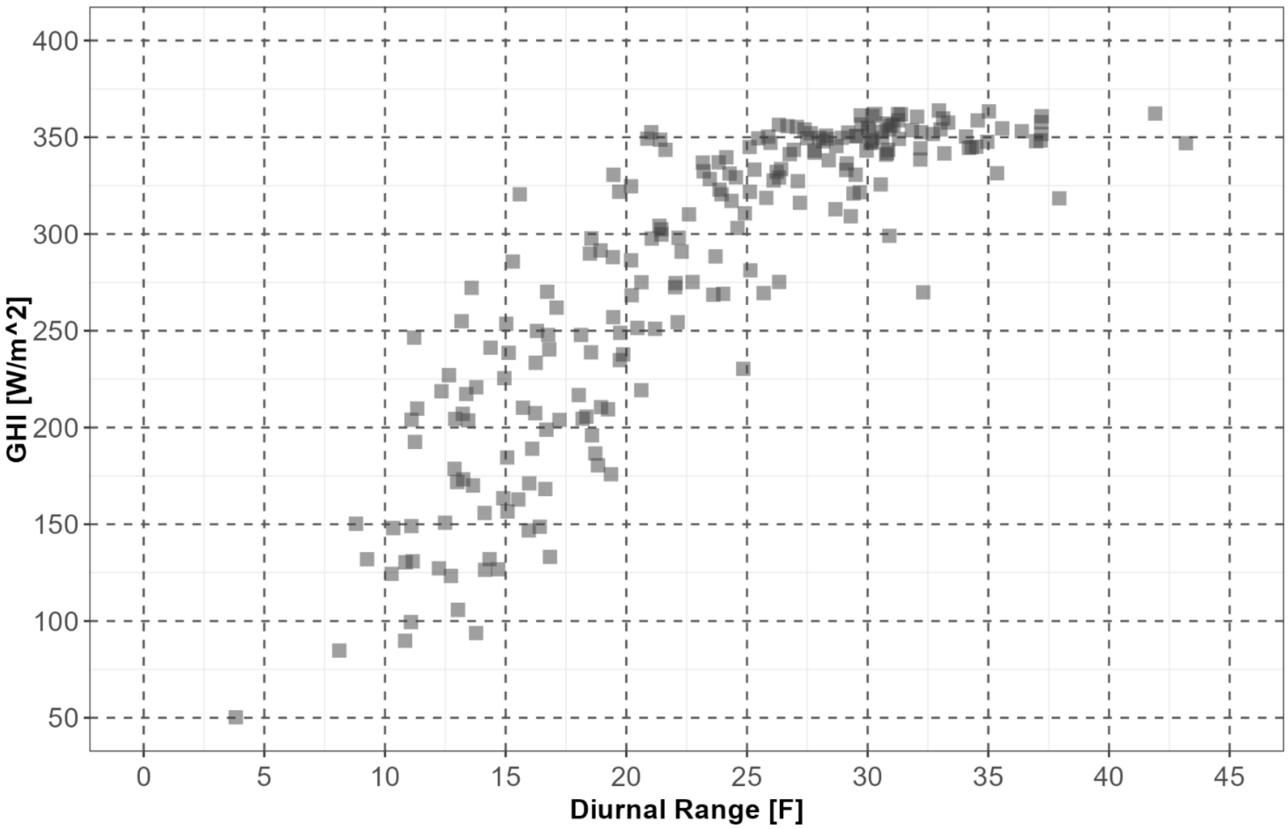

In Figure D - 53 above, for a given diurnal temperature range, there is a much smaller variance in the GHI compared to that in Figure D - 52. Furthermore, it is clear that as the diurnal temperature range (along the x-axis) increases the solar GHI (along the y-axis) tends to increase as well, and the ERA5 GHI seems to reach a plateau for higher diurnal ranges. The correlation coefficient here is much larger, about 0.85.

For each of the remaining 363 days of a year, the correlation coefficient is calculated between the ERA5 daily average GHI and the ERA5 diurnal temperature range for the 5 days surrounding the day of interest. From the resulting distribution of 365 correlation coefficients, the minimum, median and maximum are 0.45, 0.78, and 0.89, respectively. Thus, it could be concluded that, for any five consecutive days of a year, their ERA5 daily average GHI and diurnal temperature range, on average, are strongly correlated at the West solar location.[86]

[86] For the "Central" solar location, the minimum, median and maximum correlation coefficients are 0.23, 0.62, and 0.80, respectively. For the "East" solar location, the three corresponding correlations coefficients are 0.32, 0.61, and 0.75, respectively. Therefore, for these two solar locations, the ERA5 GHI and diurnal temperature range are moderately correlated, for which the method developed in this section should apply.

Then, it is assumed that the climate scenario GHI and diurnal temperature range also have the same correlations as the ERA5 data sets. The method of using the climate scenario diurnal temperature range to estimate a climate scenario GHI is as follows. For a climate scenario date, for example, 3/4/2032, calculate its climate scenario diurnal temperature range, then randomly select a nearby diurnal temperature range (details to be presented in an example) from the distribution of ERA5 diurnal temperature ranges for the 5 days surrounding March 4th: March 2nd, 3rd, 4th, 5th, and 6th for the 43 years from 1980 to 2023. Then, the ERA5 hourly GHI data on the same date as the randomly selected ERA5 diurnal temperature range becomes the climate scenario hourly GHI for 3/4/2032.

This method is presented in more detail in the following example. For the West solar farm, download from the Climatology Lab's climate scenario A's daily minimum and daily maximum temperatures for climate scenario years 2019 to 2049.

For a specific day of a year, for example, January 1st, the first day of a year, there are 31 climate scenario dates: 1/1/2019, 1/1/2020, 1/1/2021, ..., 1/1/2049. The climate scenario A diurnal temperature ranges (DTRs) are calculated for the 31 climate scenario dates, and then categorized into temperature bins of size 5 F. For example, if DTR = 0.56 F, then it is categorized into the bin [0 F, 5F). If DTR = 12.3, then it is categorized into the bin [10 F, 15 F), etc. The 31 climate scenario A diurnal temperature ranges and temperature bins for the West solar farm are plotted in Figure D - 54 below.

Figure D - 54: Climate Scenario A Diurnal Temperature Range vs Temperature for West Solar Location for January 1

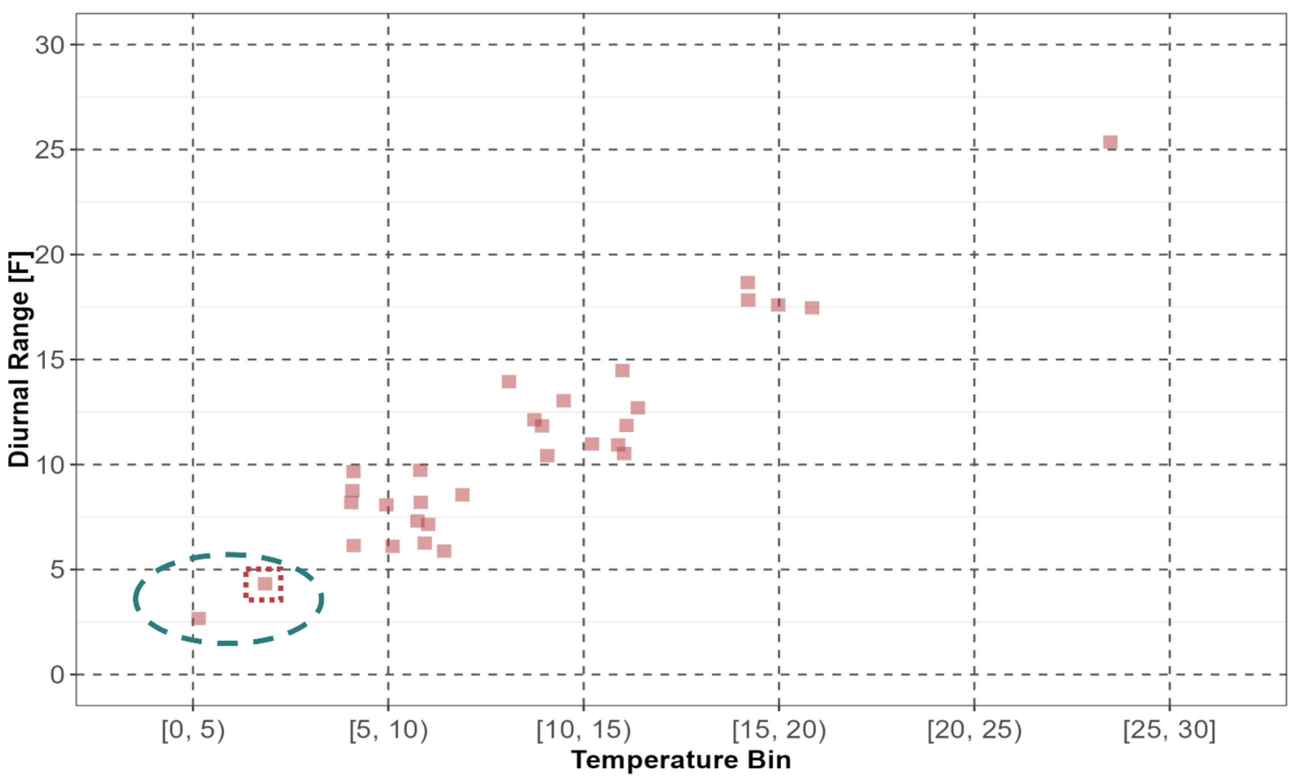

Along the x-axis in Figure D - 54, there are six temperatures bins in units of F, starting with [0, 5), which is followed by [5, 10), and so on, and ending with [25, 30]. All 31 climate scenario A's diurnal temperature ranges are plotted along the y-axis and grouped into these six bins. For each of the 31 climate scenario A diurnal temperature range data points, there is a corresponding date of January 1st from 2019 to 2049. For example, in temperature bin [0 F, 5 F) at the left side of the x-axis, there are two climate scenario A DTRs, at 2.7 F and 4.3 F, plotted as red squares inside the dashed green oval. The DTR of 2.7 F corresponds to climate scenario date 1/1/2036, while the other DTR of 4.3 F corresponds to 1/1/2035. Interestingly, there is no DTR in temperature bin [20 F, 25 F).

Next, to estimate the climate scenario A GHI for either of the two DTRs in temperature bin [0 F, 5F) in the dashed green oval, randomly select a nearby ERA5 DTR (calculated for the West solar farm) from the five days surrounding January 1st: December 30th and 31st, January 1st, 2nd, and 3rd for the 43 historical years 1980 to 2023. Using the five days surrounding January 1st (instead of just January 1st) allows more ERA5 data to become available to be randomly selected. There are 220 (from five days surrounding January 1st $\times$ 43 years) ERA5 DTRs which were previously plotted in Figure D - 52.

Each of the 220 ERA5 DTR is then categorized into a temperature bin of size 5 F as was done for the climate scenario A DTRs. The 220 ERA5 DTRs and temperature bins for the West solar farm are plotted in Figure D - 55 below.

Figure D - 55: ERA5 Diurnal Temperature Range vs Temperature for West Solar Location for January 1

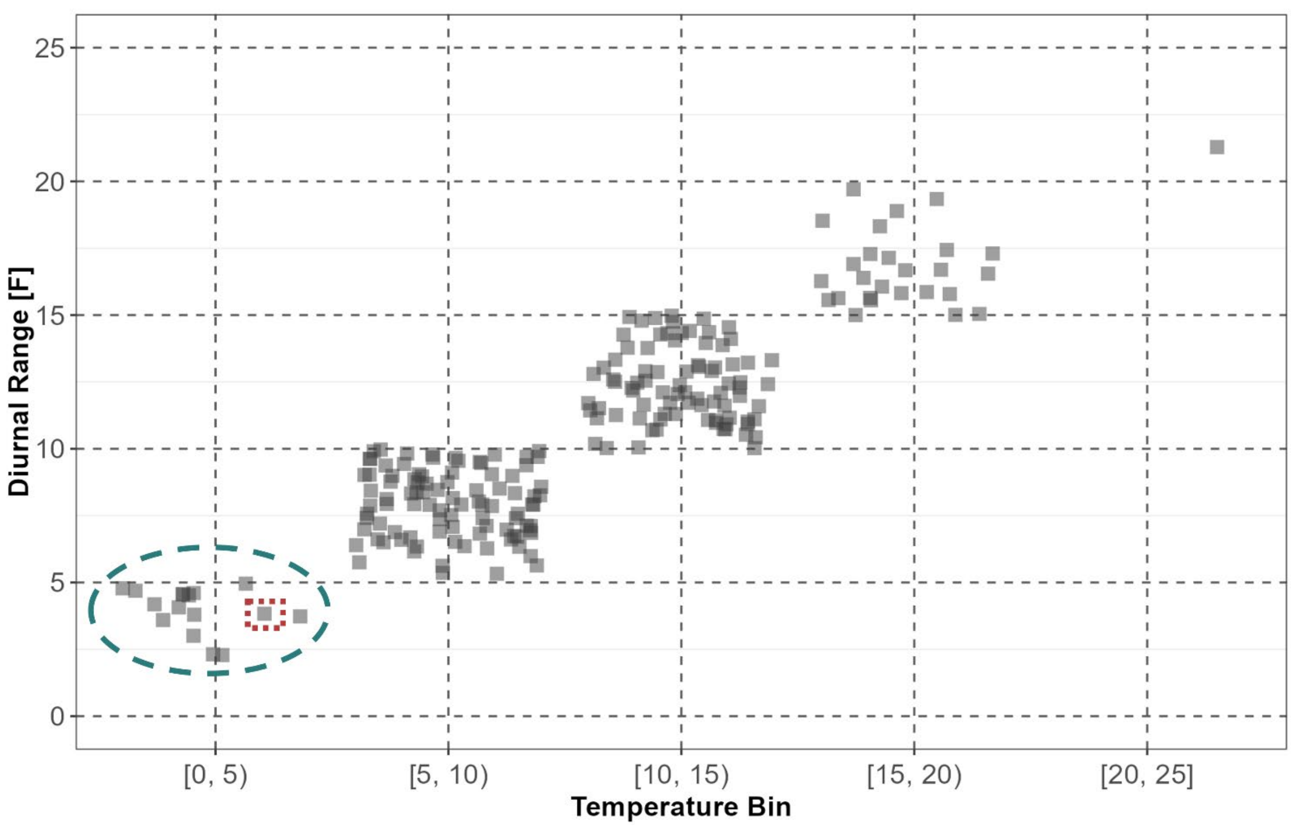

Thus, for the two climate scenario A DTRs in temperature bin [0, 5) in Figure D - 54 (inside the dashed green oval), the nearby ERA5 DTRs are those in the same temperature bin, *[0 F, 5 F),* in Figure D - 55 (inside the dashed green oval). There are 16 ERA5 DTRs in the [0, 5) bin in Figure D - 55 that could be randomly selected. Each of 16 ERA5 DTRs has a corresponding historical date which is listed in Table D - 25 below.

Table D - 25: The ERA5 Dates corresponding to the 16 Diurnal Temperature Ranges in the Temperature Bin [0 F, 5 F) in Figure D - 55.

The 16 ERA5 Dates in Temperature Bin [0 F, 5 F)
12/31/1992
12/31/1993
1/1/1997
1/1/2002
12/30/2002
1/3/2003
12/31/2003
1/1/2004
1/2/2004
1/3/2004
12/31/2005
12/30/2008
12/31/2008
12/31/2020
1/1/2021
1/2/2021

As an example, the 4.3 F climate scenario A DTR with corresponding climate scenario date 1/1/2035 (plotted inside the dashed red square and inside the dashed green oval in Figure D - 54) could be paired with a randomly selected ERA5 DTR plotted inside the dashed red square and inside the dashed green oval in Figure D - 55. The ERA5 DTR inside the dashed red square is 3.80 F and its corresponding historical date is 12/31/2005, which is listed in the bold font in Table D - 25. Therefore, the ERA5 hourly GHIs of that historical date, 12/31/2005, are assigned to be the climate scenario A hourly GHIs of climate scenario date 1/1/2035.

By pairing a climate scenario DTR with a randomly selected ERA5 DTR from the same temperature bin, the climate scenario date (corresponding to the climate scenario DTR) is thus paired with a selected ERA5 historical date (corresponding to the randomly selected ERA5 DTR). Finally, the climate scenario date would be assigned the ERA5 GHI hourly values of the randomly selected ERA5 historical date.

Therefore, using the method as presented in the example above, the cliamte scenario A GHI has been estimated for climate scenario date 1/1/2035. Following the same procedure, the climate scneario A hourly GHIs could also be calculated for the remaining 30 climate scenario dates for January 1st from 2019 to 2049.

It should be noted that the highest climate scenario A DTR, at 25.4 F, with a corresponding climate scenario date 1/1/2021, is catogorized into the highest temperature bin [25 F, 30 F] in Figure D - 54. However, in Figure D - 55, there is no ERA5 DTR data in temperature bin [25 F, 30 F]. In that case, the next closest ERA5 temperature bin is chosen, which is [20 F, 25 F] in Figure D - 55, and an ERA5 DTR within the temperature bin is randomly selected to pair with the highest climate scenario A DTR. But there is only one ERA5 DTR value in temperature bin [20 F, 25 F], which is 21.3 F and has a corresponding histoircal date 1/2/2012. Therefore, ERA5 24 hourly GHIs on 1/2/2012 are thus assigned to be the climate scenario A hourly GHIs on climate scenario date 1/1/2021.

Thus, this process assigns historical ERA5 hourly GHIs to all 31 January 1st for years 2019 to 2049 of climate scenario A plotted in Figure D - 54. The same process could be followed to assign ERA5 hourly GHIs to the remaining 364 calendar dates for years 2019 to 2049 of climate scenario A. Of course, using the same process would result in all the days in years 2019 to 2049 of climate scenarios C and G being assigned ERA5 hourly GHIs.

This methodology was presented to the CWAC.[87] Some climate scientists suggested further analysis of the climate scenario temperatures (which were used to calculate diurnal temperature ranges) to determine if there are biases. Another suggestion was to analyze for correlations between neighboring grid points. However, it was acknowledged that the analyses should be performed by climate scientists. Aside from these issues, there was no objection to the methodogly discussed in this section.

It is interesting to note in Figure D - 56 below that at each of the solar farm locations and for each month (along the x-axis), the aggregate climate scenario diurnal temperature range (plotted in the red boxplots) is higher than the ERA5 diurnal temperature range (plotted in the gray boxplots). It was also discussed in the RMJOC report that over the entire region, climate scenario temperatures (from 2020 to 2049) are higher than those in a historical time period.[88] It could be that the higher climate scenario temperatures are related to the higher climate scenrio diurnal temperature ranges.

[87] Climate and Weather Advisory Committee Meeting on 4/3/2025: https://www.nwcouncil.org/meeting/climate-and-weather-advisory-committee-2025-04-03.

[88] *Climate and Hydrology Datasets for RMJOC Long-Term Planning Studies: Second Edition (RMJOC-II) Part I: Hydroclimate Projections and Analyses*" at https://www.bpa.gov/-/media/Aep/power/hydropower-data-studies/rmjoc-ll-report-part-l.pdf.

Figure D - 56: Comparing ERA5 and Aggregate Climate Scenario Diurnal Temperature Range by Month at Each Solar Location

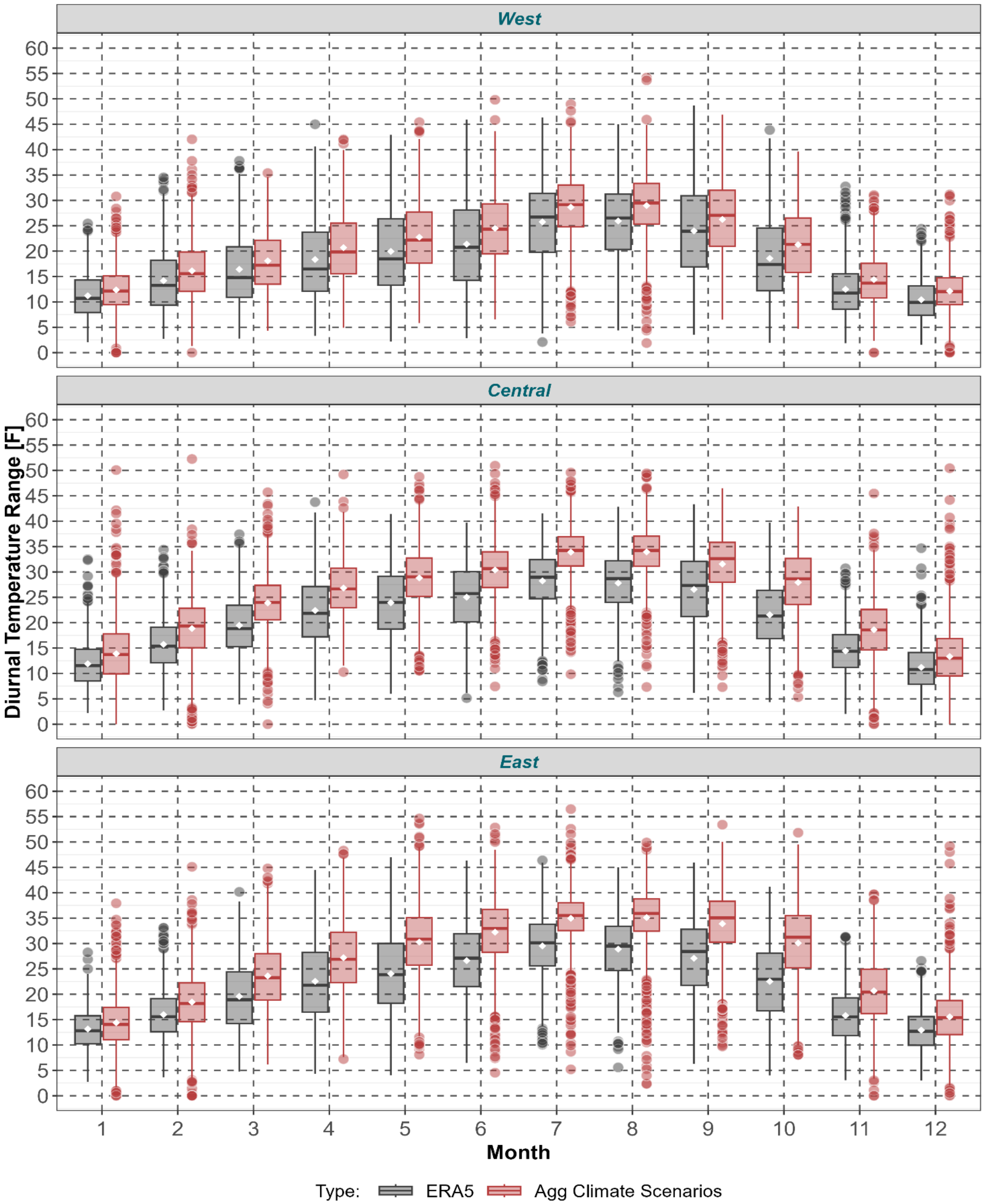

In any case, at each loaction and for each month, the distribution of climate scenario diurnal temperature ranges (red boxplots) are higher than the distribution of ERA5 diurnal temperature ranges (gray boxplots). Therefore, since the diurnal temperature range is highly or moderately correlated with GHI, then it could be deduced that the climate scenario GHIs will be higher than those of ERA5, at each location and for each month. This is discussed in the next section.

ERA5 and Climate Scenario GHI

The ERA5 hourly GHIs are embedded in the TSL model from 1980 to 2023, and their daily average GHIs at the three solar profile locations are plotted in Figure D - 57 below.

Figure D - 57: ERA5 Daily Range GHI by Month

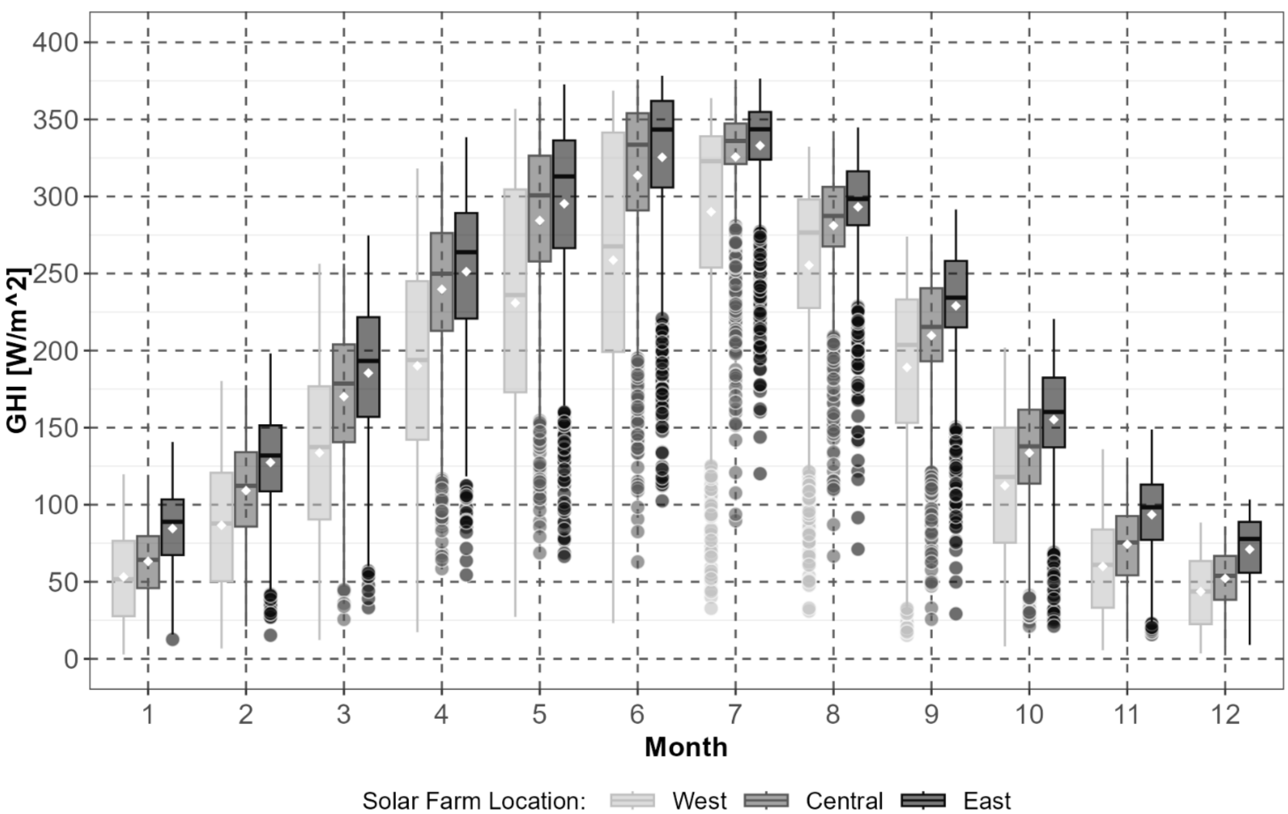

There are two clear patterns in Figure D - 57. One is the pattern across the 12 months along the x-axis, with the maximum distributions occurring in July, and the minimum distributions in December, for each of the three solar locations. Therefore, the distributions of GHI increase from January to July and then decrease to December.

The other pattern is that for each month, the distribution for the West (plotted in light gray boxplots) is less than that for the Central (plotted in the medium gray boxplots), which in turn is less than that for the East (plotted in the dark gray boxplots). Furthermore, the variance for the West is higher than those for the other two locations, which are more comparable. Finally, even during the sunnier months from months May to September, there are still some very cloudy days as plotted in the low boxplot outliers.

It turns out that the ERA5 GHI patterns in Figure D - 57 are transferred to the aggregate climate scenario (combined A, C and G) GHIs plotted in Figure D - 58. In the figure below, the same ERA5 geographical pattern in Figure D - 57 is evident: the distribution for the West (plotted in light red boxplots) is less than that for the Central (plotted in medium red boxplots), which in turn is less than that for the East (plotted in dark red boxplots). Also, for the 12 months along the x-axis, the other ERA5 monthly pattern is also clear: the distributions of GHI increase from January to July and then decrease to December.

Therefore, these GHI patterns are expected to be preserved in the capacity factors as calculated by the TSL model (to be discussed in the next section).

Figure D - 58: Aggregated Climate Scenario Daily Average GHI by Month

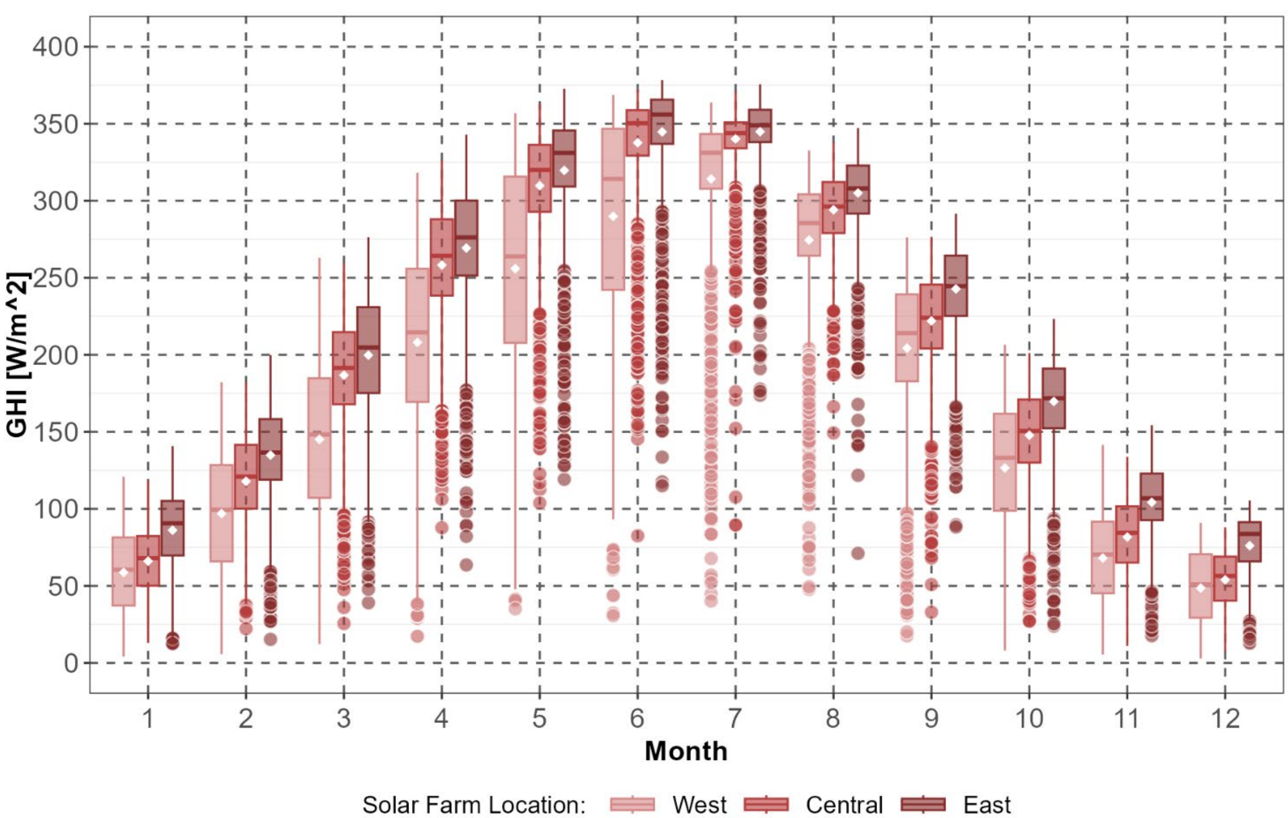

However, despite having the same GHI patterns as the ERA5 data, the aggregate climate scenario GHIs, derived from sampling ERA5 data in matching diurnal temperature bins, are higher than ERA5 GHIs, as presented in Figure D - 59 for the three solar locations.

1 **Figure D - 59: Comparison of ERA5 and Climate Scenario Daily Average GHI by Month**

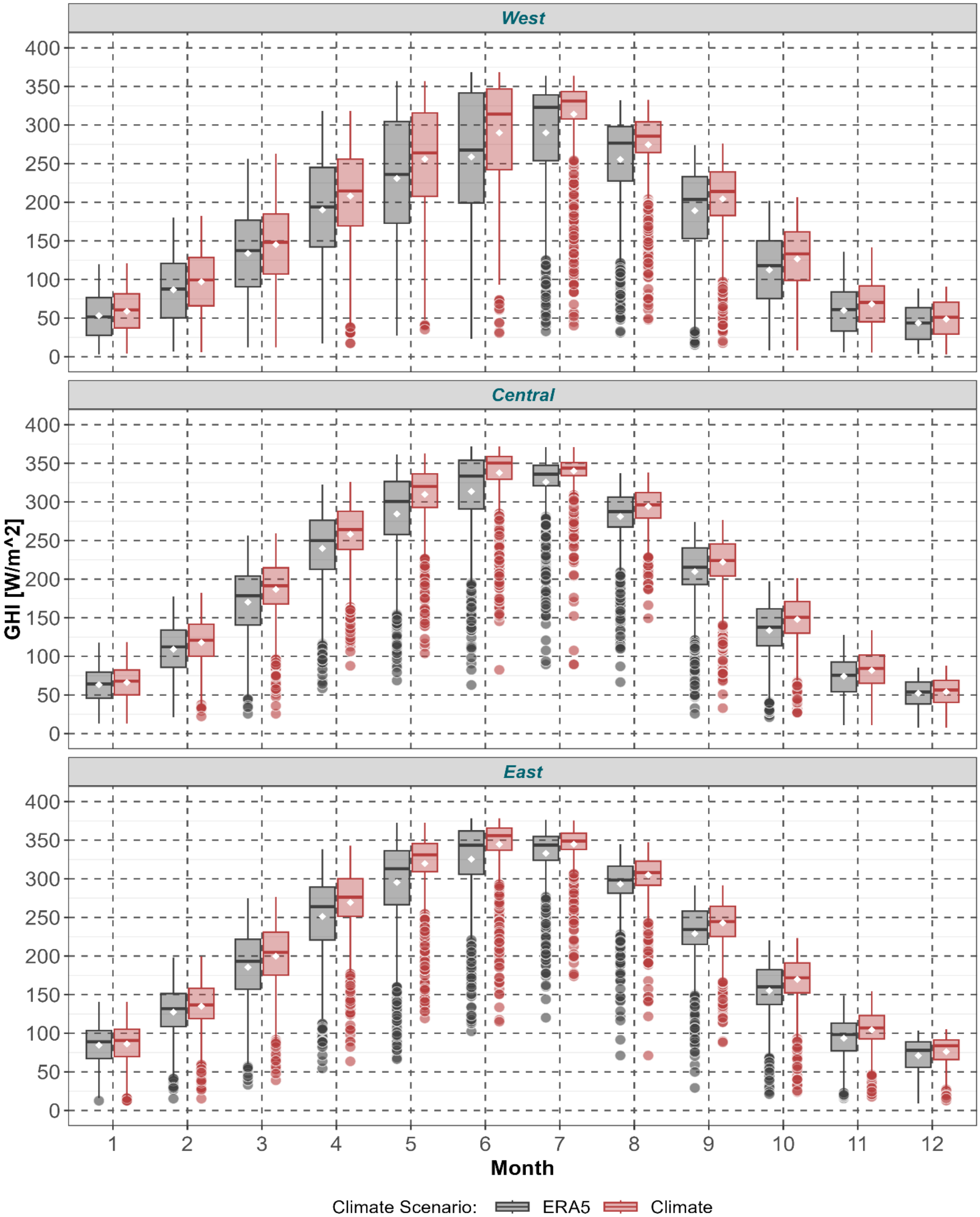

2

It is clear that at each solar farm location, the distributions of aggregate climate scenario GHIs are higher than those of ERA5 for all 12 months. The reason is that at each loaction and for each month, the distribution of climate scenario diurnal temperature ranges are higher than the distribution of ERA5 diurnal temperature ranges as presented in Figure D - 56 in a previous section. Therefore, climate scenario GHIs are assigned ERA5 GHI values from the matching higher ERA5 temperature bins which have higher ERA5 GHI values. Due to its higher GHIs, the aggregate climate scenario solar generation is expected to be higher than the ERA5 solar generation.

Climate Scenario Solar Generation

The climate scenario hourly solar GHIs whose daily averages are plotted in Figure D - 58 and Figure D - 59 are inputs into the TSL model to calculate solar generation for the 0-axis, or fixed, solar panel, and the 1-axis, or tilt, solar panel, which were chosen as reference plants for the Power Plan.[89] Both 0-axis and 1-axis panels are used for modeling existing utility scale solar generation. However, new utility scale solar generation are modeled with only the 1-axis panel. Furthermore, the 0-axis panel is used to model both existing and new behind-the-meter solar generation.[90]

In analyzing hourly solar generation data, there are many night-time hours for every day of a year where solar generation is zero, and the numerous zero CFs would distort the monthly boxplots of hourly CFs. Therefore, the daily average CFs are plotted instead. The aggregate climate scenario daily average generation capacity factors (CFs) for the 1-axis reference solar panel are plotted by month, along the x-axis, in Figure D - 60 below for the three solar locations.

[89] See Technical Appendix G - New Generating Resources in the Ninth Power Plan for more details.
[90] See Technical Appendix J - Rooftop Solar Methodology and Potential in the Ninth Power Plan for more details.

Figure D - 60: Aggregate Climate Scenario Daily Average Capacity Factors by Month

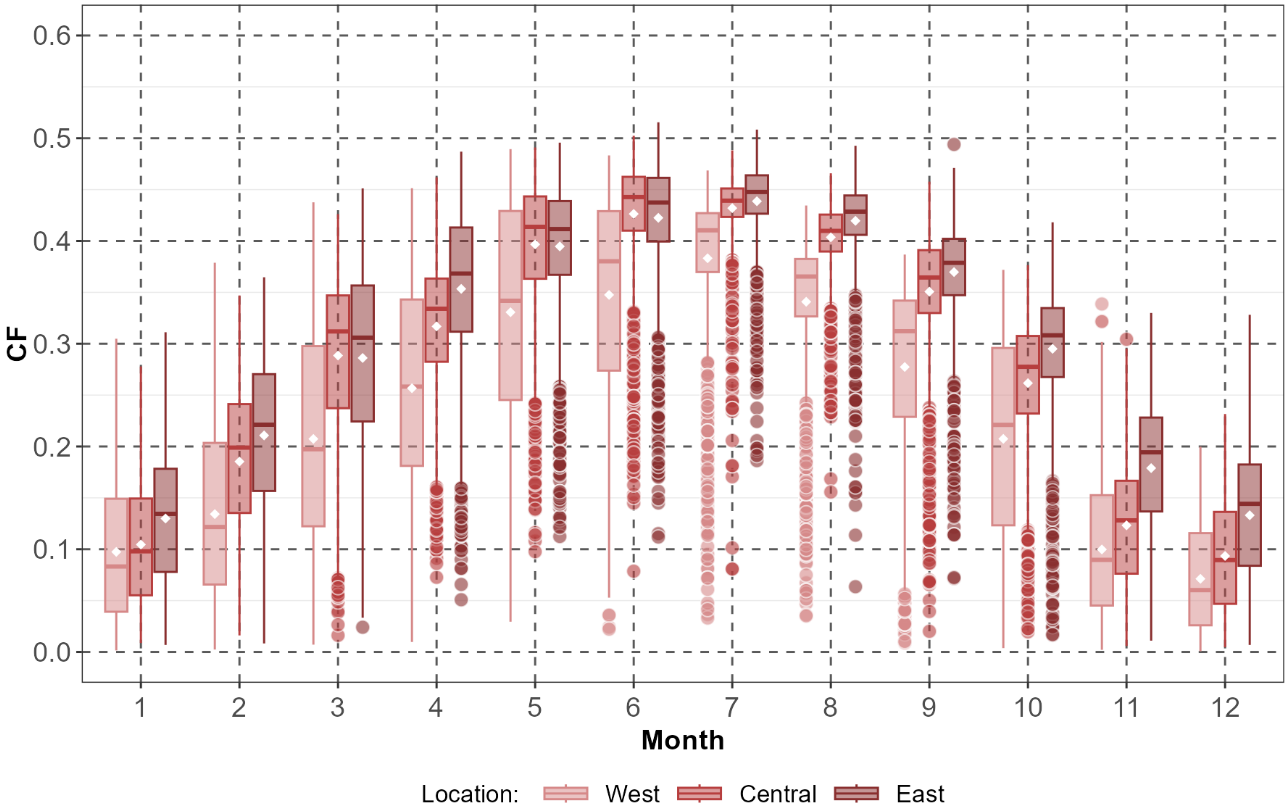

As discussed previously, the aggregate climate scenario GHI patterns in Figure D - 58 are mostly preserved in their CFs in Figure D - 60. The exceptions to the patterns are the distributions of Central CFs (in medium red boxplots) being about the same as those of the East CFs (in dark red boxplots) for the three months, March, May and June, whereas the East CFs were expected to be higher due to the East location having higher GHIs in Figure D - 58. This is due to bias-corrections on the climate scenario CFs to resemble historical solar CF data from the AURORA power system simulation model.[91] The bias corrections were performed internally in TSL.

The maximum daily average CF in Figure D - 60 is about 0.52 for the East solar farm for June, whereas the minimum is 0.0007 for the West solar farm for December. However, there are other CFs near the maximum and the minimum for other locations and other months.

In addition, the averages of the distributions (represented by the white diamonds inside each boxplot in Figure D - 60) are listed in Table D - 26.

[91] See https://www.energyexemplar.com/aurora.

Table D - 26: Averages of the Monthly Distributions of Solar Generation Capacity Factors

Month	West	Central	East
1	0.097	0.105	0.130
2	0.134	0.185	0.211
3	0.207	0.289	0.286
4	0.257	0.317	0.353
5	0.331	0.397	0.395
6	0.348	0.426	0.423
7	0.383	0.432	0.439
8	0.341	0.404	0.420
9	0.277	0.351	0.370
10	0.207	0.262	0.295
11	0.100	0.123	0.179
12	0.071	0.093	0.133

From Table D - 26, the maximum monthly average CF is 0.439 for July at the East solar farm, and the minimum is 0.071 in December at the West solar farm.

The overall annual average solar CFs for the West, Central, and East solar farms are listed in Table D - 27 below.

Table D - 27: Overall Averages of all Solar Generation Capacity Factors

Solar Farm Location	West	Central	East
Annual Average CF	0.230	0.282	0.303

The highest and lowest overall solar CFs are the East solar farm at 0.303 and the West solar farm at 0.230, respectively.

The boxplots in Figure D - 60 show the monthly and locational patterns of the aggregate climate scenario daily average solar CFs. There are small differences among the three climate scenarios in the plotted aggregate data. For completeness, daily average CFs by month of the three climate scenarios are plotted separately (instead of in-aggregate) for the three solar farm locations in Figure D - 61 below.

1 **Figure D - 61: Monthly Average Solar Capacity Factors for Climate Scenarios A, C, and G**

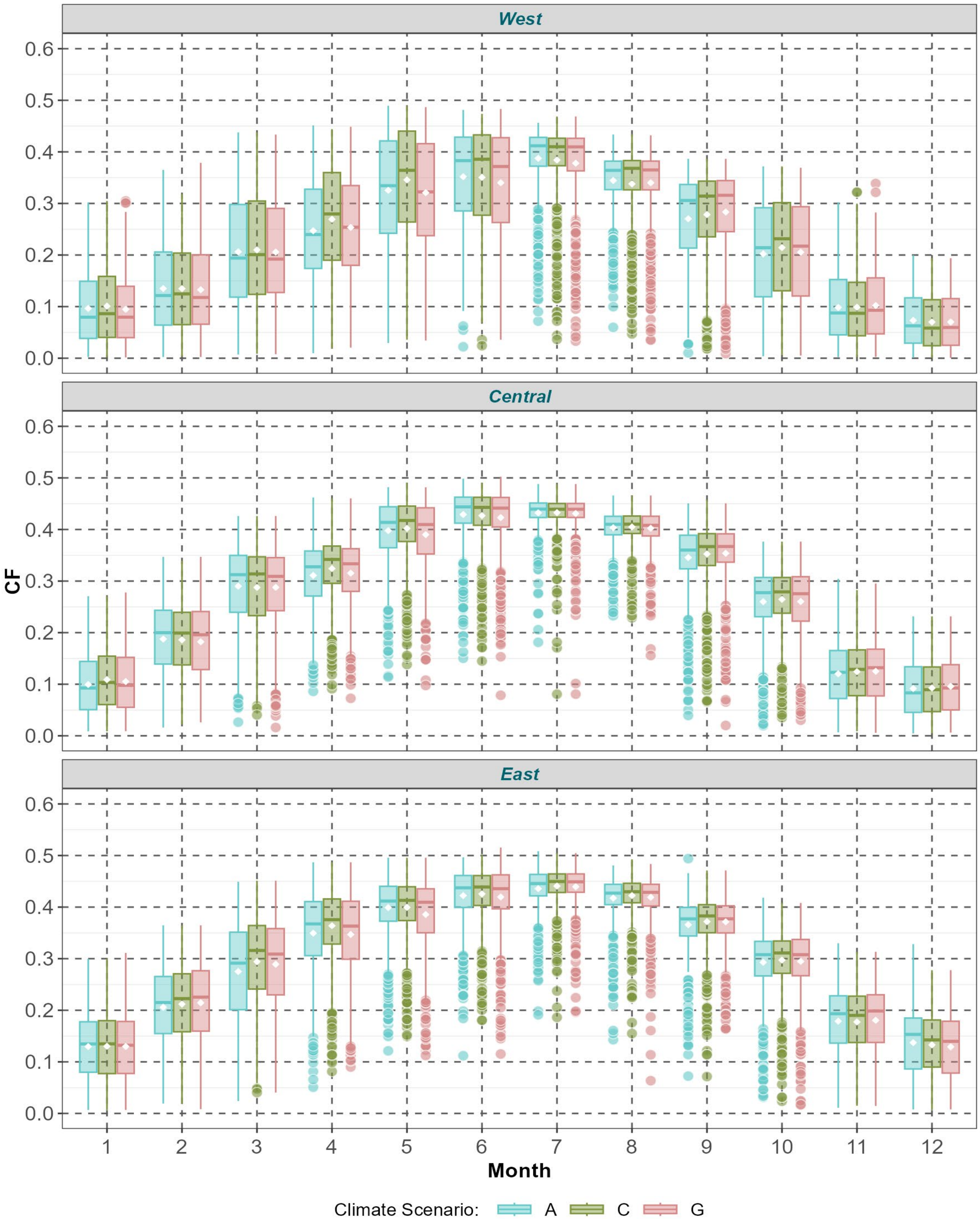

2

In Figure D - 61, solar CFs of climate scenarios A, C, and G are plotted in teal, green, and red boxplots respectively in each of the three panels. It could be seen that the differences among the climate scenarios are slightly higher for months April, May, September, and October. Otherwise, for other months at each location, the distributions of CFs among the three climate scenarios are closer to each other.

Very Low Climate Scenario Solar Generation

It is prudent to analyze the frequency and duration of very low solar generation (as was done for very low wind generation in a previous section) since during that stressful period, power system planners would have to develop a program to acquire sufficient and economical generation from other sources to meet load. As was done for very low wind generation, let very low solar generation at a solar farm be defined as those generations at or below the 10th percentile of all solar generations.

For simplicity, let the 10th percentile of all daily average CFs be represented by CF_{10}, and let those days where their CFs $\leq CF_{10}$ be referred to as low-CF days. For the three solar farms, their CF_{10}'s are listed in Table D - 28 below.

Table D - 28: The 10th Percentiles of the Distributions of Daily Average Solar Generation Capacity Factors over all Months.

10th Percentiles of CFs	West	Central	East
CF_{10}	0.042	0.076	0.118

For the aggregate 93 climate scenario years, from the three climate scenarios each having 31 climate scenario years, there are a total of 33,945 days of daily average CFs. Therefore, the number of days where their daily average CFs $\leq CF_{10}$ is about 3,394, depending on the number of ties. Specifically for the West, Central, and East solar farms, there are 3,396, 3,398, and 3,395 low-CF dates, respectively. However, among the three sets of low-CF dates, there are only 467 low-CF dates common to all three solar farms, where on those common dates, the daily average CFs of all three solar farms are less than or equal to their respective CF_{10}'s listed in Table D - 28.

However, instead of analyzing the total number of low-CF days or dates for the 93 climate scenario years, a more interpretable quantity could be the average number of low-CF days per year. For example, for the West solar farm, the average number of low-CF days is $(3{,}396 \text{ days})/(93 \text{ years}) \cong 36.5$ days per year (where the daily average CF $\leq CF_{10}$). Furthermore, the average number of low-CF days common to all three solar farm is $(467 \text{ days})/(93 \text{ years}) \cong 5.02$ days per year.

In the top panel of Figure D - 62 below, the average number of low-CF days per year for the three solar farm locations and for All-Locations (all-three solar locations) are plotted.

Figure D - 62: Low Solar Periods in Climate Scenario Solar Profiles

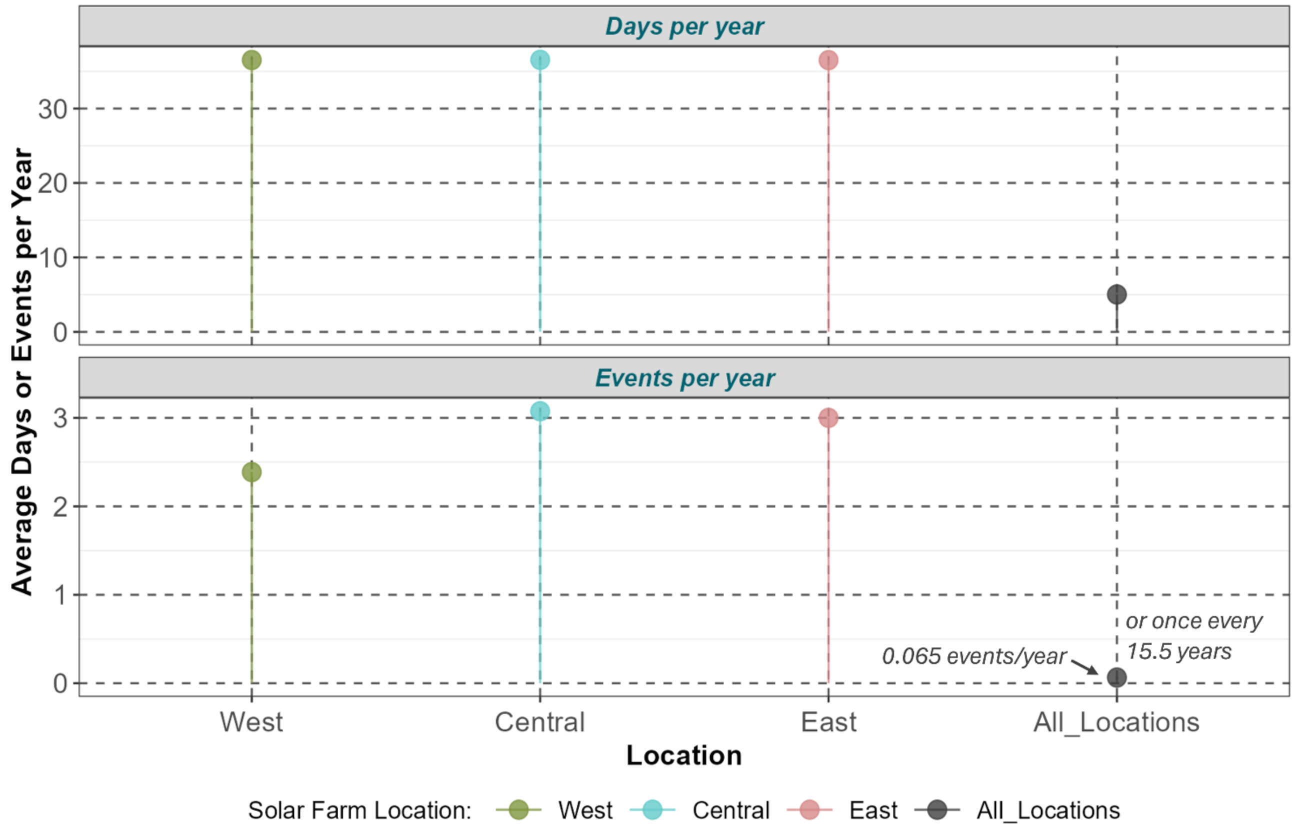

There are on average 36.5 low-CF days per year for each of the three wind fleet locations: West (green circle), Central (blue circle), and East (red circle), listed from left to right on the x-axis. Furthermore, there is on average only around five common low-CF days per year for all three solar farm locations which is plotted in the gray circle on the right side.

Among the low-CF days could be subsets of three-or-more consecutive low-CF days, which are conditions under which it is even more challenging to operate the power system to meet load. Let the subsets of three-or-more consecutive low-CF days be referred to as low-CF events. For example, for the West solar farm, among the 3,395 low-CF days, there are 222 low-CF events (where each event consists of three-or-more consecutive low-CF days) in 93 climate scenario years. And for all three solar farm locations, out of the 467 common low-CF days, there are only 6 low-CF events.

In terms of average number of low-CF events per year, it is $(222 \text{ events})/(93 \text{ years}) \cong 2.39$ average number of events per year for the West solar farm. In contrast, there is only an average of $(6 \text{ events})/(93 \text{ years}) \cong 0.065$ low-CF events per year common to all three solar farms, which is rather infrequent.

Since (0.065 low-CF events per year) is less than (1 low-CF event per year), its reciprocal, $1/(0.065 \text{ events per year}) \cong (15.5 \text{ years per event})$, has an easier interpretation. In other words, for all three solar locations simultaneously having one common low-CF event, the frequency is on average once every 15.5 years.

In the bottom panel of Figure D - 62 above, the average number of low-CF events per year for the three solar farm locations and for all-locations are plotted. Going from left to right on the x-axis, the values are: West (green circle) 2.39; Central (blue circle) 3.08; East (red circle) 3.00; all-locations (gray circle) 0.065. As mentioned previously, for the entire in-region solar fleet to have very low generation that lasts for three or more consecutive days, that happens on average once every 15.5 years.

Furthermore, from Figure D - 60, the lowest monthly distributions of daily average CFs are in January and December. Therefore, it is not surprising that among all low-CF event days, the percentage of them being in January or December is: 77% for West; 82% for Central; 87% for East; and 100% for all-locations.

Out-of-Region Climate Data

Previous sections of this Technical Appendix contain analyses of climate scenario temperatures, streamflows, wind and solar data for the Pacific Northwest. These data are considered as in-region and are inputs into the Council's analytical tools. Specifically, temperatures are inputs into the load forecast model ITRON, while streamflows, wind and solar data, along with the load forecasts, are inputs into the adequacy model GENESYS, and capital expansion model OptGen.

Since the Council's models also simulate operations of power systems in WECC that are outside of the Northwest, this section describes similar types of climate data used to model these out-or-region power systems. However, operations for these out-of-region power systems are simplified to enable reasonable model run-time.

Figure D - 63 below shows the 38 Balancing Authorities (BAs) in WECC, where those BAs (and portions of BAs) inside the area bounded by the pink dashed lines, for example, Portland General Electric (PGE in the light blue circle), represent in-region power systems.[92] In contrast, those BAs in Figure D - 63 that are outside the area bounded by the pink dashed lines, for example, Los Angeles Department of Water and Power (LDWP in the gray oval), represent out-of-region power systems. A list of all WECC BAs (and non-WECC BAs) and their acronyms are available on a Federal Energy Regulatory Commission (FERC) webpage.[93]

[92] Some generations in WAPA – Upper Great Plains (WAUW) and in the Wyoming portion of PACE are also considered as in-region.
[93] See https://mbrweb.ferc.gov/LookupData/LookupTables/lkp_baa?page=4.

Figure D - 63: The 38 Balancing Authorities in WECC

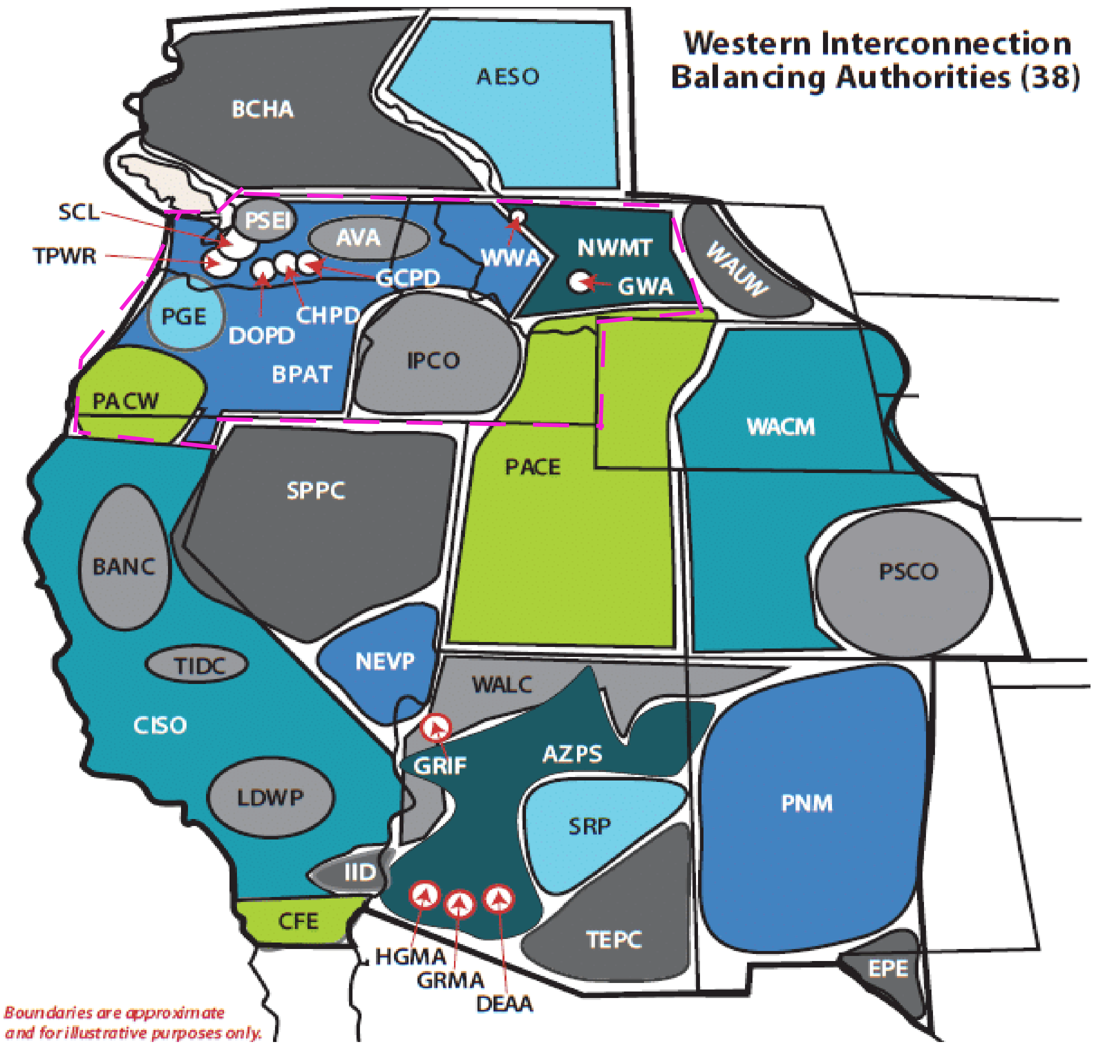

Temperature Data

For out-of-region power systems, the Council decided to use load forecasts collected from utility planning documents such as Integrated Resource Plans (IRPs), Energy Information Agency (EIA) and Federal Energy Regulatory Commission (FERC) filings.[94] Therefore, there is no need to use any temperature data as inputs for out-of-region load forecasts.

[94] See Technical Appendix L - Wholesale Market Availability Results Draft for more details.

Streamflow Data

The out-of-region climate model streamflow data are calculated for 13 regions in WECC corresponding to a subset of transmission zones defined in the Council's GENESYS model and plotted in the black circles in Figure D - 64 below.

Figure D - 64: Zonal Transmissions in the GENESYS Model

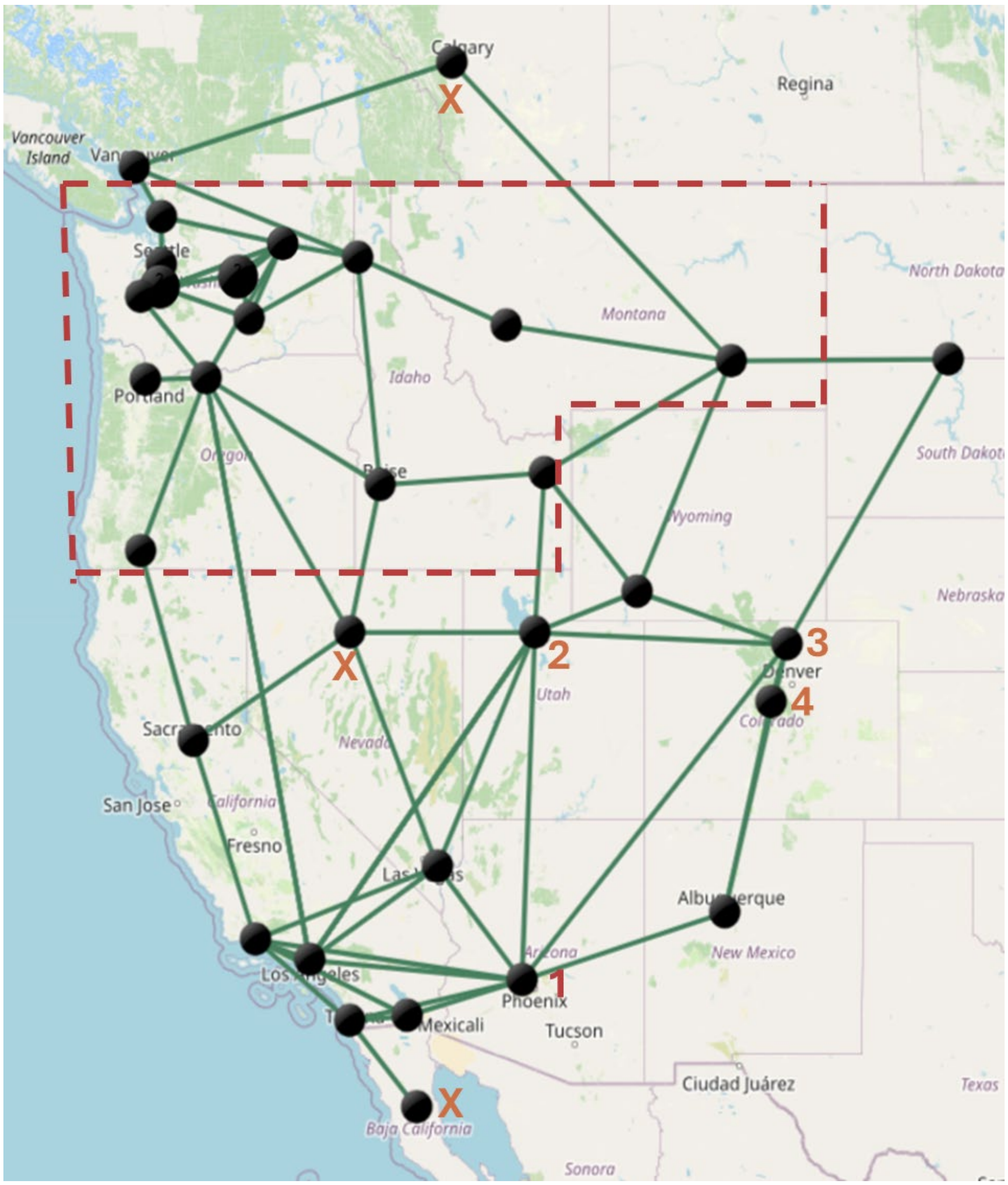

In Figure D - 64, the transmission zones inside the area bounded by the dashed red lines are considered in-region, while those outside the bounded area are considered out-or-region transmission zones. All 13 streamflow regions are various combinations of the out-of-region transmission zones, except those labeled with an orange "X."

A streamflow region could correspond to one transmission zone, for example, the transmission zone in Arizona, labeled by the orange "*1*" in Figure D - 64. This one zone comprises four WECC BAs plotted in Figure D - 63: Arizona Public Service (AZPS), Salt River Project (SRP), Tucson Electric Power (TEPC) and WAPA Lower Colorado (WALC).

Another streamflow region corresponding to one transmission zone is the one in Utah labeled by the orange "2" in Figure D - 64. However, this zone is not an entire WECC BA but a subset of the WECC BA PacificCorp East (PACE in Figure D - 63).

On the other hand, some streamflow regions correspond to combinations of multiple transmission zones. For example, the streamflow region in Colorado consists of two transmission zones labeled by the orange "3" and "4" in Figure D - 64. Respectively, they represent WECC BA WAPA Rocky Mountain (WACM in Figure D - 63) and WECC BA Public Service Company of Colorado (PSCO in Figure D - 63).

The remaining 10 of 13 streamflow regions are defined very similarly to the three examples above, which is, one or more of the transmission zones plotted in Figure D - 64 which in turn correspond to one or more WECC BAs (see Figure D - 63), or one or more subsets of WECC BAs, or both WECC BAs and subsets of WECC BAs.

Therefore, to model (out-of-region) hydro systems in the 13 streamflow regions, the Council decided to use hydro generations from the GODEEEP data set[95] developed by the Pacific Northwest National Lab (PNNL). The GODEEEP hydro generations are calculated from streamflow data (but not available in GODEEEP) derived from hydrological modeling of an ensemble of CMIP6 climate models.[96] The ensemble of CMIP6 climate models, published around 2020 or shortly after, are newer than the 10 CMIP5 models (published around 2012) that were used to produce the in-region RMJOC climate data as presented in previous sections.[97] Despite differences between the CMIP5 and CMIP6 climate models, as the climate data outside the region is disjointed from climate data inside the region, the Council decided to use the ensemble CMIP6 data because they should contain more up-to-date general trends of climate change.

For simplicity, for each of the 13 streamflow regions, all hydro generations within the region are added together to become the total hydro generation of that region. Furthermore, by assuming the total hydro generation of a region is produced by *just one* hypothetical hydro-project with a fixed (constant) power production coefficient (e.g., the H/K factor), then a representative CMIP6 "streamflow" of a

[95] See https://zenodo.org/records/13776945

[96] See https://www.nature.com/articles/s41597-025-05097-3.pdf, https://www.nature.com/articles/s41597-023-02485-5 , and https://www.nature.com/articles/s41597-023-02485-5/tables/1.

[97] See "*CMIP6 - Coupled Model Intercomparison Project Phase 6*" at https://pcmdi.llnl.gov/CMIP6. It should be noted the CMIP6 models are different from CMIP5 models, even those with very similar names developed by the same organizations (e.g., GFDL-ESM*, or CNRM-CM*). Therefore, even on the same calendar date (i.e., 6/15/2032) the CMIP6 out-of-region climate data should not be expected to be temporally co-incident to the CMIP5 in-region climate data.

region could be calculated as a ratio. The representative CMIP6 streamflows for the 13 regions then become inputs into the Council’s GENESYS and OptGen models.

Wind Data

For out-of-region on-shore wind generation, the Council decided to simulate generation at the 20 locations plotted in Figure D - 65 below.

Figure D - 65: The 20 Locations for Modeling Out-of-Region On-Shore Wind Generation

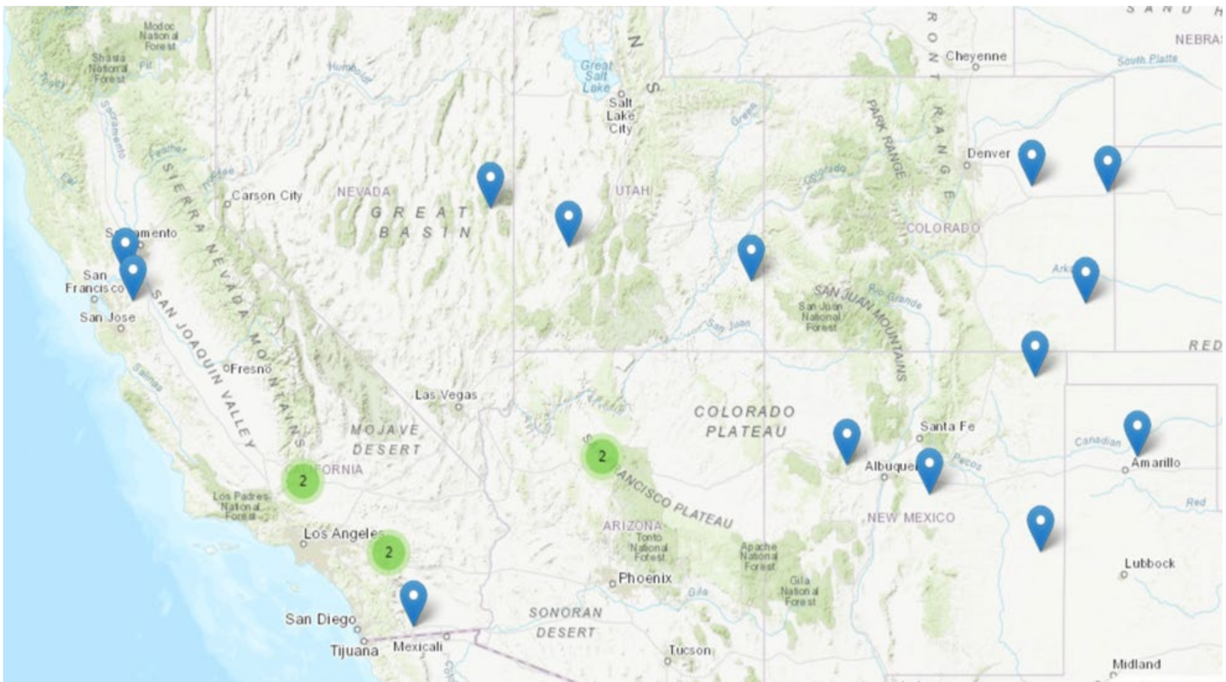

In Figure D - 65, the three green circles with the number “2” indicate that there are two wind turbine hub-heights and thus two wind generation shapes modeled at those locations. The remaining 14 locations have only one wind turbine hub-height and so only one wind generation shape.

In addition to the onshore wind generation, the Council also simulates out-of-region offshore wind generation at the six locations plotted in Figure D - 66 below.

Figure D - 66: The Six Locations for Modeling Out-of-Region Off-Shore Wind Generation

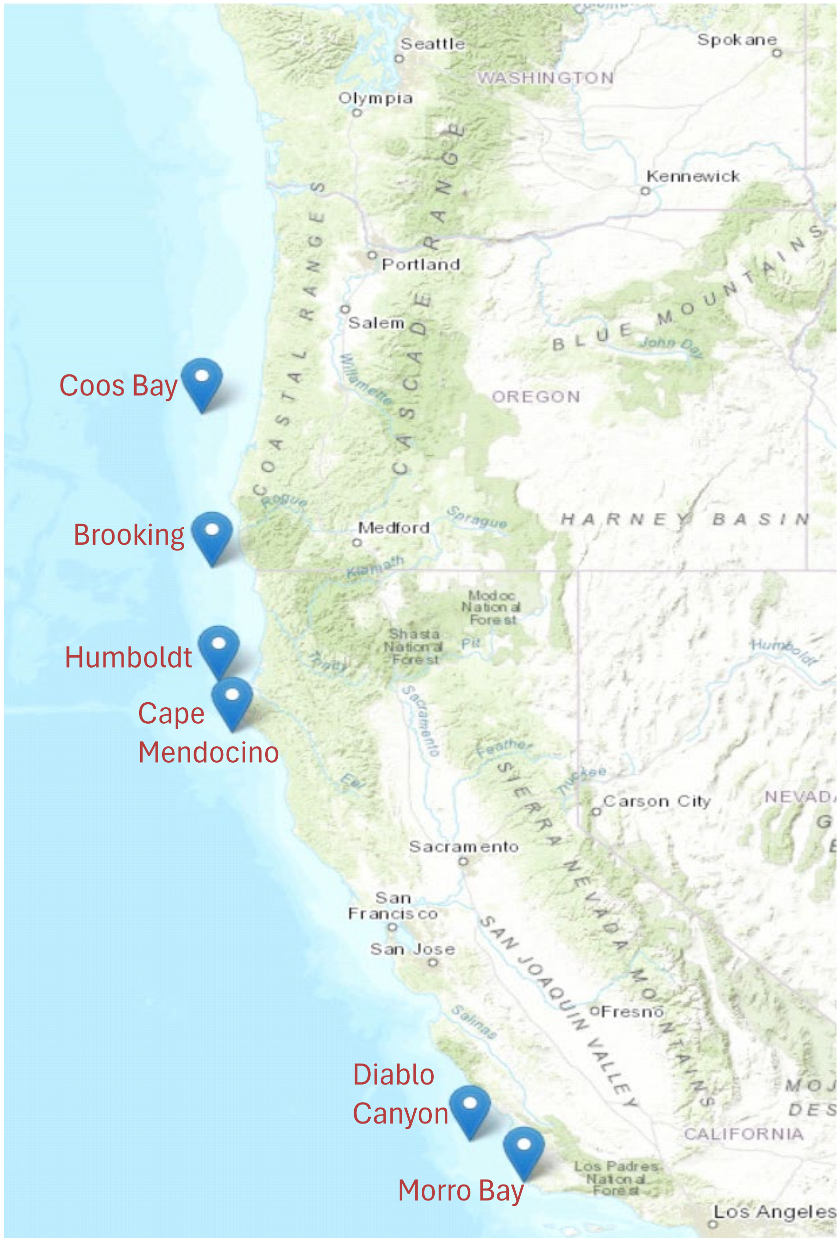

The upper two locations in Figure D - 66, offshore from the Oregon coast near Coos Bay and Brooking, could be considered as in-region. However, since at these two locations there is no CMIP5 model wind speed available from the Climatology Lab,[98] then for simplicity, they are grouped with the lower four locations off-shore from the California coast as out-of-region wind farms.

[98] Climatology Lab: https://www.climatologylab.org/maca.html.

Due to time constraint of the Power Plan, it was not feasible to incorporate climate model wind generation from the GODEEEP data set[99] at the locations plotted in Figure D - 65 and Figure D - 66 into the Council's simulation models, as was done for climate model hydro-generation discussed in the previous section.

For the Ninth Power Plan, the Council decided to use the bias-corrected historical ERA5 wind data set which is already embedded in the TSL model[100] to calculate wind generation capacity factors at the 26 locations for various reference wind turbines.[101] Similar to the development of in-region wind generation data presented in the Section "Climate Scenario Wind Generation Profiles," the historical out-of-region on-shore ERA5 wind data were bias-corrected to be similar to historical wind generation profiles (at the 20 locations plotted in Figure D - 65) from the AURORA power system simulation model[102] and the National Wind Tool Kit[103] developed by the National Lab of the Rockies. In contrast, the historical off-shore ERA5 wind data were bias-corrected to be similar to historical wind generation profiles (at the six locations plotted in Figure D - 66) downloaded from the Bureau of Ocean Energy Management (BOEM) website.[104]

Solar Data

For out-of-region solar generation, the Council decided to simulate generations at the 24 locations plotted in Figure D - 67 below.

[99] See https://zenodo.org/records/13717258
[100] See https://www.timeserieslab.com for more details.
[101] See Technical Appendices B - Existing System Parameters and Policies Draft and G - New Generating Resources Draft for more details.
[102] AURORA power system simulation model: see https://www.energyexemplar.com/aurora.
[103] National Wind Toolkit: see https://www.nlr.gov/grid/wind-toolkit.
[104] Bureau of Ocean Energy Management (BOEM): see https://www.boem.gov/renewable-energy/mapping-and-data/renewable-energy-gis-data.

Figure D - 67: The 24 Locations for Modeling Out-of-Region Solar Generation

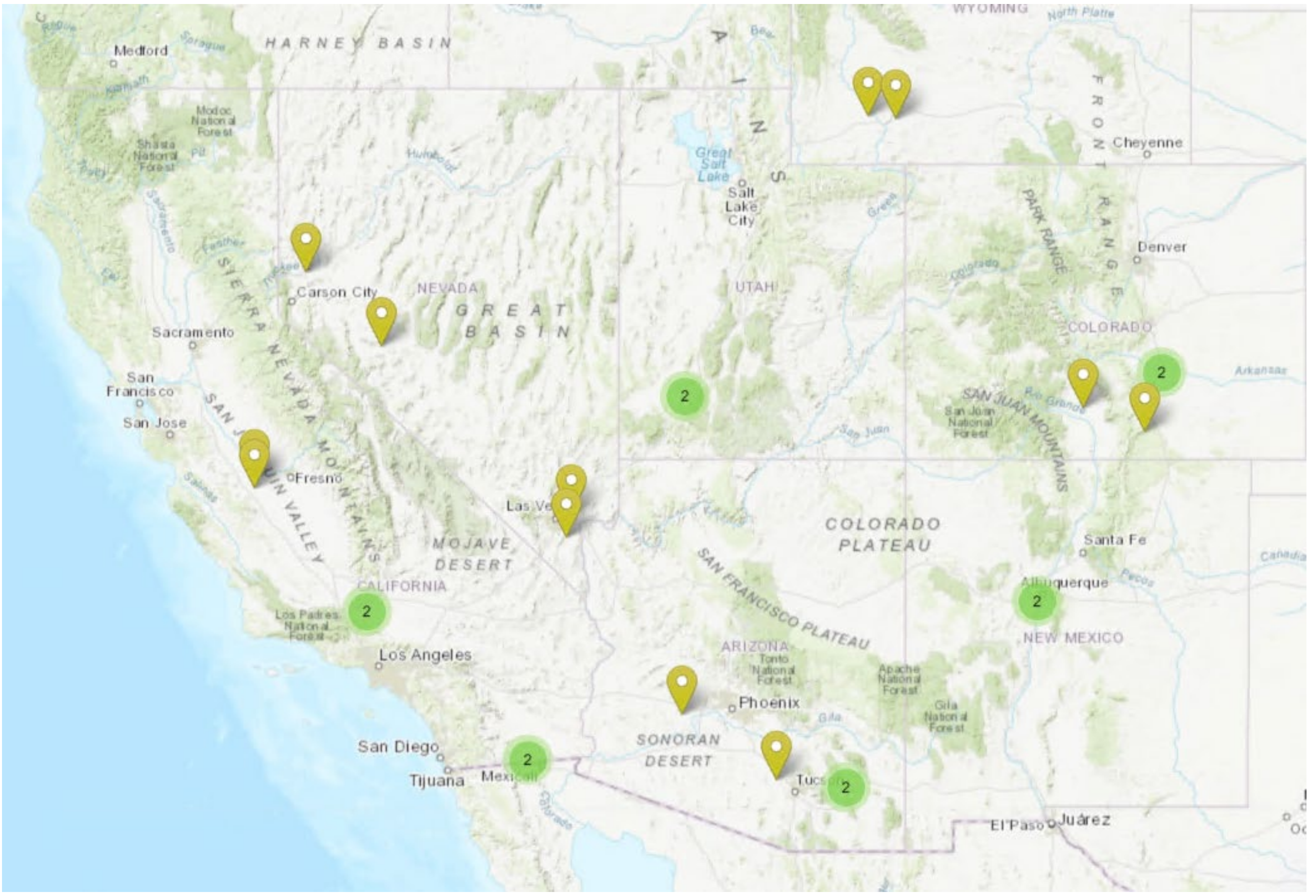

In Figure D - 67, the six green circles with the number “2” indicate that there are two types of solar-panel axis (fixed and 1-axis) and thus two solar generation shapes modeled at those locations. The remaining 12 locations have only one type of solar panel axis and so only one solar generation shape.

Similar to modeling the out-of-region wind generation, for the Ninth Power Plan, the Council also decided to use the bias-corrected historical ERA5 solar data set which is already embedded in the TSL model to calculate solar generation capacity factors at the 18 locations for various reference solar panels.[105] The historical out-of-region ERA5 solar data set were bias-corrected to be similar to historical solar generation profiles (at the 18 locations plotted in Figure D - 67) from the AURORA power system simulation model.[106] It should be noted that six solar generations in California have been adjusted to account for wildfire effects.[107]

[105] See Technical Appendices B - Existing System Parameters and Policies Draft and G - New Generating Resources Draft for more details.
[106] AURORA power system simulation model: see https://www.energyexemplar.com/aurora.
[107] See wildfire methodology section in Technical Appendix G - New Generating Resources Draft for more details.